A SPECTROSCOPIC STUDY OF HIGH MASS X-RAY BINARIES

Alastair P. Reynolds

A Thesis Submitted for the Degree of PhD
at the
University of St Andrews

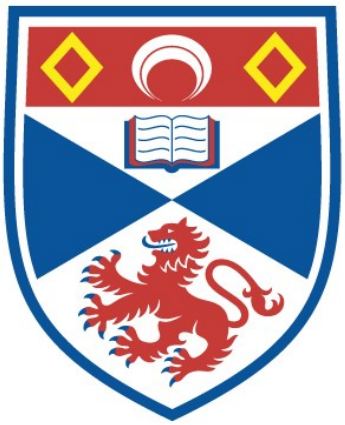

1992

THE UNIVERSITY OF ST. ANDREWS

A SPECTROSCOPIC STUDY OF HIGH MASS X-RAY BINARIES

Alastair P Reynolds

Submitted for the degree of Ph.D.

September 1991

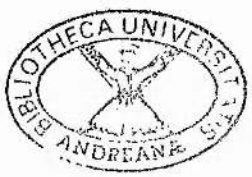

ProQuest LLC.
789 East Eisenhower Parkway
P.O. Box 1346
Ann Arbor, MI 48106 – 1346

TL
BS1

I, Alastair Reynolds, hereby certify that this thesis has been composed by myself, that it is a record of my own work and that it has not been accepted in partial or complete fulfilment of any other degree or professional qualification.

A.P. Reynolds

I was admitted to the Faculty of Science of the University of St. Andrews under Ordinance General No. 12 on 1st October 1988, and as a candidate for the degree of Ph.D. on 1st October 1989.

A.P. Reynolds

I hereby certify that the candidate has fulfilled the conditions of the Resolution and Regulations appropriate to the Degree of Ph.D.

R.W. Hilditch

In submitting this thesis to the University of St. Andrews I understand that I am giving permission for it to be made available for use in accordance with the regulations of the University Library for the time being in force, subject to any copyright vested in the work not being affected thereby. I also understand that the title and abstract will be published, and that a copy of the work may be made and supplied to any *bona fide* library or research worker.

Abstract

Observations of four massive x-ray binary stars are presented, based on data accumulated between February 1989 and August 1991. Using modern techniques of spectroscopic data analysis, velocity curves are derived for three of these systems. Two of these curves (SMC X-1, QV Nor) yield very precise mass estimates for the component stars, while the third (Cen X-3) offers a constraint on the possible masses. The fourth system (X Per) is not shown to exhibit periodic variations, despite an extensive study conducted over more than two years.

For the two systems that yielded precise masses, the component neutron stars are shown to lie within the theoretical mass range based on theories of their formation via the supernova explosion of a helium star in a close binary system. This is a marked improvement on previous studies where both stars had estimated masses which lay well outside of the expected range. The derivation of these masses incorporates the use of non-keplerian velocity corrections, arising from the non-spherical, asymmetrically illuminated primary stars. A study of the line profiles showed that the temperatures around both primary stars were consistent with the parameters in these calculations.

For the third system, the inaccuracy of the published ephemeris resulted in a lack of observations at the times of maximum and minimum velocity. The semi-amplitude is thus not well constrained, but it is shown that the observations are consistent with the assumption of a normal mass neutron star secondary. The system is shown to have undergone a gradual decrease in its orbital period which follows a parabolic trend, suggesting substantial mass-transfer.

For the fourth system, a periodicity analysis of 130 spectroscopic velocity measurements of a Be star, via Fouriergram and string-length techniques, failed to highlight any strong periodicity. The scatter in the data appears larger than would be expected for a non-variable B star. The absence of periodic velocity variations at the expected period is discussed in terms of the binarity (or otherwise) of the Be star. A transition from Be to shell-star or ordinary B star phase occurred during the study, which is not evident from the spectral variations observed in the blue.

Acknowledgements

So many people have helped this work along in the last three years that to name them all would probably double the length of the thesis. Thank you, then, to everyone who gave any amount of assistance, whether they realised it or not - fellow research students and flatmates.

The program could not have been accomplished without the generous allocation of 9 nights of observing time on the 3.9 m Anglo-Australian Telescope, (partly funded by the UK's Science and Engineering Research Council), and many part-nights on the Isaac Newton Telescope, also SERC funded. The staff of the Anglo-Australian Observatory at Epping and Siding Spring are thanked for their hospitality and technical assistance. The observers who took data for us on the INT are also thanked.

Equally important were the numerous observations taken on the 0.5 m Leslie Rose Telescope in St Andrews itself, which, while providing a data set in its own right, also assisted the analysis of the overseas data by providing high signal/noise comparison spectra. Dr R.P. Edwin is thanked for support over the course of 3 years.

The extensive literature search required for this project would have been impossible without the Library staff at St Andrews, not to mention the use of the SIMBAD data base run by the Centre de Donnees Astronomique de Strasbourg. Dr P.W. Hill is thanked for help with SIMBAD.

Financial support was via the Science and Engineering Research Council, in the form of a postgraduate studentship award. That said, couldn't have managed without the support of my parents - not just the end-of-term bale-outs, but their unstinting support and enthusiasm. Also big thanks to my sister and the rest of my family for sticking with me.

I am indebted to my supervisor, Dr R.W. Hilditch, Dr S.A. Bell, Dr D. Pollaco and Dr G. Hill for their collaboration, both in the collection of data here and abroad, and for helping me out of the rough (to use a St Andrews term). I thank my external examiner, Dr I.D. Howarth for valuable comments on concerning many areas of this study. Steve Bell and Graham Hill wrote much of the software through which the data were analysed. Steve and Roger Stapledon deserve thanks for putting me right whenever things computational got the better of me. Lastly, I owe singular thanks to Ron Hilditch for his dedication, patience, good humour and considerable faith over the last three years.

Contents

List of Figures

List of Tables

Chapter 1

Introduction

1.1 Neutron Stars and high-mass Companions

1.1.1 Overview

High-mass x-ray binaries constitute a small but decidedly diverse subset of the pulsating x-ray sources. Reviews of the subject include White (1989) and Rappaport and Joss (1984). The long-term behaviour of the systems is discussed by Priedhorsky and Holt (1986), while the physics of the pulsars is summarized by White, Swank and Holt (1983).

The several dozen systems have little in common other than the fact that in all cases a pulsar is accreting material from an early-type companion, which may be shedding mass by any of the accepted mechanisms, and perhaps in a complicated combination of processes. The spectral and luminosity classes of the stars vary, as do the orbital geometries of the systems; these are factors important in determining the interactional effects and, equally crucially, what is actually likely to be observed. Not *all* the systems (HMXBs for short) are observed to pulsate, and at least one (Cygnus X - 1) is a famous black-hole candidate, but in the following study, it will be assumed that the accreting object (pulsar) is unambiguously a neutron star, except where discussion is clearly merited.

In three of the four cases considered here, it was the detection of periodically varying doppler-shifted pulses which spurred the search for a luminous primary companion, identified by linking photometric/spectroscopic variations with the characteristic eclipse or doppler period of the pulsar, or establishing that no other suitable star lay in the x-ray error box. For the X Per system, examined in Chapter 6, the pulses were too slow, weak and noisy to yield evidence of motion, the binarity and period in this case being inferred by the semi-regularity of x-ray flare-ups.

In other cases even this proved difficult, and it is worth bearing in mind that in some systems the correct identification of the primary is by no means certain. Fortunately this is most certainly not true of any of the short-period systems observed in this study, although the Be/x-ray systems are especially problematic, due to their generally long periods. The latter systems are particularly difficult to study, since there is at present no canonical model for the primary. The presence of excretion disks and complicated wind geometries cannot be ruled out, and the stars may be in highly eccentric orbits. Also, the low eclipse probability means that in most cases only an upper bound can be placed on the mass-function.

1.2 The Optical Companion Stars

The companion stars have been observed to fall into two categories. In the 'supergiant' (luminosity class I-II) systems, the neutron star is in association with evolved stars which are approaching Roche-lobe overflow, or in which the star is in a phase of stellar wind mass loss. These systems all have relatively short orbital periods, facilitating observations on large telescopes, but are distinguished by the differing pulse periods of their companions. Conversely, the Be/x-ray (luminosity class III-V) systems have orbital periods ranging from (it is believed) days to years, and a similarly wide spread in their associated pulse periods. For instance, X Per is the slowest known compact pulsator, with a period of thirteen minutes, while A 0538-66 (not observed here due to poor weather) has the most rapid pulsation of a high-mass x-ray system, 69 milliseconds. These classes of star will be discussed with some reference to the examples considered for study herein, without preempting the results described later on.

1.2.1 Roche-lobe overflow and wind systems - SMC X-1, Cen X-3 and QV Nor

These "ordinary" early-type systems can be studied spectroscopically provided there is no masking by the emission line spectrum of an accretion disk. (The light leaving the disk is typically reprocessed x-radiation from the central source). The ratio of x-ray to optical luminosity in these systems is generally less than unity, with the companions being bright, evolved early spectral types, close to Roche-lobe overflow (RLOF from hereon), which have often been described as undermassive for their luminosity.

The total light output from these systems is, in most cases, determined by the surface area of the primary which is presented to the observer. Its ellipsoidal or Roche-lobe shape ensures a continuous brightness variation as a function of orbital phase (the ellipticity effect). In the absence of other effects such as x-ray heating, gravity darkening is enhanced at the 0.5 phase of the cycle, when the x-ray source is transitting the star. The minimum with the x-ray source behind the primary is shallower. Given a knowledge of the primary's effective temperature, information about the degree of its Roche lobe filling, and an a priori assumption about the inclination of the orbital plane, then analysis of the light curve of an eclipsing system ought to yield an unambiguous mass-ratio. This approach has not been very succesful in the HMXBs, owing to the fact that the light curves depend on far more than these basic parameters. In reality, one appeals to the light curve for information concerning the inclination, and so on, only when the mass-ratio has already been determined spectroscopically. Even when the mass-ratio is known, interpretation of the light curve may be fraught with difficulty. The compact companion may have a pronounced heating effect on the facing hemisphere of the star at periastron, raising the depth of the primary minima. The magnitude of this effect may be comparable to the cooling caused by gravity darkening. Additionally, the disk acts as a source of reprocessed radiation, and also serves to complicate the eclipse geometry. The disk may also cast an x-ray shadow, damping the effect of x-ray heating seen on the primary, or localising it in hotspots whose positions on the star may shift in accordance with the motion of the disk. (The disk may display complex optical modulation over orbital and superorbital timescales.) Clearly, with this many essentially free parameters, any attempt to solve uniquely the light curve will be forlorn,

since many configurations of the system could generate similar modulations. What one can hope for is simply to arrive at a model consistent with the observations, while making the fewest assumptions. For instance, in the case of disk-fed accretion, one can postulate that the star probably fills its Roche-lobe to within a few percent by volume, since the disk must be supported by overflow from the primary star. With the mass-ratio known from the velocity curve and pulse timing, one may then investigate the distortion of the light-curve away from that due to a simple ellipsoidal or Roche-lobe figure in rotation, caused, one presumes, by the action of the disk and the x-ray flux. The picture then derived may feed back into the original assumption, since corrections to the mass-ratio may be computed, accounting for the accurate geometry of the system (see Chapters 3 and 4). Two typical light curves for accretion (supergiant) powered objects are shown in Figure 1.1, from Ilovaisky (1985). X-ray heating fills in the minimum of SMC X-1.

The massive binaries have spectra dominated by the optical companion, with absorption lines moving in phase with the primary. The Balmer lines are frequently subject to contamination, both from cool components in gas flows, and from emission in the disk (assumed comparatively weak). The question of x-ray heating is also of interest (see Chapters 3 and 4). For this reason, most recent workers have cautioned against the use of Balmer lines for velocity determination purposes, a guideline adhered to in this study wherever practicable, with the general caveat that it may be a question of all or nothing, when the spectra are faint, noisy and far from numerous!

Antiphased emission features have been reported for the disk systems, shown to arise close to the dense object, but having amplitudes smaller than expected for the x-ray source orbital velocity, indicating that they arise in the accretion disk, close to the impact point for the stream of matter trailing off the primary. The most common feature seen in emission, other than H_α, has been the HeII emission line at 4686 Å.

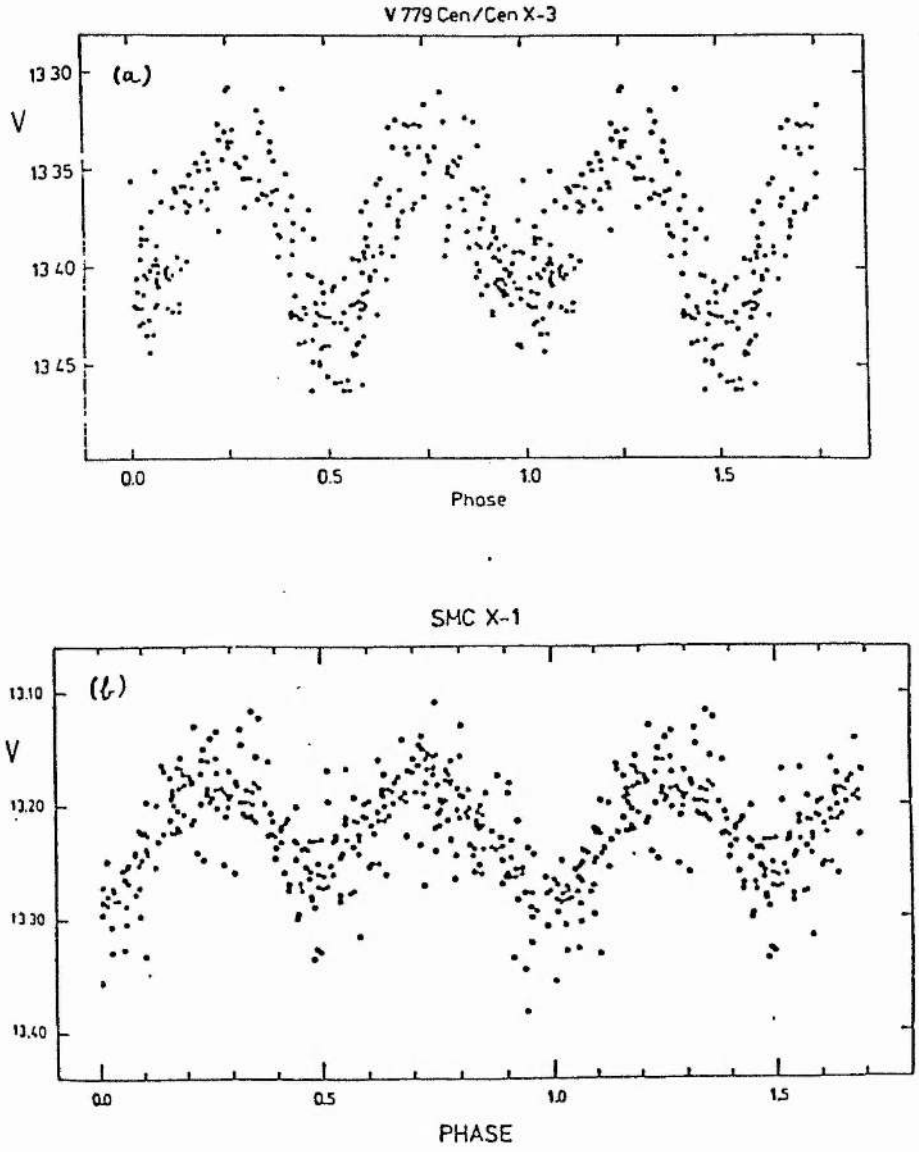

Figure 1.1: The light curves of Cen X-3 and SMC X-1

1.2.2 Be/x-ray binaries - X Per

Harmanec and Kriz (1975) conjectured that all Be stars occur in binary systems, even those hitherto assumed to be isolated cases. Be stars are known to be common among the optical companions of the high-mass pulsating x-ray systems. The frequency of Be stars among these systems is consistent with the fraction of emission line stars among the early types, bearing in mind that Oe stars are often classified as Be stars. Selection effects are important, since the x-ray luminosities of the Be/x-ray binaries are generally subcritical, an order of magnitude fainter than the short-period accretors, and may be subject to extended interludes of quiescence.

Be stars are known to be hot, rapidly rotating stars with emission lines in their spectra. The basic Struve theory of a ring of circumstellar matter supported by the centrifugal force of the star has proved untenable. The stars are not in general rotating near their critical velocities as Struve had assumed (see Chapter 6). It is now known, partly from IRAS studies, that the morphology of the Be circumstellar cloud is more complex than this. Plavec (1985) covers the currently fashionable theories, most of which are not easily reconcilable. The condensation of the wind in the equatorial plane in a disklike morphology (two-component model) has been invoked to explain the discrepancy between the wind strength as inferred by the pulsar luminosity and that implied separately by the IR excess and the UV spectrum (see Section 1.4).

Controversy exists over the question of whether or not Be stars form during or after the main-sequence era of a star. A single B star undergoing post main-sequence contraction might produce a Be-type gas shell, although this would presumably be a 'one-off' event rather than the semi-recurrent envelope regeneration necessary to account for the transient accretion objects, in which replenishment may be occurring on a short, yearly timescale.

The most popular single-star explanation not explicitly requiring binarity is the non-radial pulsation (NRP) model (Baade, 1985). Some short periodicities possibly linked to NRP have been seen in the spectroscopic and photometric data. In the case of X Persei, a reported variability in the x-ray flux on a 22.5 hour basis has been ascribed to periodic ejection of material, driven by NRP (Penrod and Vogt, 1985).

However, Slettebak (1985), on the basis of a detailed survey, suggests that the Be phenomenon occurs among unevolved main sequence stars. This lends credence to the binary hypothesis, which provides an automatic mechanism for the formation of envelopes around normal main-sequence stars. Advocates of the single star hypothesis, on the other hand, must explain how rotational instability arises in a main-sequence star that is undergoing gradual expansion rather than contraction (Harmanec, 1987).

The binary model, as summarised by Harmanec (1985) and Plavec (1985), postulates that the Be envelope is an accretion structure arising from mass transfer. This hypothesis fails to explain the persistence of the envelope where the mass transfer episode clearly occurred much earlier in the history of the system—those Be stars, for instance, in conjunction with dead companions such as neutron stars or white dwarfs. To complicate matters, at least one of the Be/x-ray systems may contain *two* disks (Giovanelli and Żiolkowski, 1990). Most of the HMXB literature explicitly assumes that the Be stars are not evolved and are deep within their critical lobes.

X-ray flare observations have been a valuable technique for illuminating the orbital characteristics of many Be/x-ray binaries. Phases of enhanced emission, possibly following a period of quiescence, are expected in systems in which the orbit of the pulsar is highly eccentric, bringing it much nearer the companion at periastron than at apastron, when there may be no infall to speak of, or infall supported only by residual accretion of matter collected during the previous flare-up passage.

A serious problem is that those systems with long period orbits prove difficult to analyse from a purely Doppler-effect based approach; pulse periods are also longer in these systems. The only orbital data available may therefore be optical, and even then, it may not be feasible to follow a system throughout the entirety of one cycle. At best, therefore, one may only be able to a obtain an optical mass-function in the long period systems. Even if the orbits are solved for masses, other geometric variables may remain undetermined. It would be of interest to know the inter-relationship between the inclination of the orbital plane and the axis of rotation of the Be star (Ruusalepp, 1981), for this would enable predictions to be made about the occurrence time and duration of x-ray bursts. If the neutron star orbit is inclined to the plane of ejected circumstellar material, it may intersect twice in every orbit, causing two possibly closely

spaced enhanced phases of x-ray emission. Alternatively, if the orbit and the envelope are coplanar there will be one extended periastron outburst.

1.3 The X-Ray Spectra and Pulse morphologies

Joss and Rappaport (1988) note that the pulse period distribution of the known systems is consistent with a constant number per logarithmic interval in period, although there is a marginal excess for periods in the 300 second range. Those objects possessing either very long or very short pulse periods are likely to have been selected out of the observational set. It is to be expected that the real systems undergo massive alterations in their pulse periods over their lifetimes - probably being created with extremely short spins which are then reduced by interaction of the initially very strong pulsar magnetic field with the surrounding interstellar medium. Subsequent evolution may be expected to take the form of accretion-powered spin-up episodes, leading to circularisation of the orbit and pulse periods of around a second. Figure 1.2 illustrates some sample pulse profiles (from Joss and Rappaport, 1984).

By contrast with the symmetric, narrow pulses of the isolated radio pulsars, these are seen to be wide, asymmetric, and somewhat irregular. Furthermore, there is no obvious pulse-period dependent morphology for these profiles, nor is there any correlation with the widely varying x-ray luminosities, spread over five decades. The luminosities are not well determined, even when distance estimates are available, owing to the restricted spectral coverage of the detectors and the uncertain nature of the pulse geometry.

The spectra themselves differ little in detail, although cyclotron lines have been observed in two of the systems. Typically, the x-ray spectra show broadband emission lacking sharp spectral features, with the power mostly being emitted in the 2-20 KeV range. Not only are the fluxes at source rather poorly determined, but the problem of the beaming geometry cannot be avoided, particularly in discussions of the effect of the flux on the neighboring star (pencils or fans?). The spectra are usually described by a

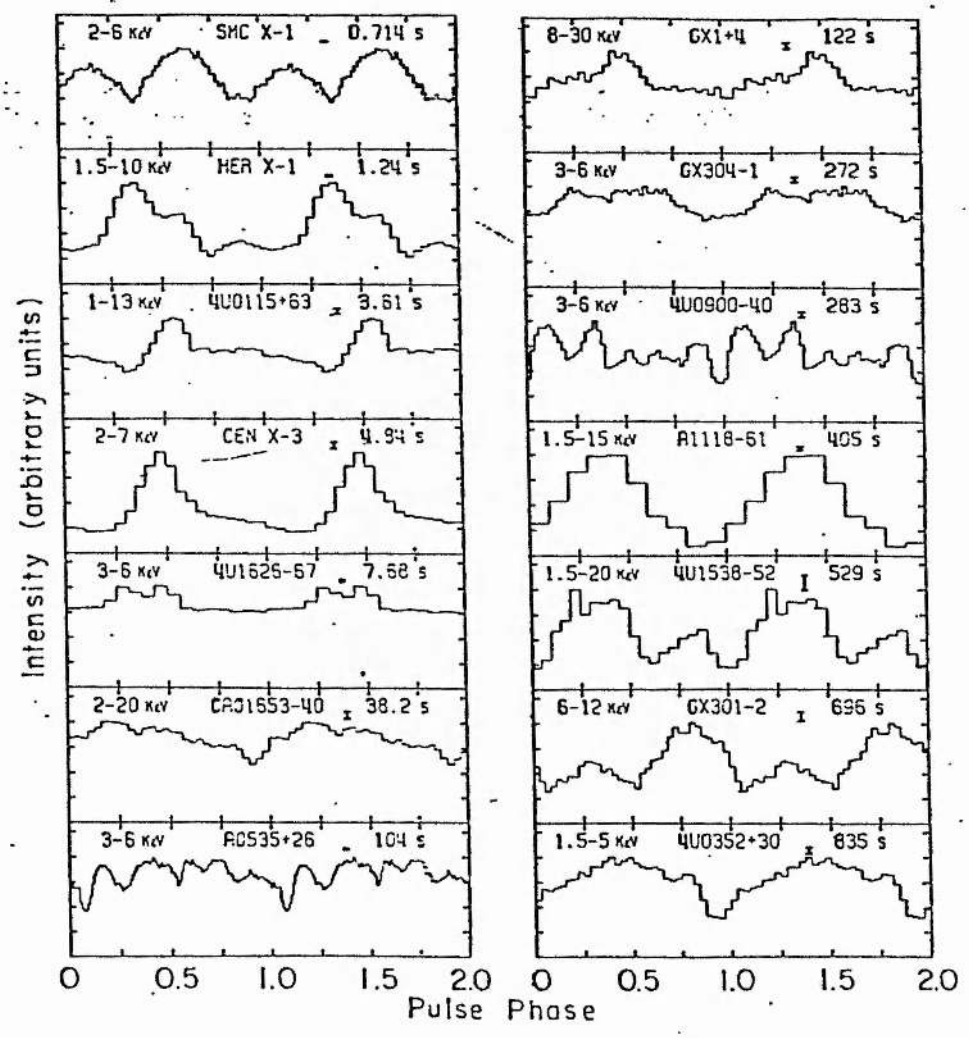

Figure 1.2: Sample pulse profiles for 14 x-ray pulsars.

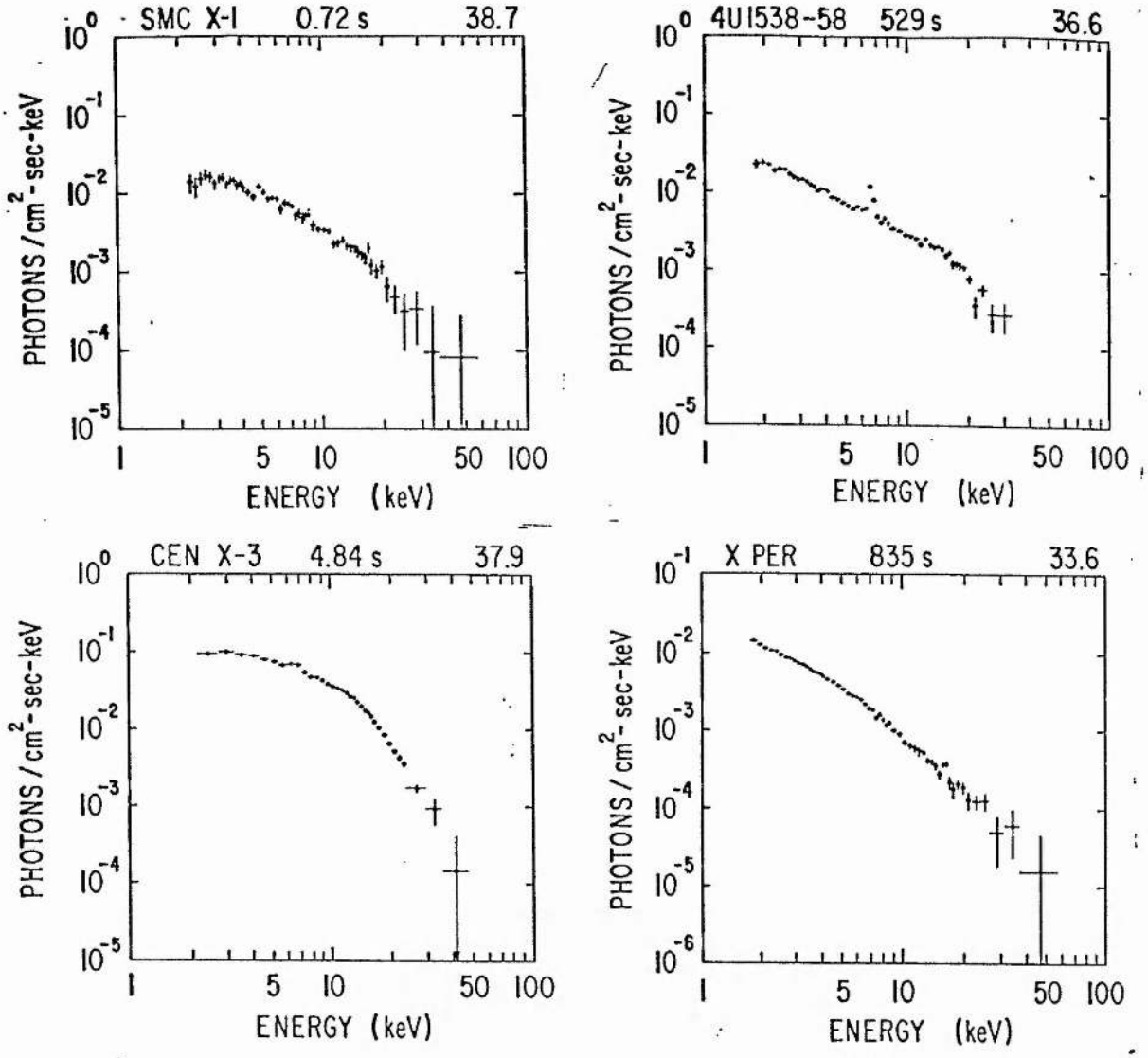

Figure 1.3: Phase-averaged spectra of the systems from Chapters 3-6.

modified, approximately flat power law, with a sharp cut-off at high energies, though sometimes the cut-off is not very pronounced. The phase-averaged spectra for the 4 systems studied in detail in this study are depicted in Figure 1.3, from White et al (1983). The exception to the rule is X Persei, which is best fitted thermally (and is a very faint intrinsic x-ray source compared to the others).

1.3.1 X-Ray Absorption

OB winds are driven by the transfer of momentum from the supergiant radiation field by scattering in the UV band (White 1989, and references therein). A cavity will form

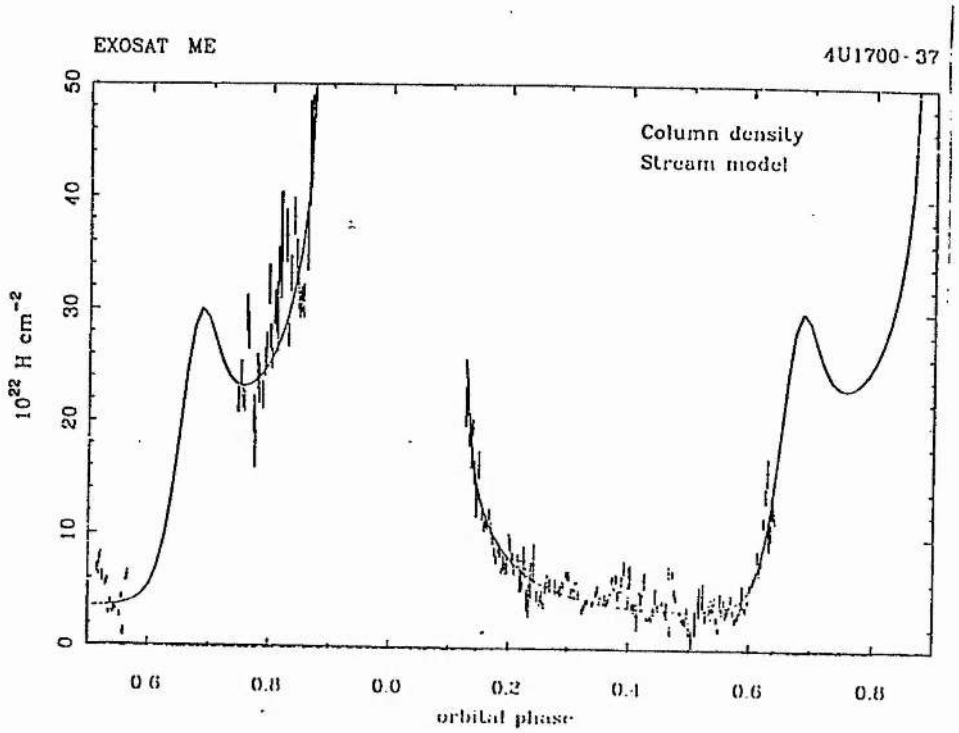

Figure 1.4: Absorption as a function of phase for X1700-37.

in the wind surrounding the x-ray source as UV line transitions are destroyed, thus dampening the radiative acceleration of the wind. This feature can be utilised to study the density distribution of the wind and the outer atmosphere of the OB star, as the neutron star moves out of eclipse. Marked asymmetry exists in the eclipse profile before and after phase 0.5 - see figure 3. The decrease following eclipse egress is well modelled (Solid line) due to a decrease in absorption through the wind, in accordance with a velocity law. The increase at 0.6 is modelled by including a gas stream trailing behind the compact object (From White, 1989 and references therein).

This asymmetry may arise due to a gas stream trailing behind the neutron star, or x-ray disruption of the accelerated wind. The object X1700-37 is a non-pulsating x-ray source not believed to be a black-hole candidate, and is therefore of essentially the same class as Corbet's stellar-wind driven sources (see below), except that some factor prevents observation of pulses.

1.4 Pulse and Orbital Period Correlations

Pulse and orbital periods are known for at least seventeen high-mass x-ray pulsators (Corbet, 1986). Despite the low reliability of some of these estimates (for instance, see Chapter 6), certain trends are nonetheless clear. There is a marked correlation between the two periods, seemingly depending on the prevalent mass transfer mechanism, and thus the evolutionary state of the primary. The systems fall into three types, with the Be/x-ray cases displaying this most obviously. They lie along a positively sloped line when pulse period is plotted against the orbital period (see Figure 1.5 and Table 1.1 , from Corbet). This might seem to indicate some mass transfer driven evolutionary trend from long-period to short periods in both pulse and orbit.

If the neutron star rotates with the keplerian period of the accretion disk where it encounters the magnetosphere, then a particular wind-density will lead to a relationship between pulse period and orbital period (White, 1989 and references therein). However, assumptions about expected Be mass-loss rates do not predict the correct pulse-period association. The picture is worse for the supergiants, where wind loss is assumed to be much higher. Rather than postulate unrealistically high magnetic field strengths, it has been suggested that the current pulse-period association is a relic of a phase when supergiant wind loss was less active.

Simplistic attempts to probe Be wind loss from the standpoint of the known pulse-period correlation indicate that the winds have to be much slower than had been thought plausible. Recent work suggests that the Be wind profile does vary considerably from pole to equator. Waters and van Kerkwijk (cited in White, 1989) have apparently produced good theoretical predictions of the Be correlation based on this picture. The outbursts of the Be/x-ray binaries can be classified into two different types. Type I outbursts are linked to the orbital period and trigger a hundredfold luminosity increase. Type II outbursts are unique events which typically last for tens of days and are associated with luminosity changes up to ten times higher than in the type I cases. Both types may occur in one system at separate occasions.

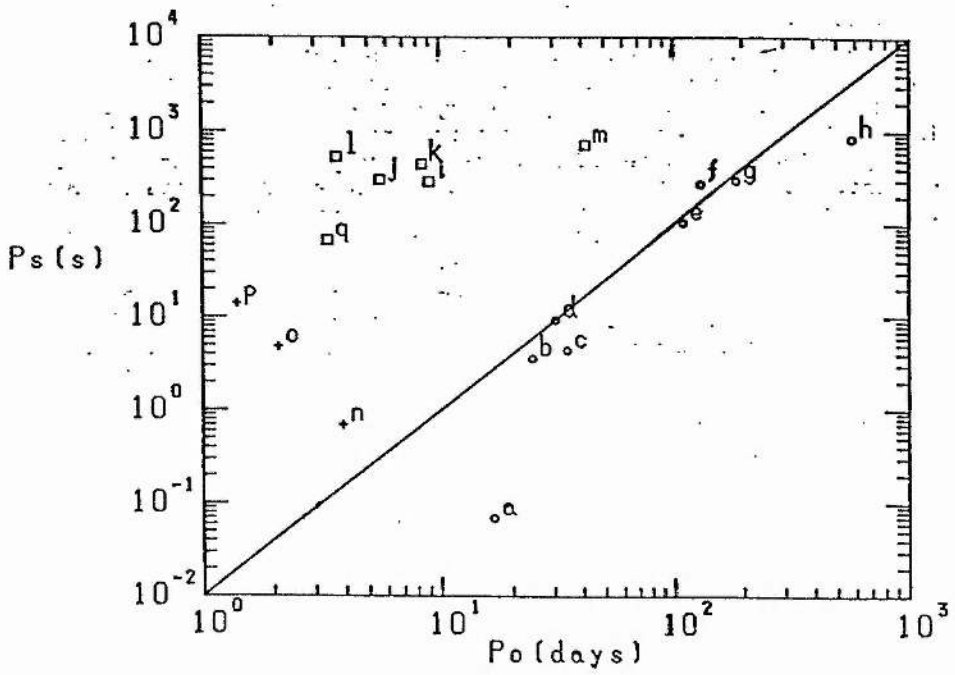

Figure 1.5: Orbital and pulse periods for HMXBs.

Other systems display significant long term variations in overall behaviour. One observes well defined phases characterized by *ON* and *OFF* states in the x-ray emission. This may imply long-term depletion of the Be envelope. GX 304-1 is a known Be/x-ray binary displaying such behaviour; others are 4U0115+63, and possibly 4U1145-61 (Preidhorsky and Holt, 1986) . In the case of GX 304-1, it would seem that the Be envelope has been on the wane since 1978; recent x-ray observations have detected a flux 25 times less than the expected quiescent level. It seems unlikely that such apparently significant changes will be permanent. More probably, this drastic short-term behaviour will turn out to be part of a broadly uniform pattern for Be/x-ray binaries that will only emerge when long-term monitoring becomes possible. X Persei is a long period Be/x-ray binary (a weak but non-transient x-ray source) in which variations in the Be envelope had not been seen thus far.

Conversely, those systems where stellar wind accretion from a supergiant primary, and Roche-lobe overflow onto an accretion disk are the active transfer processes have their own well defined zones on this map, though the pattern is less obvious than the Be

	Source	Spec. Type	P_s [seconds]	P_o [days]	e	group	L_x	
a	A0538-66	B2IIIe	0.069	16.65	>0.4	1(3?)	1E39	
b	4U0115+63	Be	3.6	24.3	0.34	1	8E36	
c	V0332+53	Be?	4.4	34.	0.31	1	?	(a)
d	2S1553-542	?	9.3	30.6	<0.09	1	?	
e	A053335+26	BOVe	104	111	.2-.4	1	2E37	
f	GX304-1	B2Ve	272	133	?	1	3E36	
g	4U1154-61	B1Ve	292	188	?	1	6E36	
h	X Per	0.95III-Ve	835	580?	?	1	1E34	
i	Vela X-1	BO.5Ib	283	9.0	0.09	2	6E36	
j	1E1145.1-614	BII	297	5.6	?	2	3E36	
k	4U1907+09	OBI	437	8.4	?	2	4E37	(b)
l	4U1538-52	BOI	529	3.7	?	2	4E36	
m	4U1223-62	B2Ia	700	41.5	0.447	2	1E37	
n	SMC X-1	BOI	0.7	3.9	$<7\times10^{-4}$	3	6E38	
o	Cen X-3	O6-8(f)p	4.8	2.1	8×10^{-4}	3	4E37	
p	LMC X-4	O7III-V	13.5	1.4	<0.09	3	4E38	(c)
q	4U1700-37	O6.5f	67.4?	3.4	?	2?	3E36	(d)

Table 1.1: Key for HMXB pulse-period diagram.

systems. The RLOF correlation is based on only three objects, but appears analogous to that seen in the class of objects known as the intermediate polars, in which the neutron star has been replaced by an accreting white dwarf. The *observed* tendency seems to be for a gradual spin-down of the pulsar, with a corresponding reduction in the orbital period. It must be that the dominant long-term process is a spin-up, (ie a tendency toward synchronisation of period and spin) in order to generate the anti-correlation. Therefore, the correlation we observe is *in spite* of accretion, arising when the systems in general are x-ray quiet. This phase is not observed in any binaries for the obvious reason that they will not have been identified as x-ray sources. However, the onset of strong mass loss at the end of the primary's life will again spin up the pulsar. This final period of strong accretion results in binary pulsars in which the magnetically weakest component (oldest) is the most rapid rotator (eg PSR 1913+16).

The wind-driven objects do not display much of a correlation at all, simply occupying a domain on the pulse-period map. Studies of the pulse histories (eg Nagase, 1988) show a random walk behaviour, with no overall trend either to spin up or down. This suggests that the density and flux of material around the stars is also subject

to random fluctuations. It is generally argued that the wind cannot form a disk (see Chapter 5), although some have objected that the x-ray luminosity implies RLOF. The light curves do not support the presence of a large or bright disk, since they are basically ellipsoidal.

1.5 The evolutionary scenarios for the HMXBs

It now seems clear that the short-period HMXBs can be explained fairly successfully in a framework of the subsequent conservative evolution of close binary systems containing early-type stars. In this respect, the close HMXBs (RLOF and wind-driven systems) can be considered as normal by-products of stellar evolution. This is in stark contrast with the LMXBs where the fraction of x-ray binaries formed, per unit time, and among stars of the same mass, is between 10^5 - 10^7 less (van den Heuvel, 1983); these are exceptionally rare objects. The HMXBs can therefore be thought of as "par for the course"; their small number in the sky at any one time is due to the brief time over which they are likely to be active as x-ray objects (no more than a few tens of thousands of years, before the x-rays are quenched by the onset of large mass ejection).

The fact that the optical star in the HMXB has survived the supernova detonation of the secondary shows that it must have been the more massive star at the time of the explosion. This then requires extensive mass transfer from the supernova progenitor to the primary via case B or C mass transfer (the primary here referring to the observed optical star, not the more massive or luminous star prior to the explosion). As much as 80 % by mass of the progenitor may be shed onto the companion, leaving a helium core. Van den Heuvel summarizes the expected evolution of the helium stars for various mass ranges. Since this is of interest, in view of the derived component masses discussed throughout this study, the findings will be briefly reiterated.

(1) If a solitary helium star weighs less than 2 $M_\odot$, the entire core is incinerated via carbon deflagration, and explodes as a supernova without leaving a remnant. In a binary, the carbon deflagration does not occur, the envelope having been shed, and a CO white dwarf is left behind.

(2) If the helium star lies between 2 - 3 $M_{\odot}$, the CO core does not become degenerate and quietly ignites carbon burning. A degenerate O-Ne-Mg core is left behind, approaching the Chandrasekhar limit. In a single star, helium shell burning sets in and tips the core over into a neutron star. In a binary, the envelope is shed leaving a O-Ne-Mg white dwarf.

(3) If the helium star is heavier than around 3 $M_{\odot}$, the O-Ne-Mg core is larger than the Chandrasekhar limit and evolves through all stages of nuclear burning until an iron core is attained. The core eventually collapses, leaving a neutron star formed in a photodisintegration supernova (or a black hole).

The third scenario then suggests that the immediate precursor to a HMXB would be a Wolf-Rayet (WR) binary, the result of case B mass transfer in a massive close system. The WR star is the more evolved, having already reached core helium burning, but is the less massive component. Observations of WR binaries reveal that the companions (primaries in the designation used here) are O- and early B-types still burning hydrogen in their cores. The periods and masses of these binaries are quite consistent with them later becoming HMXBs, provided the WR component has lowered its mass to 10 $M_{\odot}$ by wind loss, and, as van den Heuvel adds, may also satisfy the parameters of some of the Be/x-ray binaries.

Figures 1.6 and 1.7 (from van den Heuvel, 1983, and the references therein) displays scenarios for the formation of a short period HMXB and a Be/ns type system, depending on the initial masses of the binary components.

There are however difficulties with reconciling the conservative scenario with the short-period systems. Some authors have argued that the primary cannot accept the matter being transferred to it by the progenitor within the required timescale; it ends up spilling out over its own Roche lobe, leading to a contact configuration. This problem means that for short period systems (5 days or less), contact is inevitable so long as q is less than 0.4. If q is 0.3, for instance, the period cannot be less than 9 days. For these two constraints, the period *after* the explosion will always be more than 10 days; in other words, there is no way at all to form post-supernova HMXBs with periods shorter than 10 days in conservative evolution. The problem can be alleviated by postulating a

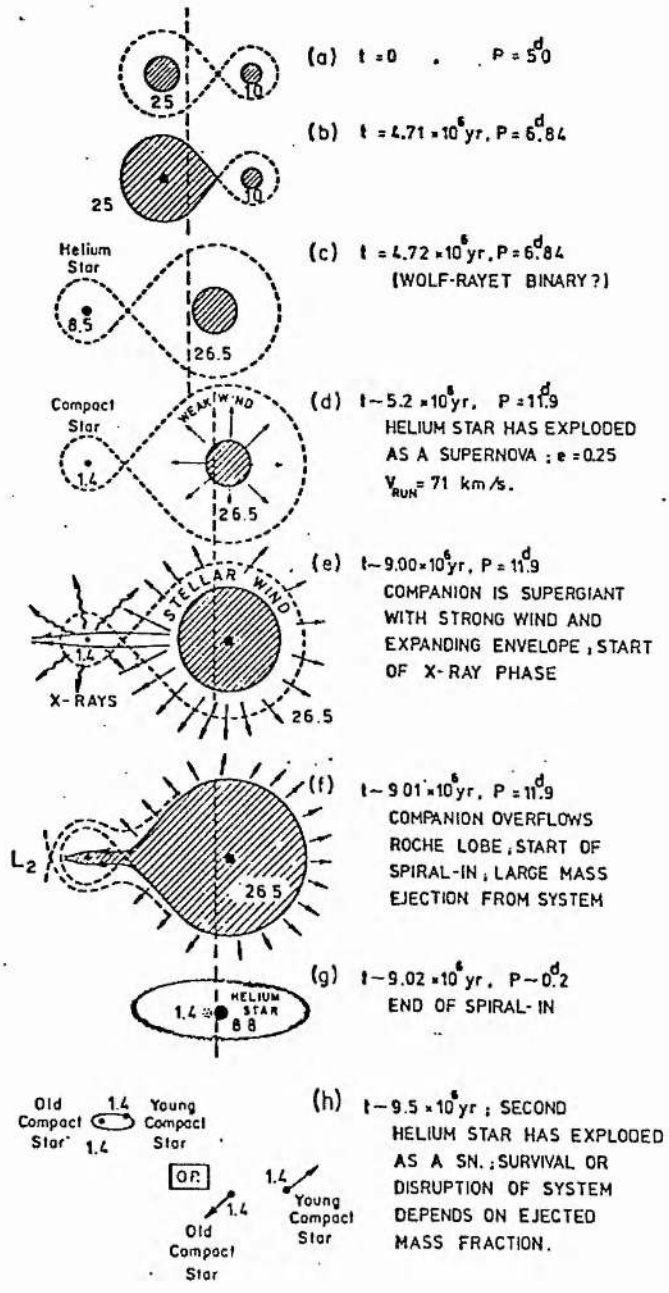

Figure 1.6: Conservative evolution for short-period HMXB.

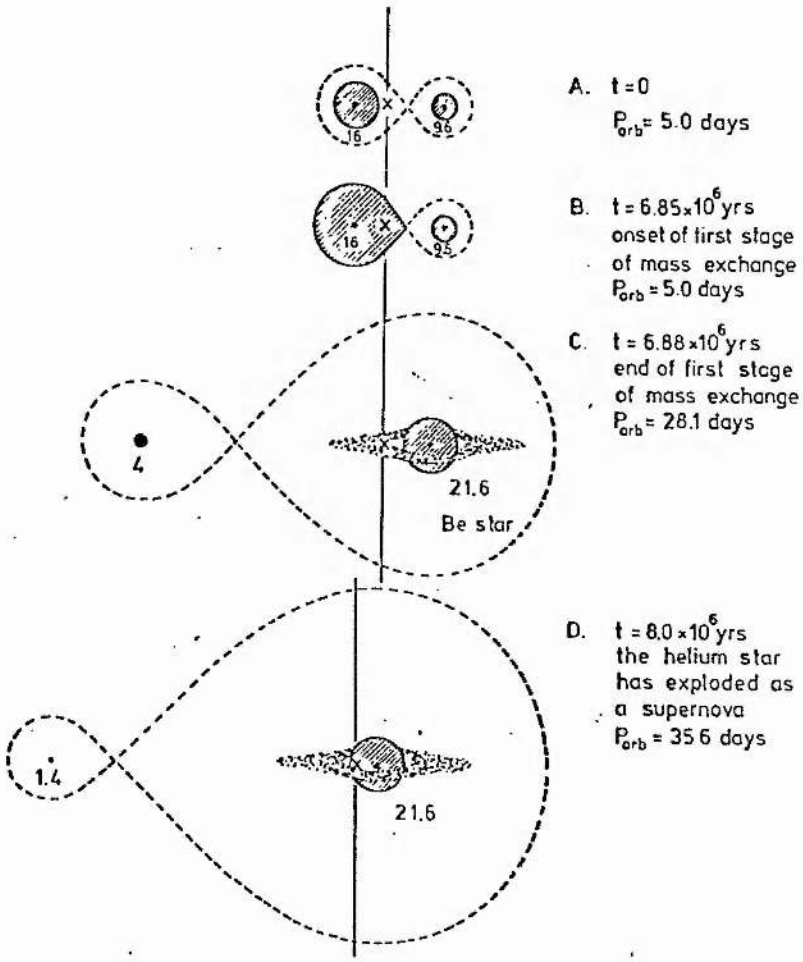

Figure 1.7: Conservative evolution leading to Be/x-ray system.

period of angular-momentum loss during a common-envelope phase, during which the period is shortened. The resulting theoretical models strongly resemble systems like SMC X-1 and QV Nor.

It is now believed (Rappaport and Joss, 1983, van den Heuvel, 1983, Arnett and Schramm, 1973) that the masses of the remnants in these binaries will straddle the Chandrasekhar mass to within 0.2 $M_{\odot}$, owing to the limiting mass of the core in the progenitor (which will have undergone extensive mass loss).

1.5.1 Future evolution of the HMXBs

Inevitably, the optical star in the binary will reach the end of its normal lifetime. There will be extensive mass loss from the system as a whole, possibly characterised by an episode of beaming, similar to that seen in SS 433, as the bulk of inflowing matter is expelled perpendicular to the disk, with a spiral-in phase leading to a short-period helium star/neutron star binary. The RLOF driven HMXBs have already embarked on this final stage, and it will also occur in the Be/x-ray binaries once they have evolved off the main-sequence. Whether or not the system remains bound after the second supernova explosion depends on the extent of mass removed from the binary; the disrupted component(s) might then explain the large space velocities of some of the isolated radio pulsars. Alternatively, the end-state might be a white-dwarf/neutron star binary.

1.6 The component masses of the HMXBs

1.6.1 Mass determination via spectroscopy in the HMXBs

In all three cases of short period system discussed in this study, the following observational facts were already to hand: a reliable estimate of K_x, the semi-amplitude of the pulsar's orbit as revealed by pulse timing, $A_x \sin i$, the semi-major axis of the secondary's orbit, revealed by the maximum delay in seconds of the pulse, and θ_e, the half-angle of the x-ray eclipse. Typical errors on these parameters would be in the 5

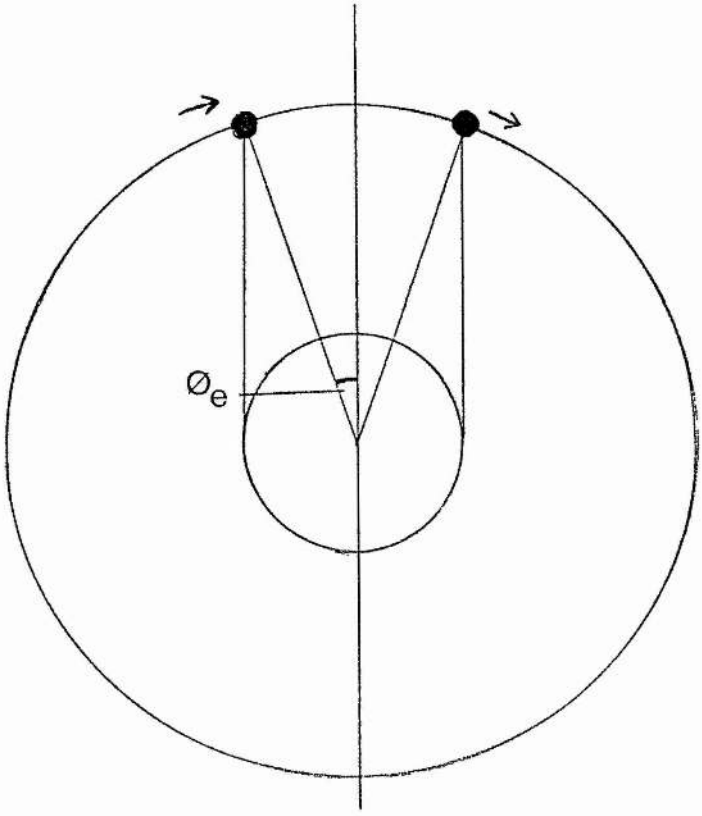

Figure 1.8: Eclipse geometry in an HMXB system.

- 10 % range, although the first two are sensitive to the eccentricity and net spin-up rates of the pulsar. These observations, coupled with an optical velocity curve, permit the independent derivation of the system masses with recourse to only a few external assumptions.

Based on an assumed geometry, the eclipse timing (when the x-ray source is occulted by the primary) determines the inclination angle, i. The eclipse geometry is represented schematically in Figure 1.8. For ease of calculation, if the primary is represented by a sphere, Equation 1.1 holds (see Rappaport and Joss, 1983, and Avni, 1976. Chanan, Middleditch and Nelson, 1976, investigated the eclipse geometry without the assumption of sphericity. For eclipse durations appropriate to SMC X-1 and QV Nor (20-30°), and mass-ratios of around 10, this author finds that the simplified estimate of i is quite accurate, in general not more than $\approx 1°$ from the Chanan et al result. For $q = 10.01$ and $\theta_e = 30°$, for instance, both predictions are for $i = 70.0°$).

$$R_c \approx a\,[\cos^2 i + \sin^2 i \sin^2 \theta_e]^{1/2} \tag{1.1}$$

where R_c is the radius of the sphere whose volume equals the actual volume of the star, and where a is the separation between the centres of mass of the two stars.

This volume may be related to the mass-ratio between the *x-ray star* and the *optical star* q by an empirical expression, Equation 1.2 :

$$R_L \approx a\,[A + B\log q + C\log^2 q] \tag{1.2}$$

Here R_L is the effective radius of the critical lobe. For corotation, the constants become $\approx$ 0.376, -0.227 and -0.028 respectively. Often the above expression is reduced to Equation 1.3 :

$$R_L/a = 0.38 - 0.2\log q \tag{1.3}$$

Alternatively, various authors have computed theoretical grids relating the above parameters (eg Mochnacki, 1984). If R_c is then taken to be some fraction β of the critical lobe (in effect a parameter defining the extent to which the star fills out the lobe), then the inclination angle can be obtained from the eclipse duration as in Equation 1.4 :

$$\sin i \approx [1 - \beta^2(R_L/a)^2]^{1/2}/\cos\theta_e \tag{1.4}$$

Therefore, provided the x-ray data are sufficiently "clean" with regard to the times of ingress and egress, the inclination may be deduced. In practice, this usually involves considerable uncertainty (see Chapter 4 for instance). Part of the difficulty arises because the presence of gas-streaming may destroy the symmetry of the absorption about maximum eclipse. Secondly, the atmospheres of B-stars are not sharp occulting surfaces (see Chapter 5, for instance), which may mean that the size of the critical lobe is underestimated, with the x-ray source "shining through" even though it is geometrically obscured. Thirdly, the sheer faintness of the source may hamper a precise determination of the flux change with time (as seems to be the case in Chapter 4). Nonetheless, it is usually possible to deduce i to within a few degrees, provided the orbit is well-determined, and the evolutionary status of the star can be inferred independently (how well it fills its lobe). Caution should be administered, however, in adopting the inclination estimates of previous workers. In the case of QV Nor, for instance, a different estimate of the mass-ratio suggests a lower value of i than found previously.

This adopted i then enables the mass-function to be solved for the companion star, Equation 1.5 :

$$f(M) = 1.0385 \times 10^{-7} K_{opt}{}^3 P = \frac{M_x \sin^3 i}{(1+q)^2} \tag{1.5}$$

where $f(M)$ is in solar masses and P in days, and the orbit has been assumed circular (a satisfactory assumption in most cases). The kind of uncertainties that these parameters lead to in the final derivation of the masses and sizes has been discussed briefly in Chapter 4.

In the longer period systems, the likely absence of eclipses means that i cannot be deduced so easily, and the lack of proximity will mean that the light variations will be slight. In the Be stars, for example, the inclination might be determined from a study of theoretical and observed line profiles, (eg Corbet et al, 1986), or polarimetric studies, since these stars are expected to exhibit preferential outflow when seen "equator-on". The absence of an estimate for i is usually unimportant since it is rarely the case that the other parameters are known precisely.

1.6.2 Comparison with theory

Most of the systems discussed in this study were observed at least once in the nineteen seventies. The spectroscopy performed was based on image tubes and photographic plates, frequently over more than one cycle. Most of the orbital solutions were poorly determined, owing to the scatter in the data, and often relied on the ad hoc weighting of various velocity points in order to produce a sinusoidal variation of the right amplitude. The lines measured were chosen fairly indiscriminately, with a wide use of Balmer lines where it was perhaps unwise. No attempts were made to correct for distorted stellar geometries, heating assymetries, etc (although their possible importance was recognised by most authors). Nonetheless, masses were determined, but with errors that echoed the technology of the time.

The masses of the neutron stars in these systems range from $\approx$ 1 - 2 $M_{\odot}$, as displayed in Figure 1.9, reproduced from Rappaport and Joss (1983) : It is believed that the masses of the stars should lie in the region of 1.4 $\pm$ 0.2 $M_{\odot}$. Obviously the most extreme case, the component 4U 1538-52 of the QV Nor system, is only poorly determined. This theoretical mass range covers the evolution both via collapse of the degenerate core of an evolved star and also accretion-indued collapse (AIC) of a white-dwarf in a binary. In the case of the HMXBs, the former is thought to be the most

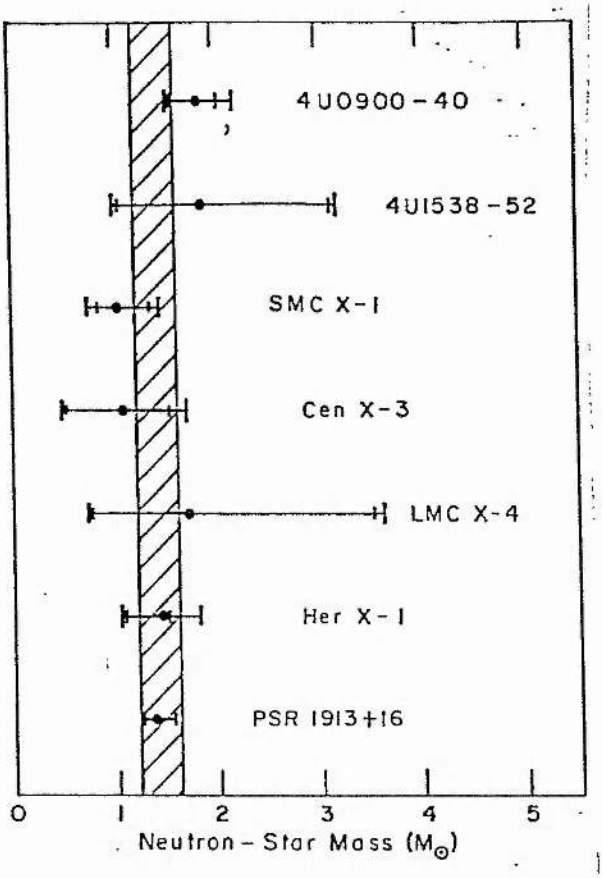

Figure 1.9: Empirical knowledge of neutron-star masses.

probable track, since AIC requires exceptionally fine-tuning of the accretion flow and its composition in order to occur, in addition to the fact that the star must lie within 1 % of the Chandrasekhar limit. The details of the evolved star model have already been discussed in Section 5 earlier in this chapter.

The primary star masses have been the subject of some contention, since many authors have claimed evidence for their undermassiveness in respect to their luminosity (or overluminosity for their given masses). This topic was discussed at length by Savonije (1980). There seems to be no *a priori* reason why this should occur, particularly in view of the weakness of the illuminating flux from the secondary. It is therefore sometimes suggested that the primaries must have shed a lot of mass during their evolution, and that the helium cores are therefore larger than usual. This has been argued against on the grounds that the rates for the winds/RLOF transfer required are unrealistic. Savonije admitted that it was "certainly not impossible" that the problem might boil down to systematic errors in the mass and luminosity derivations. Later, van Paradijs (1983) concurred that "the differences seem too small to conclude that there is a general overluminosity...", although Cen X-3 had been shown to be undermassive.

The issue of the undermassiveness does still crop up in the literature (for instance, Giovanelli and Ziokowski, 1990), and a new analysis of the systems, incorporating CCD detector technology, cross-correlation velocity determinations and computed corrections for off-centre illumination in the primaries, was obviously germane.

1.6.3 This study

The work reported in this thesis is based on two separate runs of observing time in 1989 and 1990, as well as observations taken in St Andrews. In early 1989, an application was submitted to PATT (the panel for the allocation of telescope time on SERC-funded instruments) applying for 4 nights of bright time in two 2-day units on the Anglo-Australian Telescope, in order to study the HMXBs LMC X-4 and SMC X-1. An application was also submitted asking for a single night of service time on the same telescope to study the peristron passage of A 0535-66, a unique HMXB which, in terms of its pulse-period relationship, is intermediate between the Be/x-ray sources and the RLOF systems. The result of the application was an allocation of four consecutive nights shared with a separate St Andrews program, together with one night of remote time for A 0535-66. The subsequent observations were hampered by poor weather, with the result that LMC X-4 was not successfully observed. The observations of SMC X-1 are described in Chapter 3. No observations of A 0538-66 were secured owing to rain on the desired night.

In the same round, time was also applied for on the Isaac Newton Telescope, studying three Be/x-ray systems with contentious periods or geometries: X Persei, BQ Cam and A0535+26. Two sets of ten to fourteen day runs were requested in bright time. Though this application was deemed unsuitable for scheduled PATT time, owing to the uncertain ephemerides of the systems, we were able to arrange long-term studies of these stars during twilight and on nights when other observations were impractical. Some of these data are discussed in Chapter 6.

In October 1990, 5 nights of AAT bright time were requested in order to study Cen X-3 and QV Nor. This application was rewarded with 5 nights in March 1990, the results of which are described in Chapters 4 and 5. Follow-up observations on

these two systems, together with new observations of 4U 1145-61, a system with a poorly determined spectroscopic orbit, were requested for the equivalent semester in 1991. The awarding committee felt that the observations of QV Nor obtained on the previous run were adequate, while the specific observations of Cen X-3 (at the times of maximum and minimum velocity) could be best obtained by means of several spectra taken in service time. Service time was therefore applied for through the usual channel, but was then deemed unsuitable for such a study by the AAO since the few service nights in a semester would only be decided upon at short notice. Nonetheless, we were able to arrange to have spectra taken at the beginning and end of two consecutive nights, during another observer's scheduled time. Unfortunately, the observations were not taken owing to instrumental problems. No further telescope time was requested, since there would have been insufficient time to include any new observations in this study.

1.7 References

Avni, Y., 1976. *Astrophys. J.*, **209**, 574.

Baade, D., 1987. *The Physics of Be stars, eds. A. Slettebak and T.P. Snow (Dordrecht: Reidel), p361.*

Chanan, G.A., Middleditch, J., Nelson, J.E., 1976. *Astrophys. J.*, **208**, 512.

Corbet, R.H.D, 1986. *The Evolution of Galactic X-Ray Binaries, ed. J. Trumper, W.H.G. Lewin, and W. Brinkman (Dordrecht: Reidel), p63.*

Corbet, R.H.D., Charles, P.A., van der Klis, M., 1986. *Astr. Astrophys.*, **162**, 117.

Eggleton, P.P., 1986. *The Evolution of Galactic X-Ray Binaries, eds. J. Trumper, W.H.G. Lewin, and W. Brinkman (Dordrecht: Reidel), p87.*

Giovanelli, F., Ziolkowski, J., 1990. Acta Astronmica, **40**, 95.

Harmanec, P., 1985. *The Physics of Be Stars, eds. A. Slettebak and T.P. Snow (Dordrecht: Reidel), p339.*

Hovaisky, S.A., 1985. *Interacting Binaries, eds P.P. Eggleton and J.E. Pringle (Dordrecht: Reidel), p205.*

Joss, P.C., Rappaport, S.A., 1984. *Ann. Rev. Astr. Astrophys.*, **22**, 537.

Mochnacki, S.W. , 1984. *Astrophys. J.*, **55**, 551.

Nagase, F., 1988. *Physics of Neutron Stars and Black Holes, ed. Y. Tanaka (Universal Acacdemy Press, Tokyo).*

Penrod, G.D., Vogt, S.S., 1985. *Astrophys. J.*, **299**, 653.

Plavec, M.J., 1985. *The Physics of Be stars, eds A. Slettebak and T.P. Snow (Dordrecht: Reidel).*

Preidhorsky, W.C., Holt, S.S., 1986. *Long Term Cycles in Cosmic X-Ray Sources (Space Science Preprint).*

Rappaport, S.A., Joss, P.C., 1983. *Accretion driven stellar x-ray sources, eds Lewin and van den Heuvel (Cambridge University Press).*

Ruusalepp, M., 1981. *Be stars, IAU symposium 98, eds M. Jaschek and H-G Groth (Dordrecht: Reidel).*

Savonije, G.J., 1980. *Astr. Astrophys.*, **81**, 25.

Slettebak, A., 1985. *The Physics of Be Stars, ed A. Slettebak and T.P. Snow (Dordrecht: Reidel).*

White, N.E., 1989. Astron Astrophysics Rev., **1**, 85.

van den Heuvel, E.P.J., 1983. *Accretion driven stellar x-ray sources, eds Lewin and van den Heuvel (Cambridge University Press).*

van Paradijs, J., 1983. *Accretion driven stellar x-ray sources, eds Lewin and van den Heuvel (Cambridge University Press).*

Chapter 2

Observations and Data Analysis

2.1 Introduction

This chapter concerns the details of observing, reducing and analysing the CCD and Reticon spectra which form the basis of this study. The following three chapters are based on observations taken with the 3.9m Anglo Australian Telescope at Siding Spring near Coonabarabran, New South Wales, on two separate observing runs. Chapter 3 is based on data acquired in October 1989, while Chapters 4 and 5 are based on data taken in March 1990. Chapter 6 is largely based on Reticon observations taken in St Andrews, using the 0.5m Leslie Rose Telescope and spectrograph, from February 1989 to March 1991, with supplementary observations taken with the 2.5m Isaac Newton Telescope on La Palma, on various service nights in 1990. Since these are all means of obtaining digitized spectra, the data reduction and analysis methodologies are very similar.

2.2 Observations

The HMXB studies published to date (see subsequent chapters for references) frequently relied on Balmer lines for radial velocity determination. In attempting to improve on this, spectral regions were selected which contained a number of good photospheric

lines, consistent with obtaining the best signal/noise ratio. At the intermediate dispersion used on both of the AAT runs, 33 Å mm^{-1}, the spectral coverage was in excess of 400 Å. For the first run, the spectral region chosen ran from $\lambda\lambda$ 4000 - 4400. After reducing and analysing those data, the decision was made to recentre the next blue observations on 4500 Å, in order to observe three good helium lines (see Chapter 5). The observations of QV Nor described in Chapter 4 were made in the red, covering $\lambda\lambda$ 6300 - 6700. Although this choice of region effectively gave only one measurable line, the extreme redness of the star prevailed against observations in the blue region, as previous workers had found.

Observations on the AAT were made using the ADAM and ADAMCCD data acquisition environments (the latter having now superceded the former). Flat-fields were obtained at all wavelength regions used, at the start and end of each night. Although this is not strictly necessary, since the aim of the flat-field is ultimately to give pixel to pixel variations in the detector, independent of the illuminating source, it was thought advisable to obtain them at every grating setting. Focussing of the spectrograph was performed in the early evening prior to the observing session.

Cu-Ar and Cu-Ne comparison lamps were used for the blue and red regions respectively, having ascertained that there would be sufficient lines in the red for calibration purposes. The arcs were taken before and after every spectrum taken, even if the telescope remained at a set coordinate during a series of integrations. The integration times for the various objects are discussed in their relevant chapters but were in the region of 10 - 20 minutes for the program stars. Radial velocity standard stars were also observed as a matter of course. For both runs, the mean of the O-S, (observed-minus-standard velocities) was within its own error margin of zero, thus leading us to conclude that the derived velocities from the target stars were on the IAU system. On both runs, a number of bright B-star secondary standards were also observed, to serve as possible cross-correlation templates.

The INT observations were performed in much the same manner, except that the spectra were taken at a wide variety of central wavelengths and dispersions, largely determined by other programs running concurrently on the same instrument. Not all the images were flat-fielded, owing to poor signal/noise in some of the flats. The derived

velocities have been assumed to lie on the standard system (see Chapter 6 for a full discussion).

The Reticon observations followed much the same logic; the "flat-field" in this case being a lamp which bathes the detector array without passing through any optics. A gross overall response must still be divided out of the flat to obtain the pixel variations (see next section). Typical exposure times were fifty minutes to an hour. The spectrograph has been shown to produce velocities on the IAU system (see Chapter 6, and references therein).

2.3 Reduction

2.3.1 Reduction of CCD frames

Reduction and analysis of all CCD images proceeded in the same manner. Much use was made of FIGARO (Shortridge, 1986), the STARLINK data reduction package. FIGARO routines were used to subtract bias counts, remove cosmic ray events from the CCD frames, obtain the pixel-to-pixel variation and divide this out of the image, subtract the sky background and finally extract out a one-dimensional spectrum. The use of the bias frame is not critical to spectroscopy, since one is not usually concerned with exact flux calibration, and any offset will be removed during the sky subraction.

The methodology of premliminary reduction of CCD frames has been discussed in the FIGARO manual. The flat-field is first summed spatially to give an overall spectral response along the chip. This response is a combination of the spectral distribution of the lamp and the colour sensitivity of the chip itself. The pixel-to-pixel variations are superimposed on this response, and to obtain them one needs to divide out the underlying response, either by employing a smoothing routine, or simply fitting a polynomial to the signal. This smoothed response can then be divided row by row out of the original flat-field frame, yielding a normalised "flat" image, the variation in which is entirely due to the individual quantum behaviour of each CCD pixel. It is this true flat-field which can then be divided out of each observational and comparison-source

frame.

Sky-subtraction consists simply of taking two strips of sky lying either side of the spectrum, such that their combined width in pixels equals the width of the spectrum. Of course, when the seeing is poor, the spectrum may spread out rather severely; in which case, the image should be extracted from the optimum part of the spectrum and the sky slices selected well away from the star. Sky subtraction is particularly important in the red, where night sky lines offer severe contamination around 6300 Å. The presence of spurious absorption or emission features in the reduced image would signal that the sky subtraction had been performed erroneously.

The extracted spectra each have a corresponding comparison-source frame, which may be selected from either of the two comparison-source spectra taken before and after the program image. The comparison-source is extracted spectrally, over a range of pixels chosen to match the region of the detector in which the spectrum lay. One then has a pair of one-dimensional spectra for every star. These images are then read into a SPICA one-dimensional memory file, consisting of alternating arc/star spectra. These may then be extracted into FITS format files using SPICON (Hill, 1983). SPICON creates pixel calibrated "S" and "F" format files, using a specific reference line in the comparison-source which has been manually identified by the user (typically some well-defined line near the middle of the spectrum). The referencing of this line then saves computation during the calibration stage, performed using the DAO software package REDUCE (Hill, Fisher and Poekert, 1982). Comparison-source spectrum measurement is facilitated by the use of a standard plate (Aitken, 1935), to predict the whereabouts of lines in the spectrum, on the basis of inputted spectrograph constants. The standard plate coefficients can be obtained using the program STDPLATE (Hill and Fischer, 1982). Alternatively they may be arrived at by the trial measurement of an comparison-source frame, using some guessed parameters, which will then lead to improved plate coefficients being printed out by REDUCE. The plate is deemed sufficiently accurate when the "predictor" is able to pick up all (or most) of the lines in the adopted line list. REDUCE then uses the plate coefficients to measure each comparison-source semi-automatically, outputting an comparison-source file which contains the linearization parameters, enabling the spectrum to be wavelength calibrated without effort. The residuals between the expected and the measured position of each

line are expressed by a low-order polynomial, with bad lines being discarded in the process. Helicentric corrections for all stellar spectra were computed using the program RVCORR (Bell). The outputted linearized "W' FITS files then need only to be rectified prior to measurement, producing normalised "R" files. The rectification process can unfortunately be highly subjective, particularly when the spectra are noisy and the continuum levels ill-defined. Manually selected sections of spectrum are used to produce an interpolated continuum file which may then be used to rectify a sequence of similar spectra, but if the spectra are noisy, or highly variable, one is consigned to the task of individually rectifying each. This step also enables one to edit out bad spectral features and interpolate between adjacent points (for instance, cosmic ray events not eliminated earlier may be pruned). The spectra may also be log-linearized to "U" files, although this step, taken to aid computation of the cross-correlation function, is now included automatically in the cross-correlation process.

2.3.2 Reticon frames

The reduction of the spectra obtained on the 0.5m Leslie Rose Telescope is simplified since the spectra begin life as 1-dimensional images. These need only be flat-fielded before reading into SPICA, and are subsequently treated in an exact manner as the CCD images. Some rebinning of the precalibrated frames is necessary if they are to be cross-correlated against AAT frames, since the CCF program is happier with spectra that share the same start and end points, as well as the same incremental steps between data points.

2.4 Analysis of spectra

The details of measuring, with regard to adopted windows and templates, is discussed individually in each of the relevent chapters. Extensive use has been made of the powerful cross-correlation process to obtain the velocity separations between program and template spectra. The program utilised was VCROSS (Hill, 1982), which can now handle ordinarily linearized spectra.

VCROSS takes two spectra, one of which is a carefully chosen "template" of known radial velocity. The other spectrum is then measured against this standard, in effect "slid along" until the best match spectrally has been obtained, visualised in terms of a peaked function centered on the offset velocity of the program star. Formally, the procedure is best discussed in the logarithmic domain.

If we define an independent parameter $x = \log \lambda$, then we have (Simkin, 1974), $x' - x = \log(\lambda'/\lambda) = 1/2 \log[(1-\beta)/(1+\beta)]$, where β is the ratio v/c. Thus, a linear shift in the logarithmic domain corresponds to a particular velocity, independent of λ.

If the observed spectrum is $s(x)$, the template spectrum $t(x)$, then the cross-correlation function (CCF) is, in an idealised sense:

$$C(z) \equiv \int_{-\infty}^{+\infty} s(x).t(x-z)\,dx \tag{2.1}$$

which will be a maximum when $t(x)$ has been shifted by z. For the actual data, the spectra are of course not continuous functions, but have been sampled regularly over N "pixels", such that, for the program star,

$$\sigma_s^2 = \sum s(x)^2/N \tag{2.2}$$

and similarly for the template, where σ is the rms error of the spectra (McLean, 1981). This then leads to the *normalised* CCF:

$$C(z) = \sum(s(x).t(x-z))/(N.\sigma_s.\sigma_t) \tag{2.3}$$

If $S(k)$ and $T(k)$ are then defined as the Fourier transforms (FT) of the two spectra, such that:

$$S(k) = \sum s(x).e^{[-2\pi ikx/N]} \tag{2.4}$$

And similarly for the template, the FT of $C(z)$ is then $C(k)$, such that:

$$C(k) = S(k).T^*(k)/(N.\sigma_s.\sigma_t) \tag{2.5}$$

The inverse transform is then:

$$C(z) = \sum S(k).T(-k)\,e^{[2\pi ikx/N]}/[N.\sigma_s.\sigma_t] \tag{2.6}$$

The procedure is therefore to compute the FTs of both spectra, take the conjugate of the program star, multiply them both together, then take the inverse transform of

the product. This inverse transform, once normalised, yields the measurable CCF. This peak can then be fitted by any theoretical function in order to best define its centroid. In this study, the peaks were always fitted by gaussians, although the choice of a parabola or lorentzian would not have made a great deal of difference.

In computing the CCF, one has the option of defining windows across the desired spectral regions, such that bad features do not contribute. For this study, such features would include Balmer and other unwanted lines, continuum, emission and interstellar features. No twin peaks were ever seen, since the secondary components (accretion disks, etc) contribute only a few per cent of the total brightness of the system.

The choice of best template can be something of an art form, and the various pros and cons are discussed where relevant in the subsequent chapters. In general, the window/template combination that gives the narrowest CCF is probably the best.

The derived velocities must now be used to obtain an orbital solution, and this is achieved using the program RVORBIT (Hill). Since eccentric orbit solutions were not considered likely, and since the period would in general be well known from x-ray observations, the adoption of the best sinusoidal fit was simply a matter of a least-squares solution being applied to the data. The time of maximum positive velocity, T_{+ve}, was usually put in as a free parameter, since the ephemerides of these objects are not particularly good. The details of this stage are discussed in the chapters themselves, as is the question of the intrinsic reality of the derived semi-amplitude: how closely does K_{opt} actually compare with the keplerian motion of the star? This is a complex area which has been approached tentatively in Chapters 3 and 4, on the basis of computed corrections for velocity distortion produced via the light curve synthesis/solution code LIGHT2 (Hill, 1989). Developed for the analysis of contact and detached "ordinary" binary systems, LIGHT2 has been used to model Roche distortions and ad hoc heating models. This is on a "better-than-nothing-at-all" basis, and the results must be treated with a degree of caution, since it is generally argued that a full treatment of x-ray heating is impossible without detailed non-LTE calculations (van Paradijs, 1983). We have therefore derived solutions with and without heating corrections, using the procedure for determining the masses outlined in Chapter 1.

2.5 References

Aitken, R.G., 1935. *The Binary Stars, (McGraw Hill, New York).*

Hill, G., 1982. Publs Dom. Astrophys. Obs, **16**, 67.

Hill, G., 1983. *Private Communication*

Hill, G., 1989. *Private Communication*

Hill, G., Fisher, W.A., 1982. Publs Dom. Astrophys. Obs, **16**, 159.

Hill, G., Fisher, W.A., Poeckert, R., 1982. Publs Dom. Astrophys. Obs, **16**, 27.

Mclean, B., 1981. *Phd Thesis, Univ. St Andrews*

van Paradijs, J., 1983. *Accretion driven stellar x-ray sources, eds Lewin and van den Heuvel (Cambridge University Press)*

Shortridge, K., 1986. *Figaro Users Manual, Starlink project*

Chapter 3

A spectroscopic study of SMC X-1

3.1 The status of SMC X-1

SMC X-1 is the pulsating, eclipsing x-ray source associated with the B0 supergiant Sk 160 (Sanduleak 1968). It is believed to be located in the nearside of the Small Magellanic Cloud (SMC), although its distance is not particularly well-determined for a cloud object, owing to an apparent discrepancy between the probable distance of the primary and the calculated x-ray accretion rate, which is nearly an order of magnitude in excess of the theoretical Eddington limit for the pulsar (Howarth 1982). Because optical and x-ray eclipses have been observed, the system geometry and component masses can be elucidated by combining pulse-timing, spectroscopy and eclipse-duration data. Primini and Rappaport (1977) published orbital parameters of the x-ray star derived from analysis of pulse arrival times, showing that the orbit was highly circularised, with $e \leq 0.0016$, and $K_X = 301.5 \pm 4$ kms^{-1}, with a $P_{orb} = 3.892$ day and $P_{pulse} = 0.72$ s.

Early evidence for an accretion disk came from van Paradijs and Zuiderwijk (1977), showing that ellipsoidal light variations and x-ray heating effects were insufficient to account for the observed light curve. The minimum at photometric phase 0.5, although filled in by x-ray heating, is deeper than expected, indicating that the

x-ray object is associated with an occulting source. This source must also contribute an additional source of optical flux between phases 0.1-0.15, and 0.85-0.9, generally ascribed to reprocessing of x-rays by the disk. SMC X-1 is therefore of the same family of systems as LMC X-4 and CEN X-3, where the accretion disks are powered by Roche lobe overflow from an early supergiant primary. As in the case of LMC X-4, there is evidence for disk precession, ie modulation in the x-ray luminosity over superorbital timescales of months, however there is disagreement concerning the presence or otherwise of any such modulation in the optical light curve (Khruzhina and Cherepashchuk, 1983 versus van Paradijs and Kuiper, 1984).

Early workers (Hutchings et al, 1977, hereafter HCCO) found no evidence for a stellar wind in the optical spectrum of the star, concluding that this was consistent with the presence of a disk. This is not now believed to be the case, with UV studies showing the presence of weak winds in the fainter SMC stars (Hammerschlag-Hensberg et al, 1984 and references therein) including Sk 160, the weakness possibly due to depletion of wind-driving trace elements in the SMC (Hutchings, 1982). The weakness of the wind suggests that the x-ray object is powered predominantly by accretion from Roche lobe overflow.

Previous to our study, there had been only two attempts to derive optical orbital elements for this system (HCCO, and references therein), based upon image-tube photographic spectroscopy at a dispersion of 26 Å mm^{-1}; these factors, together with velocities determined by measurement of individual absorption lines (which are broadened due to rotation), combine to result in substantial errors for the orbital parameters.

3.2 Observations and Reduction

20 spectra of SMC X-1 were obtained between 10-13 October 1989 by Graham Hill and the author, using the RGO spectrograph on the AAT in conjunction with the 25 cm camera and the 1200B grating, with the GEC CCD detector. The spectral range chosen covered 3990-4410 Å, with a dispersion of 33 Å mm^{-1}, giving a wavelength on pixel of 0.7 Å. Exposure times were 1200 seconds. The point-to-point scatter in measured velocities over one night is fairly representative of the observing conditions

experienced; by far the best session was the night of 6/7 October, night 3, and the final night was the worst. Typical s/n was 20-30. Reduction and measurement were carried out in standard fashion, using FIGARO routines (Shortridge 1986) to perform bias-subtraction, flat-fielding and cosmic-ray removal of the raw CCD images. Spectra were then extracted in 1D format and processed with the DAO programs REDUCE and VCROSS.

A variety of cross-correlation templates were tested, including co-added spectra of SMC X-1 and co-added B-star spectra obtained on the same observing run. Gaussian profiles were fitted to the CCFs generated in VCROSS, utilising the top 33 % of the profile.

The most successful templates were derived from RETICON observations of B-stars taken on the Leslie Rose 0.5 metre telescope at St Andrews, rebinned to match the lower resolution of the AAT data. A B3 V star, HR1174, gave the least scatter in the velocity measurements, although its spectral and luminosity class were in principle less well suited to the program star than a B1 I star also used as a comparison. Although SMC X-1 is an early B supergiant, its lines are broadened by rotational velocity in excess of 200 km s^{-1}, meaning that a sharp-lined early template will have less spectral similarity than a broad-lined dwarf star of later spectral class. Poor s/n spectra were discarded prior to measurement, as were measured velocity points more than 2 σ from the computed solution.

The adopted orbital solution was based upon a cross-correlation window using the entire spectral region from 4000 Åto 4395 Å, which is free from interstellar absorption bands. Some caution has to be applied here, for the Balmer lines can be unreliable velocity indicators in the high-mass x-ray binaries, since cool, H-rich gas-streaming between the primary and secondary can distort the profiles of the photospheric H lines. However, owing to the low quality of some of the spectra, and the proximity of the HeI lines to the end regions of the spectra, it was deemed necessary to include as much spectral information in the cross-correlation window as possible, particularly as the expected velocity amplitudes were not much greater than the intrinsic measurement errors. Lines near the ends of a λ calibrated spectrum are liable to give spurious velocity values due to the difficulty of constraining the dispersion polynomial at the

red and blue extremes of the arc, and should be treated with caution; hence the choice of window. The velocities are shown in Table 1.

The parameters derived from the uncorrected velocities (assuming no non-Keplerian distortions) are shown in Table 2.

Based on the x-ray data of Primini and Rappaport (1977), $K_x = 301.5 \pm 4\,\mathrm{km\,s^{-1}}$, therefore $q = 13.1 \pm 1.1$. This leads to $f(m) = 0.0049 \pm 0.0013\,M_\odot$. The above authors give the eclipse duration as $\pm\,28°$. Assuming that the primary component fills its Roche lobe completely (which is reasonable from the existence of the disk), $i = 65°$. However, the classical Roche surfaces do not take into account the heating effect of the secondary, which may mean that the stellar surface slightly underfills the Roche lobe. This would lead to an upward revision of i, however, for the purposes of this solution no such effect is assumed. The derived masses are discussed in Section 3. The time of maximum positive velocity occurs 0.04 days sooner than would be expected from the epheremis derived from the data of HCCO and the period of van Paradijs quoted therein, a shift which can be explained in terms of the uncertainties in the original parameters rather than a secular period change.

A CCF window using solely the HeI lines at 4026 Åand 4388 Åresulted in a much increased velocity scatter when compared with the orbital solutions derived from the entire-spectrum window. K_{opt} was found to be $19 \pm 5\,\mathrm{km\,s^{-1}}$, less than the value derived from the previous solution.

An apparent shift in the systemic velocity was observed between the solutions. The V from the window including the Balmer lines was $172.7 \pm 1.5\,\mathrm{km\,s^{-1}}$, which is consistent with the average velocity of the SMC, while that derived from the HeI lines alone was $180 \pm 4\,\mathrm{km\,s^{-1}}$, in agreement with the adopted value of $180\,\mathrm{km\,s^{-1}}$ of HCCO. There is no independent means of determining the systemic velocity of the secondary in these systems from x-ray timing alone, since there is no "standard clock" present. Measurements of the HeII 4686 Åline by HCCO showed an antiphased velocity amplitude lower than the expected semi-amplitude of the degenerate object, probably indicative of a "hot spot" associated with the impact point between the gas-stream and the hypothetical accretion disk. HCCO reported a value for the systemic velocity

Table 3.1: Radial velocity data for SMC X-1

H.J.D	Phasing	Observed Velocity	O-C Residuals
2447000+	T_{+ve}	$Km\,s^{-1}$	$Km\,s^{-1}$
811.89134	0.001	205.38	+9.7
811.92386	0.009	192.88	-2.7
811.94101	0.013	194.81	-0.8
811.95706	0.018	193.48	-2.0
812.04605	0.040	196.88	+2.0
812.88971	0.257	171.22	-0.4
812.94991	0.273	163.71	-5.7
813.88337	0.512	148.88	-0.9
813.89096	0.514	153.49	+3.7
813.92695	0.524	154.10	+4.1
813.96152	0.532	149.17	-1.0
813.99582	0.541	151.49	+1.0
814.87925	0.768	165.71	-9.6
814.88791	0.770	169.68	-6.0
814.96981	0.792	193.98	+15.0
814.98028	0.794	175.97	-3.0
815.05700	0.814	173.61	-8.1
815.07120	0.818	186.51	+4.4

Table 3.2: Orbital Parameters for SMC X-1

V_{opt}	172.7 ± 1.5 km s^{-1}
K_{opt}	23.0 ± 1.9 km s^{-1}
e	0.000†
Ω	0.000†
P_{orb}	3.892380†
T_{+ve}	43067.0776 ± 0.0613

† — adopted value

of the HeII line which was lower than that for the photospheric lines, ie blueshifted, which could be ascribed to a redshifted absorption profile arising in the cool gas-stream, although the observed profile did not apparently support this conjecture. Our spectral range unfortunately does not extend to this line.

Because the solution derived from the HeI lines gave a smaller semi-amplitude, gas-stream distortion of the Balmer lines seems unlikely, as gas-streaming is generally supposed to suppress orbital variations. All subsequent results derived from velocities are therefore based on the full-spectrum measurements.

3.3 Corrections for x-ray heating

3.3.1 Modelling the situation in SMC X-1

As is well known, the proximity of the two stars in any close binary will lead to a pronounced "reflection effect", the result of which is to suppress the observed velocity amplitudes away from the Keplerian orbits. It is difficult to correct for the effect in an x-ray system since there is no clear way of determining the true isotropy of the x-ray emission, other than assuming that the neutron star must not greatly exceed its Eddington limit. The problem is compounded by the generally poor distance estimates available. Conversely, if the x-ray source is sufficiently soft, the effect will be to cause the formation of partially filled in absorption or even emission lines in the heated area

of the photosphere (Milgrom, 1977), even if the ratio of optical to x-ray luminosity is large. If the assumpton is made that the continuum strength is unaffected, the lines in emission will shift the average line centre integrated over the entire stellar disk, such that the velocity amplitude is exaggerated. This assumption is valid only for soft x-ray fluxes, which do not penetrate down to the the continuum forming layers. SMC X-1 is a hard x-ray source, which means that the x-rays will be absorbed deep in the atmosphere or directly reflected as outgoing x-rays (Basko et al, 1974). The strength of the continuum in the heated region will therefore be important, and one would not expect to see a pronounced velocity gradient with line wavelength, due to the relative isotropy of the heating (in contrast to some of the other systems modelled by Milgrom and co-workers). While the presence of a soft component cannot be ruled out, it seems likely that the hard flux will outweigh its effects in line forming regions.

In addition, the presence of the accretion disk has important consequences, since the optically thick disk will not only cast an x-ray shadow on the inner lobe of the primary, but will also act as a source of optical radiation reprocessed from x-rays. Therefore, estimates of the localised heating effect on the primary are subject to uncertainty.

Models were run utilising LIGHT2 (Hill), a sophisticated light curve synthesis program, developed for generating and solving the light curves of all types of binary system but without the inclusion of accretion disks. The program generates velocity corrections in two ways; by averaging a velocity based on contributions from elements of the disk, each element weighted according to the flux at that point, or by calculating theoretical gaussian or lorentzian profiles and giving the velocity correction corresponding to a specific measurement on that profile. Depending on the form of the heating effect, these corrections may not have the same sign, let alone the same magnitude. In this study, however, the corrections were basically of the same order, with the flux-weighted velocities showing a slight ($\approx$ 2 km s^{-1} at most) increase in size over the adopted gaussian profiles, based on the lower 33 % of the line (appropriate, since CCF measurements were of this portion of the profile).

Due to natural limitations of the code, it was impossible to represent accurately the dimensions of the neutron star, and a range of models was run selecting the radius

and polar temperature of the secondary to produce the required (calculated) luminosity of 6×10^{38} erg s^{-1}, for an x-ray source at the distance of the SMC (Corbet 1984), assuming a simplistic black-body model. However, the duty cycle of the RLOF systems is large, > 50% (Joss and Rappaport, 1984), implying that the radiation is strongly collimated. For SMC X-1, Joss and Rappaport show a variation of 50 % over one pulse in the 2-6 KeV region, where most of the x-ray power is emitted. Taking the x-ray spectrum shown by White et al (1983), approximate linearity is seen between the log(photons/cm^2-sec) and the energy in KeV, between 2-30 KeV. However, the x-ray spectrum is averaged over one pulse cycle, and so represents a biased estimate in terms of the luminosity between pulses, which is the required parameter for evaluating the heating effect. Furthermore, Cen X-3 and SMC X-1 are notable among the pulsars in that there are no significant energy dependent variations in the pulse-phase profile except at low energies (White et al, 1983), where the interpulse is weakly visible. The possibility exists therefore that the x-ray luminosity as seen by the star may be lower, perhaps nearer 4×10^{38} erg s^{-1}.

3.3.2 The calculations in detail

No attempt has been made to model the eclipse or x-ray flux reprocessing effects of the accretion disk, and hence obscurations of the limbs of the B-star near primary eclipse are not included properly in the calculation of the profile distortion, since the modelled secondary occults only a very small fraction of the primary's stellar disk, at most $\approx$ 0.7 %.

The program generates corrections to be applied to the observed velocities based on assumed values of q and K for one of the components, assuming that Roche geometry applies and that the stars corotate. The process is clearly iterative, since q is dependent on the solution of the velocity curve, and the corrected velocities will necessarily revise the system parameters, meaning that the calculated heating effect is not strictly consistent with the solution at any one stage in the iteration. However this discrepancy rapidly becomes very small, in this case becoming negligible after only two steps.

As expected, the correction leads to a revised value of K_{opt} which is larger than

the initial estimate. Furthermore, as the initial estimate of L_x is highly conjectural, small additional innaccuracies in the model are probably not relevant. For spherical accretion, the Eddington limit is $\approx 10^{38}$ erg s^{-1}, requiring the system to lie *closer* than is reasonable from a study of the properties of the B-star (Howarth 1982). There is, therefore, either some error in the calculated L_x, or a shortcoming in the modelled accretion process. However, with the assumption of a black-body secondary, an uncertainty in the luminosity of a factor of ≈ 6 scales the T_{polar} of the "neutron star" by ≈ 1.5, meaning that the calculated heating effect will be similar for a range of x-ray brightnesses. The adopted "bright" luminosity was 6×10^{38} erg s^{-1}, compared to the conjectured figure of 4×10^{38} erg s^{-1}. If the lower figure was in fact correct, the adopted temperatures would be too high by a factor of ≈ 1.1. To investigate the sensitivity of the results to the choice of L_x, four calculations were made. The primary star's polar temperature was fixed at 25000 K for each calculation (Howarth, 1982, and references therein), although the real temperature may deviate from this value by a few thousand kelvin, owing to the difficulty of spectral classification.

In the "bright" calculation, T_{polar} was fixed initially at 98282 K for a radius = 0.05 the component separation, A, based on $A_x \sin i = 53.46$ lt-secs, with i taken to be 65° (and fixed at this value for the entire calculation, ignoring the very weak dependence of i on q, and $q = 13.10$, from $K_{opt} = 23.0$ km s^{-1} and $K_x = 301.5$ km s^{-1}. The corrected velocities were used to re-solve the orbit, leading to a revised $K_{opt} = 27.6 \pm 1.9$ km s^{-1}, with a small change in V_{opt} to 173.1 ± 1.6 km s^{-1}. This then led to $q = 10.92$, requiring that the temperature of the secondary be rescaled to 97518, for the same radius of 0.05 A. This model led to corrections which gave an orbital solution with $K_{opt} = 27.1 \pm 2$ km s^{-1}, $V_{opt} = 173.2 \pm 1.6$ km s^{-1}, $q = 11.11$. This solution, with the temperature rescaled to 97286, then produced $K_{opt} = 27.5 \pm 1.9$ km s^{-1}, $V_{opt} = 173.0 \pm 1.5$ km s^{-1}, $q = 10.97$. The phasing for individual data points was fixed at the phase values given by the original solution, and not the phasing given by the iterative solutions in the above calculations, which in any case do not differ by more than about $\pm$ 0.05 at worst.

In the "dim" calculation, with $L_x = 4 \times 10^{38}$ erg s^{-1}, the procedure was the same as above, with the temperatures scaled accordingly. For $q = 13.10$, T_{polar} was initially 88740 K. This generated corrections which led to a revised $K_{opt} = 26.3 \pm 1.9$ km s^{-1}, with $V_{opt} = 173.1 \pm 1.6$ km s^{-1}, giving a q of 11.47. For this mass ratio, the temperature

had to be scaled to 88294 K. This then led to velocity corrections giving K_{opt} = 26.7 km s^{-1}, V_{opt} = 172.9 km s^{-1}, leading to q = 11.29. With this q, the temperature was rescaled to 88294 and the velocity corrections recomputed. These then generated K_{opt} = 26.5 ± 1.9 km s^{-1}, V_{opt} = 172.9 ± 1.5 km s^{-1}, q = 11.36, ie a satifactorily converged solution.

In the "superbright" calculation, with $L_x = 8 \times 10^{38}$ erg s^{-1}, the same procedure was followed, with the temperatures scaled accordingly. For q = 13.10, T_{polar} was initially 105530 K. This generated corrections which led to a revised K_{opt} = 28.5 ± 2.0 km s^{-1}, with V_{opt} = 173.1 ± 1.6 km s^{-1}, giving a q of 10.57. For this mass ratio, the temperature had to be scaled to 104646 K. This produced velocity corrections giving K_{opt} = 28.5 km s^{-1}, V_{opt} = 173.1 km s^{-1}, leading to q = 10.58. With this q, the temperature was rescaled to 104648 and the velocity corrections recomputed. These then generated K_{opt} = 28.5 ± 2.0 km s^{-1}, V_{opt} = 173.1 ± 1.6 km s^{-1}, q = 10.58, *ie* a satisfactorily converged solution after only one iteration.

A fourth calculation was run with essentially no heating, generating velocity corrections based purely on the changing profile of the B-star. Beginning with q = 13.10, the corrected velocities gave K_{opt} = 24.9 km s^{-1}, V_{opt} = 173.0 km s^{-1}, leading to q = 12.12. This then changed the model parameters such that K_{opt} became 24.8 km s^{-1}, V_{opt} became 172.9 km s^{-1}, giving q = 12.15. No further iterations were run; the principle point of this calculation being to investigate the temperature distribution on the unheated star.

As expected, the substantial difference in adopted luminosities has only a small effect on the final orbit, although the corrections themselves are significant. The mass ratios vary from 10.58 to 11.36, around a geometric mean of 10.97, which is the same as the "bright" mass ratio. The intrinsic error in each estimate of q is ≈ 1.1, due to the uncertainty in K_{opt}, which means that the *total* range of values of q, assuming L_x = (6.0 ± 2.0) × 10^{38} erg s^{-1}, is 11.0 ± 1.5.

The derived corrections from the three calculations are shown in Table 3.

The adopted velocities, residuals and derived orbital parameters are shown in

Table 3.3: Corrected velocities

Phasing	Observed Velocity	Correction †	Correction	Correction
$\Phi_0 = T_{+ve}$	$Km\,s^{-1}$	$Km\,s^{-1}$	$Km\,s^{-1}$	$Km\,s^{-1}$
		$L_x = 6.0^{\ddagger}$	$L_x = 8.0^{\ddagger}$	$L_x = 4.0^{\ddagger}$
0.001	205.38	-5.00	-6.29	-3.74
0.009	192.88	-5.31	-6.78	-4.12
0.013	194.81	-5.45	-7.00	-4.18
0.018	193.48	-5.62	-7.26	-4.22
0.040	196.88	-6.41	-8.43	-4.34
0.257	171.22	+0.52	+0.83	+0.07
0.273	163.71	+1.67	+2.68	+0.26
0.512	148.88	+4.13	+4.78	+3.57
0.514	153.49	+4.00	+4.91	+3.48
0.524	154.10	+3.65	+4.13	+3.25
0.532	149.17	+3.40	+3.80	+2.94
0.541	151.49	+3.14	+3.46	+2.78
0.768	165.71	-0.10	-0.10	+0.00
0.770	169.68	+0.00	+0.00	-0.01
0.792	193.98	-0.16	-0.17	-0.16
0.794	175.97	-0.18	-0.19	-0.18
0.814	173.61	-0.44	-0.39	-0.36
0.818	186.51	-0.48	-0.50	-0.40

† = adopted correction (subtracted from raw data)

‡ : $1.0 = 1 \times 10^{38}$ erg s^{-1}

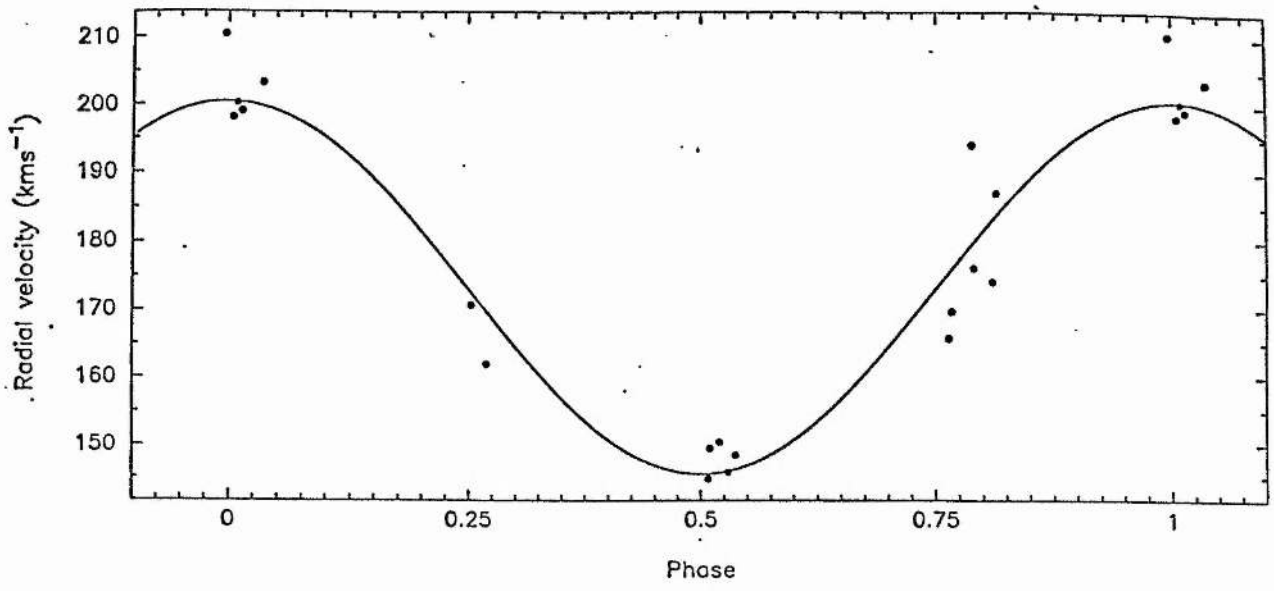

Figure 3.1: The velocity curve of SMC X-1, corrected for x-ray heating

table 4 and table 5. Figure 1 displays the velocity curve for the revised data.

3.4 Masses of the component stars

From the uncorrected data, $f(m) = 0.0049 \pm 0.0013\ M_\odot$. Based on $q = 10.97$, we have $f(m) = 0.0084 \pm 0.0017\ M_\odot$. The variation in q has the small effect of increasing i to 66.3°, from 65°. Based on these two sets of conditions, the following component masses are yielded. For $q = 13.1$, $M_x = 1.3 \pm 0.1\ M_\odot$, $M_{opt} = 17.2 \pm 0.6\ M_\odot$. For $q = 10.97$, $M_x = 1.6 \pm 0.1\ M_\odot$, $M_{opt} = 17.2 \pm 0.6\ M_\odot$. HCCO found $M_{opt} = 16.2 \pm 1.4\ M_\odot$, $M_x = 1.02 \pm 0.20\ M_\odot$. Therefore the estimates from this study consistently yield higher masses for both stars. The primary is still found to be undermassive for its spectral and luminosity class, which is characteristic of these systems. Within the quoted errors of HCCO, there is only a small discrepancy between the primary masses, although the secondary's mass estimates lie well outside their error margin. The adoption of a higher mass will naturally raise the Eddington limit, although the problem of the grossly super-Eddington luminosity is not avoided (see below).

Table 3.4: Corrected velocity data for SMC X-1

H.J.D	Phasing	Corrected velocity	O-C Residuals
2447000+	T_{+ve}	Km s^{-1}	Km s^{-1}
811.89134	0.997	210.4	+9.9
811.92386	0.005	198.2	-2.2
811.94101	0.009	200.3	-0.1
811.95706	0.014	199.1	-1.2
812.04605	0.036	203.3	+3.6
812.88971	0.253	170.7	-1.7
812.94991	0.269	162.0	-7.7
813.88337	0.508	144.8	-0.8
813.89096	0.510	149.5	+3.9
813.92695	0.520	150.4	+4.8
813.96152	0.529	145.8	-0.2
813.99582	0.537	148.4	+2.1
814.87925	0.764	165.8	-9.6
814.88791	0.767	169.7	-6.1
814.96981	0.788	194.1	+14.8
814.98028	0.790	176.1	-3.7
815.05700	0.810	174.1	-9.0
815.07120	0.814	187.0	+3.3

Table 3.5: Corrected Orbital Parameters for SMC X-1

V_{opt}	173.0 ± 1.5 km s^{-1}
K_{opt}	27.5 ± 1.9 km s^{-1}
e	0.000†
Ω	0.000†
P_{orb}	3.892380†
T_{+ve}	43067.1069 ± 0.0504

† — adopted value

3.5 Line variations in the spectrum of SMC X-1

Selected line measurements were made on rectified spectrograms of SMC X-1 through the observed phases. The line measurements were made by fitting gaussian profiles based on continuum, half-line depth and line centre cursor settings. The adopted gaussian parameters were found to be largely independent of small changes in the cursor placements. Since the spectra are not flux calibrated, this is not spectrophotometry, but obviously there will be no systematic errors in the EW measurements. Some widths and depths are displayed in Tables 6, 7 and 8.

3.5.1 Changes through phase

When plotted against phase, no significant phase dependency is observed in the H_δ widths, although there would appear to be some dependency in the H_γ measurements (see Figure 2). The corresponding Balmer depths are shown in Figure 3, and show a clear maximum line strength during the eclipse of the primary star.

By contrast, the HeI depths (Figure 4) show a convincing minimum through photometric phase 0.5 - 0.75. This is somewhat difficult to account for unless the temperature of the inner hemisphere (ignoring heating) lies between 10-25,000K; the H lines will be stronger, since Balmer line strength is a maximum at A0, whereas HeI reaches a maximum at B2, and will therefore be weaker so long as the effective

Table 3.6: Individual Balmer line measurements for SMC X-1

H.J.D	Phasing	H_γ EW	H_γ depths	H_δ EW	H_δ depths
2447000+	T_{+ve}	Å		Å	
811.89134	0.993	1.266	0.253	1.830	0.265
811.92386	0.001	1.543	0.286	1.648	0.258
811.94101	0.006	1.554	0.255	1.606	0.261
811.95706	0.010	1.614	0.261	1.741	0.252
812.04605	0.033	1.496	0.259	1.653	0.262
812.88971	0.250	1.721	0.314	1.622	0.293
812.94991	0.265	1.611	0.349	1.671	0.313
813.88337	0.505	1.419	0.276	1.527	0.249
813.89096	0.507	1.506	0.280	1.652	0.282
813.92695	0.516	1.497	0.294	1.482	0.257
813.96152	0.525	1.273	0.274	1.698	0.268
813.99582	0.534	1.479	0.255	1.527	0.251
814.87925	0.761	1.371	0.233	1.558	0.240
814.88791	0.763	1.230	0.261	1.440	0.268
814.96981	0.784	1.099	0.263	1.534	0.217
814.98028	0.787	1.220	0.248	1.361	0.277
815.05700	0.806	1.388	0.228	1.810	0.301
815.07120	0.810	1.315	0.238	1.560	0.255

Table 3.7: HeI line measurements for SMC X-1

H.J.D	Phasing	HeI 4026 EW	HeI 4026 depths
2447000+	T_{+ve}	Å	
811.89134	0.993	0.786	0.195
811.92386	0.001	0.774	0.175
811.94101	0.006	0.860	0.193
811.95706	0.010	0.681	0.166
812.04605	0.033	0.614	0.171
812.88971	0.250	0.300	0.158
812.94991	0.265	0.630	0.151
813.88337	0.505	0.722	0.160
813.89096	0.507	0.616	0.171
813.92695	0.516	0.550	0.166
813.96152	0.525	0.580	0.165
813.99582	0.534	0.615	0.163
814.87925	0.761	0.730	0.181
814.88791	0.763	0.695	0.199
814.96981	0.784	0.588	0.157
814.98028	0.787	0.609	0.170
815.05700	0.806	0.712	0.181
815.07120	0.810	0.613	0.149

Table 3.8: SiIV line measurements for SMC X-1

H.J.D	Phasing	SiIV 4089 EW	SiIV 4089 depths
2447000+	T_{+ve}	Å	
811.89134	0.993	0.589	0.130
811.92386	0.001	0.325	0.115
811.94101	0.006	0.369	0.089
811.95706	0.010	0.339	0.079
812.04605	0.033	—	—
812.88971	0.250	—	—
812.94991	0.265	0.272	0.078
813.88337	0.505	0.361	0.101
813.89096	0.507	0.627	0.123
813.92695	0.516	0.338	0.107
813.96152	0.525	0.291	0.115
813.99582	0.534	0.271	0.108
814.87925	0.761	—	—
814.88791	0.763	0.731	0.173
814.96981	0.784	0.165	0.116
814.98028	0.787	0.238	0.120
815.05700	0.806	0.428	0.185
815.07120	0.810	—	—

temperature of the rest of the star is hotter than for a B2, which is almost certainly the case. This places constraints on the strength of the heating effect, since even for the low x-ray luminosity case considered in the velocity-correction models, the temperature on the inner hemisphere is never less than 23000 K. By contrast, if there was no contribution from the secondary at all, the temperature of the substellar point gets down to 8700 K. However it is already known that the minimum when the x-ray source is transitting the star is shallower than when it is in eclipse, opposite to what would be expected from purely ellipsoidal variations. This therefore seems to favour the "dim" x-ray case over the unheated model. The "bright" case looks less favourable again, as the heating effect prevents any part of the inner hemisphere being cooler than 23700 K, with the substellar point hotter than the polar temperature. Note that these constraints do not infer the true luminosity of the x-ray source, merely the extent of the heating influence. They do however constrain the validity of the velocity corrections, and hence the mass ratios, although the masses derived in the previous section are based on the canonical "bright" value. It should be stressed that the spectrograms on which these minima and maxima are observed were not taken on the best night.

An apparent minimum is seen in the HeI EW (Figure 5) measurements at photometric phase 0.5, with the measurements at other phases showing no clear variation. This minimum may not be real due to the apparent presence of a cosmic ray near (or in) the HeI line in the spectrogram showing the smallest EW. The SiIV line at 4089 Å was also measured, where possible, although noise and the proximity of the H_δ line made it difficult to establish the continuum height in some of the spectrograms. Compared with the depths plotted by HCCO, the line is certainly stronger on average than it was in the seventies, although still inconsistent with the adopted spectral/luminosity class of the star. Based on the observational data tabulated by Kamp (1978), the average EW found for the silicon line, 0.381 Å, is more in line with a B0 IV-V than a supergiant. Unfortunately, it was on this line that the above author's model gave the severest discrepancy between predicted and observed T_{eff} versus EW, so nothing can be said concerning the temperature of the star. It is noted that there are no clear phase changes in either the EWs or the depths. A possible maximum depth during x-ray transit is based on only one spectrogram and so neither confirms nor disproves the observation of a maximum at this phase seen by HCCO. If real, this would still be difficult to interpret

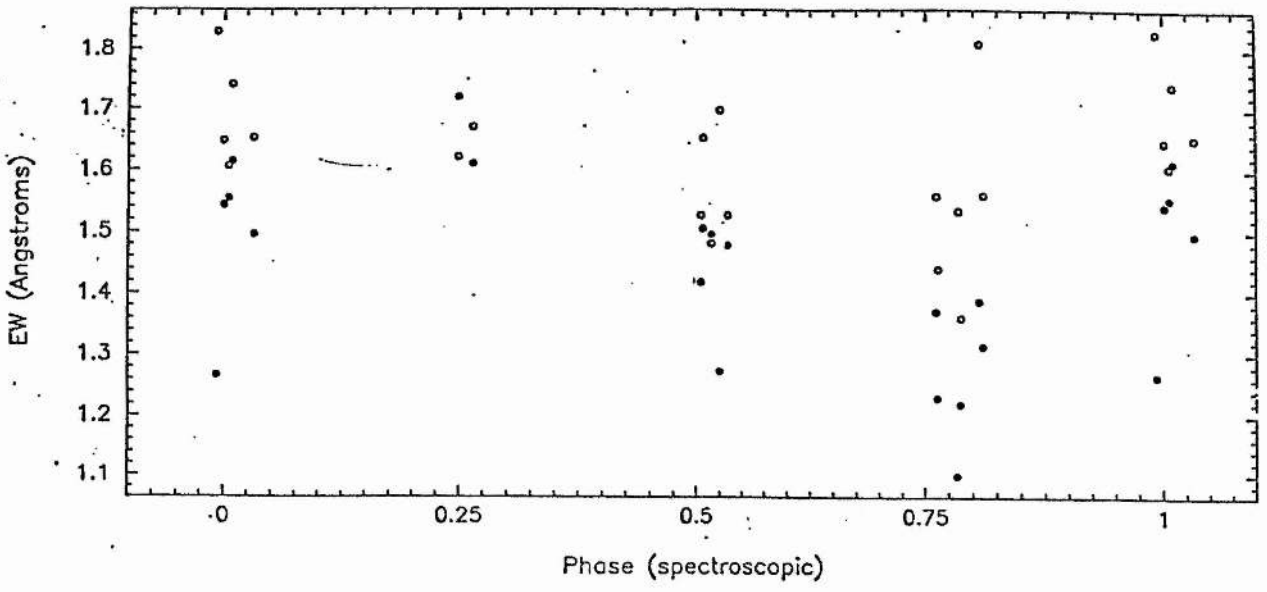

Figure 3.2: H_γ (dots) and H_δ (circles) EW measurements

on the basis of Kamp's data, since the peak in supergiant EWs is poorly defined, the observed stars having been binned into spectral classes, and may lie on either side of B0. The model atmospheres of Erhorn et al (1984) predict SiIV reaching a maximum at T_{eff} greater than 30000, irrespective of the presence of line-blanketing in their models.

These measurements are displayed in Figure 6 and Figure 7.

3.5.2 Rotational velocity measurements

The line profile measurements of the HeI 4026 Åline yield full-width half-maximum (FWHM) esimates from which V sin i may be calculated, on the basis of an established calibration. At the time of this study, no calibration was available for this line, but FWHM measurements of the HeI 4471 Åline by Hill (private communication) yielded a good correlation against the published V sin i values of Slettebak et al (1975). This relationship is displayed in Figure 3.8 . If this correlation is assumed to hold for the line measured in SMC X-1, for which gaussian profiles were used, the mean FWHM of 3.6 implies a V sin i less than 150 km s^{-1}.

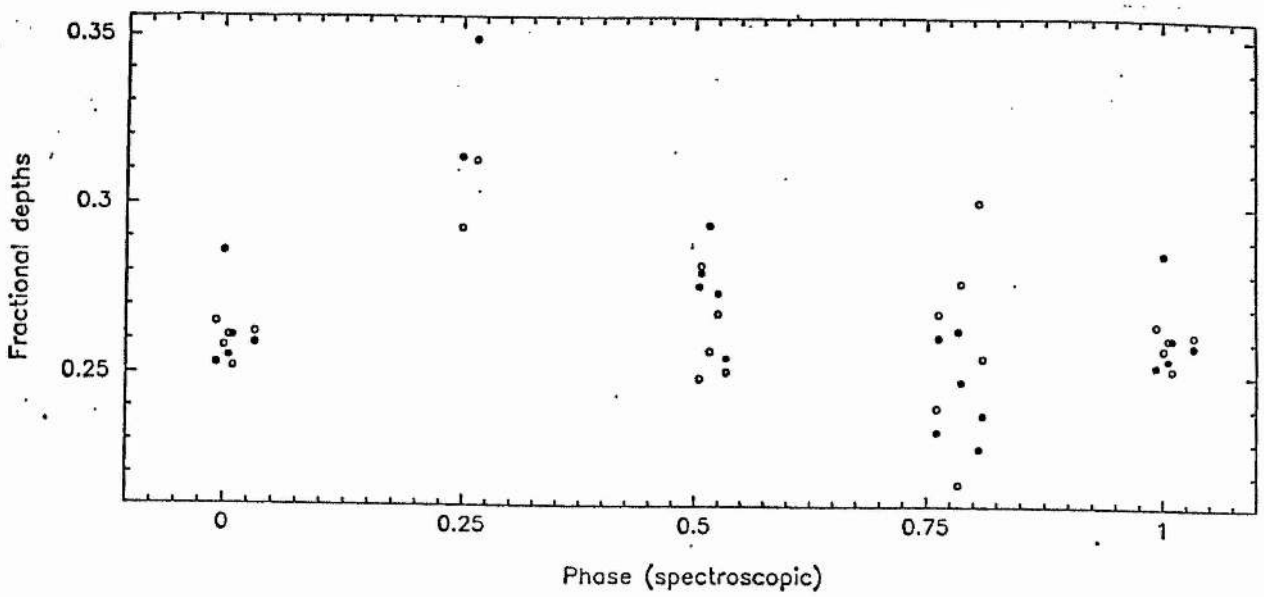

Figure 3.3: H_γ (dots) and H_δ (circles) depth measurements

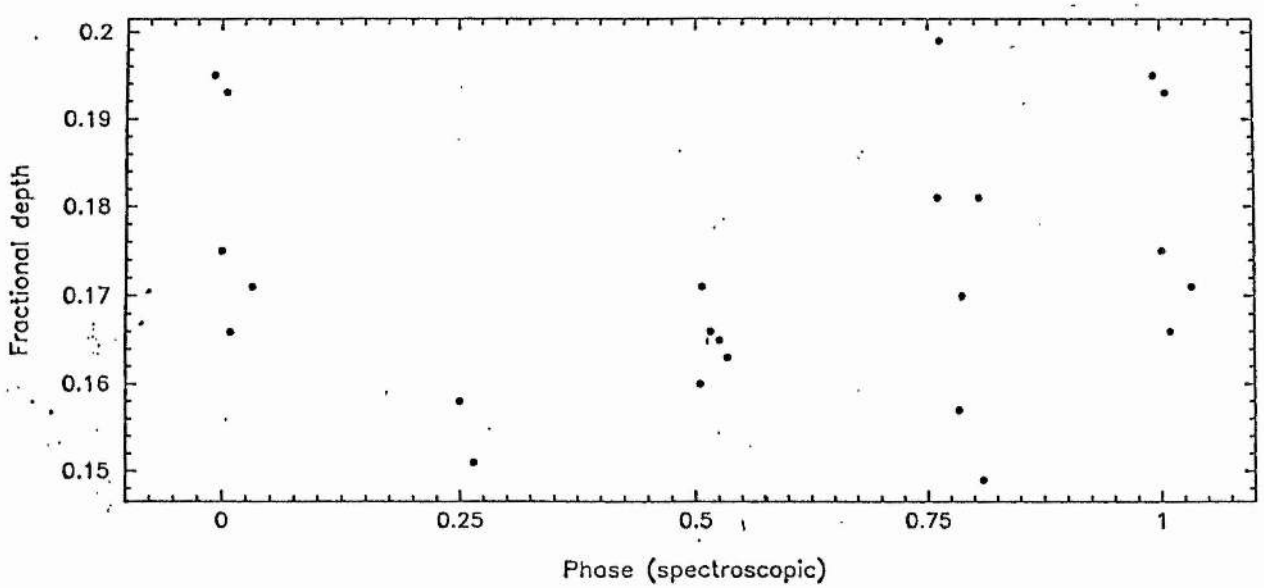

Figure 3.4: HeI 4026 Å line depth measurements

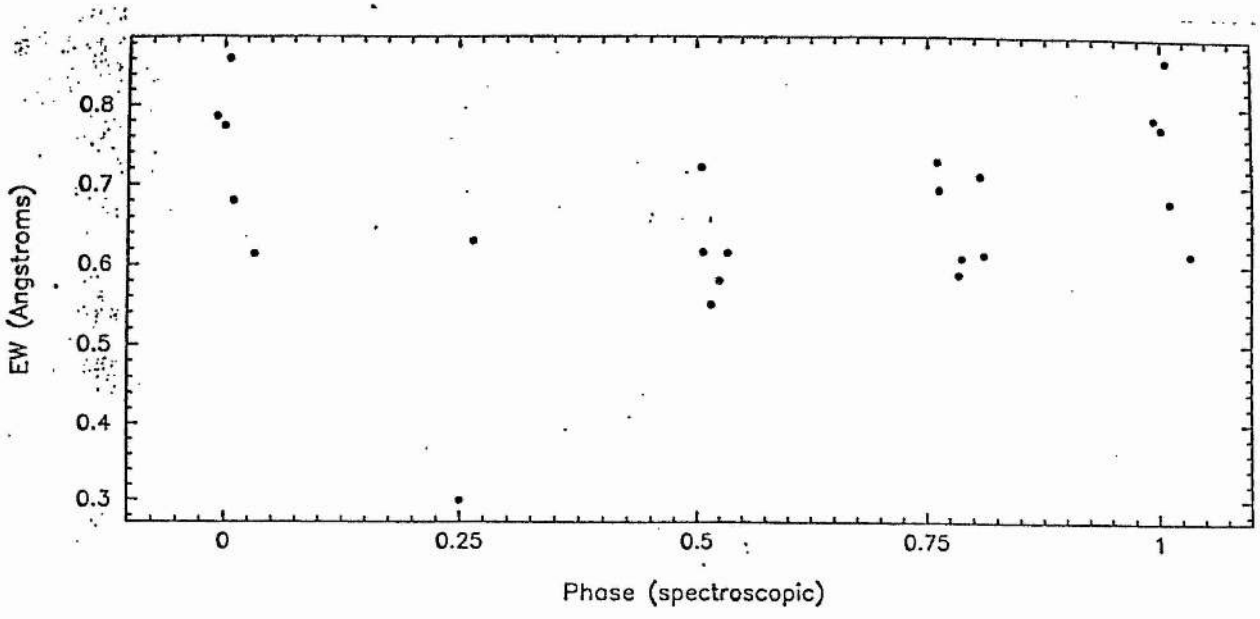

Figure 3.5: HeI 4026 Å EW measurements

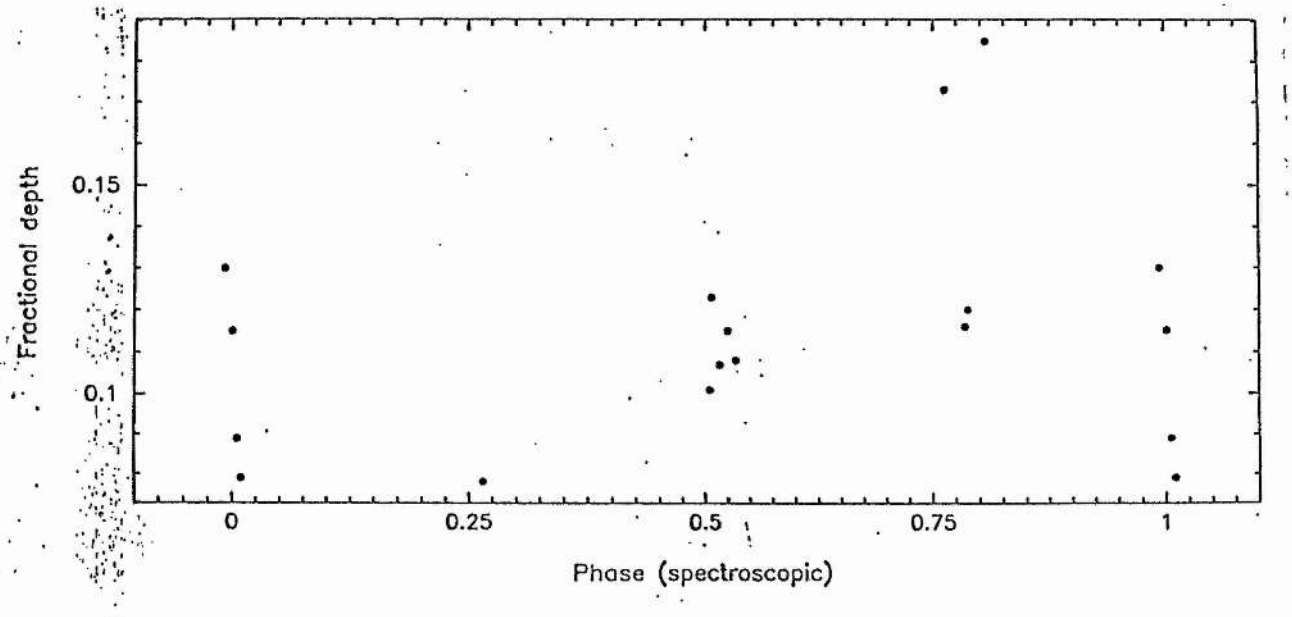

Figure 3.6: SiIV 4089 Å line depth measurements

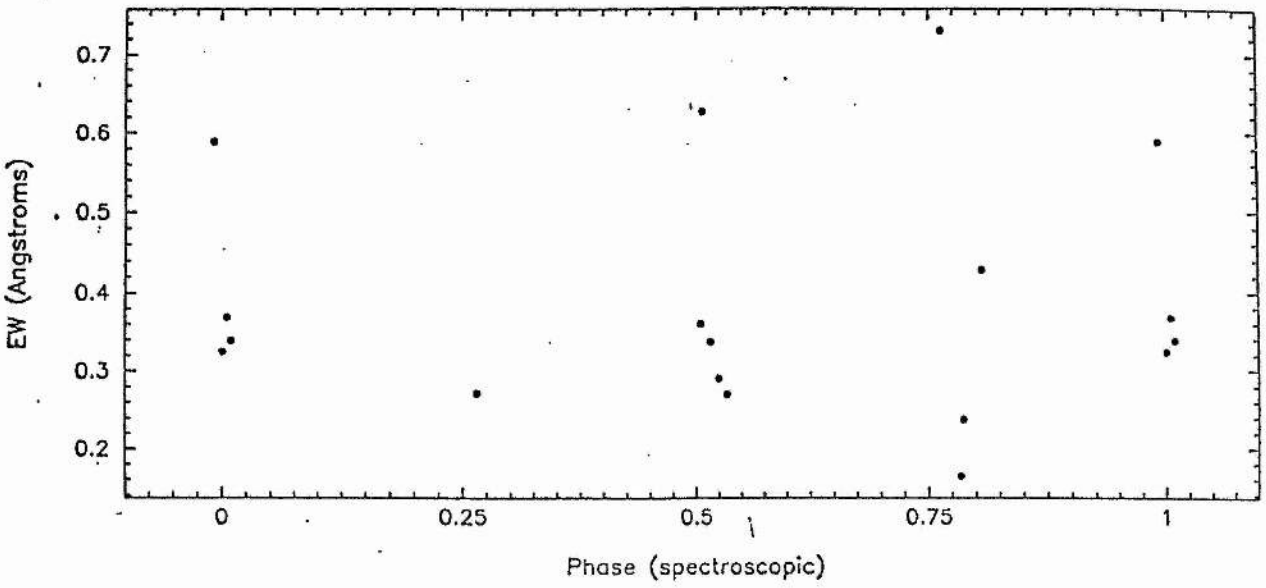

Figure 3.7: SiIV 4089 Å EW measurements

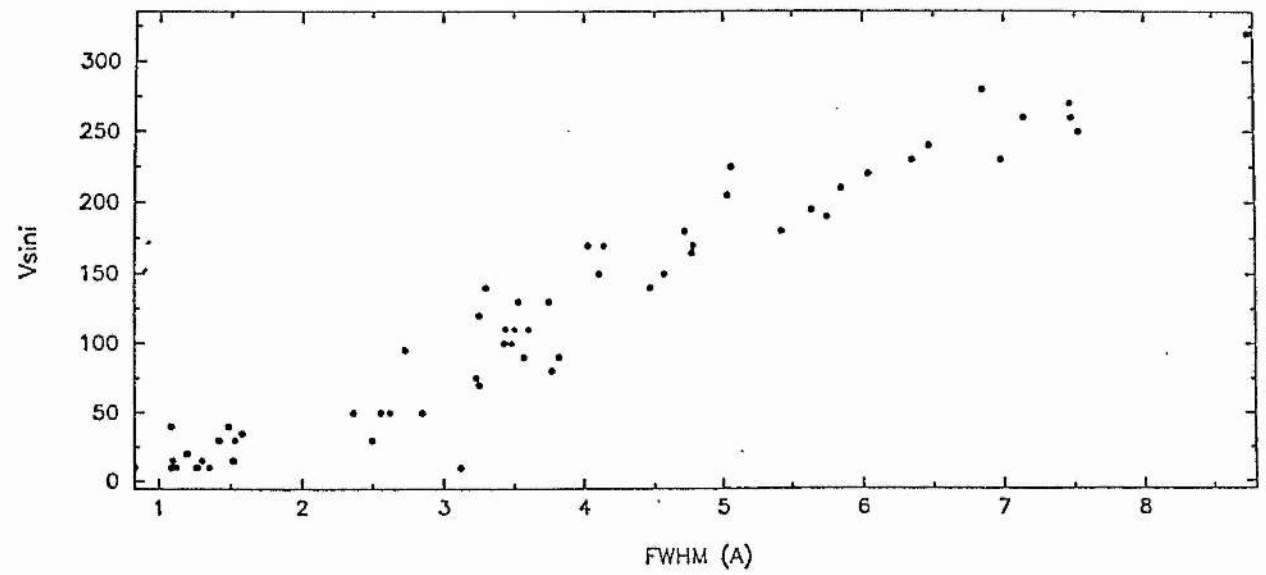

Figure 3.8: HeI 4471 Å FWHM against V sin i

This compares poorly with the expected value, since, assuming the derived mass ratio and a filled-out, corotating Roche geometry, the observed component of the rotation should be ≈ 200 km s^{-1}. The latter value was also reported by HCCO on the basis of visual FWHM estimates. The discrepancy, which is not believed to reflect the physical parameters of the system, must be ascribed to inadequacies in the fitted profile, and the absence of a reliable calibration. One factor is that different spectrograph resolutions can lead to a systematic zero-point error, even if the same line is being adopted.

If the implied rotation rate is real, and corotation assumed, the star is required to underfill its Roche-lobe by over 33 %, which is surely untenable from the standpoint of the disk and the modelled ellipsoidal variations. The only solution would be to postulate that the star is not in corotation, which is at odds with the observed circularity of the orbit, suggesting that tidal forces would also have forced corotation (or that the star would rotate faster than synchronously, as in the case of Her X-1). Unfortunately, either assumption would prevent the unique derivation of the masses outlined here, since the uncertain system geometry would preclude against determing i.

Within the context of the Roche geometry, if the inclination is fixed at 90°, and the mass-ratio taken to be 10.96, one finds that the eclipse duration prohibits against the star underfiling by more than ≈ 20 %. Thus, short of assuming that the entire framework of these calculations is flawed, these measurements must be regarded as systematic underestimates.

3.5.3 The absolute magnitude and distance of the system

The absolute magnitude of the primary has been estimated in two ways, firstly by considering the flux on the basis of the derived size of the star and the known effective temperature, and secondly by adopting a calibration scheme based on the equivalent width of a particular line.

The mass ratio derived from the heating corrections gave a volume radius (estimated from the tables of Mochnacki, 1984) of $0.588 \times a$. This gives an actual radius of

Table 3.9: HeI rotational measures for SMC X-1

H.J.D	Phasing	HeI 4026 FWHM
2447000+	T_{+ve}	Å
811.89134	0.993	3.78
811.92386	0.001	4.15
811.94101	0.006	4.18
811.95706	0.010	3.85
812.04605	0.033	3.37
812.88971	0.250	1.79
812.94991	0.265	3.93
813.88337	0.505	4.22
813.89096	0.507	3.37
813.92695	0.516	3.11
813.96152	0.525	3.31
813.99582	0.534	3.54
814.87925	0.761	3.79
814.88791	0.763	3.27
814.96981	0.784	3.52
814.98028	0.787	3.37
815.05700	0.806	3.69
815.07120	0.810	3.86

1.12×10^{10} m, implying a surface area for the equivalent spherical star of $1.6 \times 10^{10}\,m^2$. For $T_{eff} = 25000$ K, the $\log(L_{opt}/L_{\odot})$ is then 4.96. This then places SMC X-1 close to the 20 $M_{\odot}$ track on the HR diagram of Maeder and Meynet (1989) - see Figure 3.9. Since mass-loss has been assumed in their models, this is not inconsistent with the observed lower (17 $M_{\odot}$) mass of SMC X-1, and does not argue that the primary is significantly undermassive.

Adopting the luminosity derived above, and a bolometric correction of 2.4 (Underhill and Doazan, 1982, and references therin), the M_{bol} is found to be -7.68, giving M_v = -5.28. Adopting the E_{B-V} for the SMC of $0^m.04$ quoted by Westerlund (1990), a visual extinction of 0.13 magnitudes is expected. This gives a distance modulus of 18.4 based on m_v(average) $\approx$ 13.25 (van Paradijs and Kuiper, 1984). The distance is then found to be 47 kpc, which is in good agreement with the estimate of Howarth of 45 $\pm$ 5 kpc. This locates SMC X-1 as lying on the nearside of the Cloud.

The mean equivalent width of H_γ, averaged over all phases, is found to be 1.42 $\pm$ 0.01 Å, against 1.55 $\pm$ 0.02 Åof HCCO. Based on the calibration scheme of Balona and Crampton (1974), for a B0 star, the M_v of SMC X-1 is found to be -6.87 $\pm$ 0.03 , against the value found by HCCO of -6.6. The extreme values of the H_γ width give M_v ranging from -7.7 to -6.2. Adopting the E_{B-V} mentioned above, This gives a distance modulus of 19.99, significantly higher than the average for the SMC of $\approx$ 19.0. It is noted that the largest H_γ width corresponds to the photometric phase 0.5, when the illuminated side of the primary is visible, while the smallest corresponds to the geometrically opposite case. This effect is not mirrored in the H_δ widths. For the purposes of determining M_v, the values nearest the quadratures are the most appropriate, since the heated inner and cool averted hemispheres make their smallest contributions. Based on the measurements at radial velocity phase 0.993, 0.001, 0.505 and 0.507, an average M_v of -6.85 was found. The apparent magnitude at quadratures is $\approx$ 13.15, giving a distance modulus of 19.87. At best, therefore, SMC X-1 can only be as close as 94 kpc, and if the average is taken, is as far away as 100 kpc. The problem of the bright x-ray luminosity is therefore exacerbated!

The discrepancy could be alleviated by the assumption of a high intrinsic reddening for the system, or assuming a very large anisotropy in the reddening of the SMC

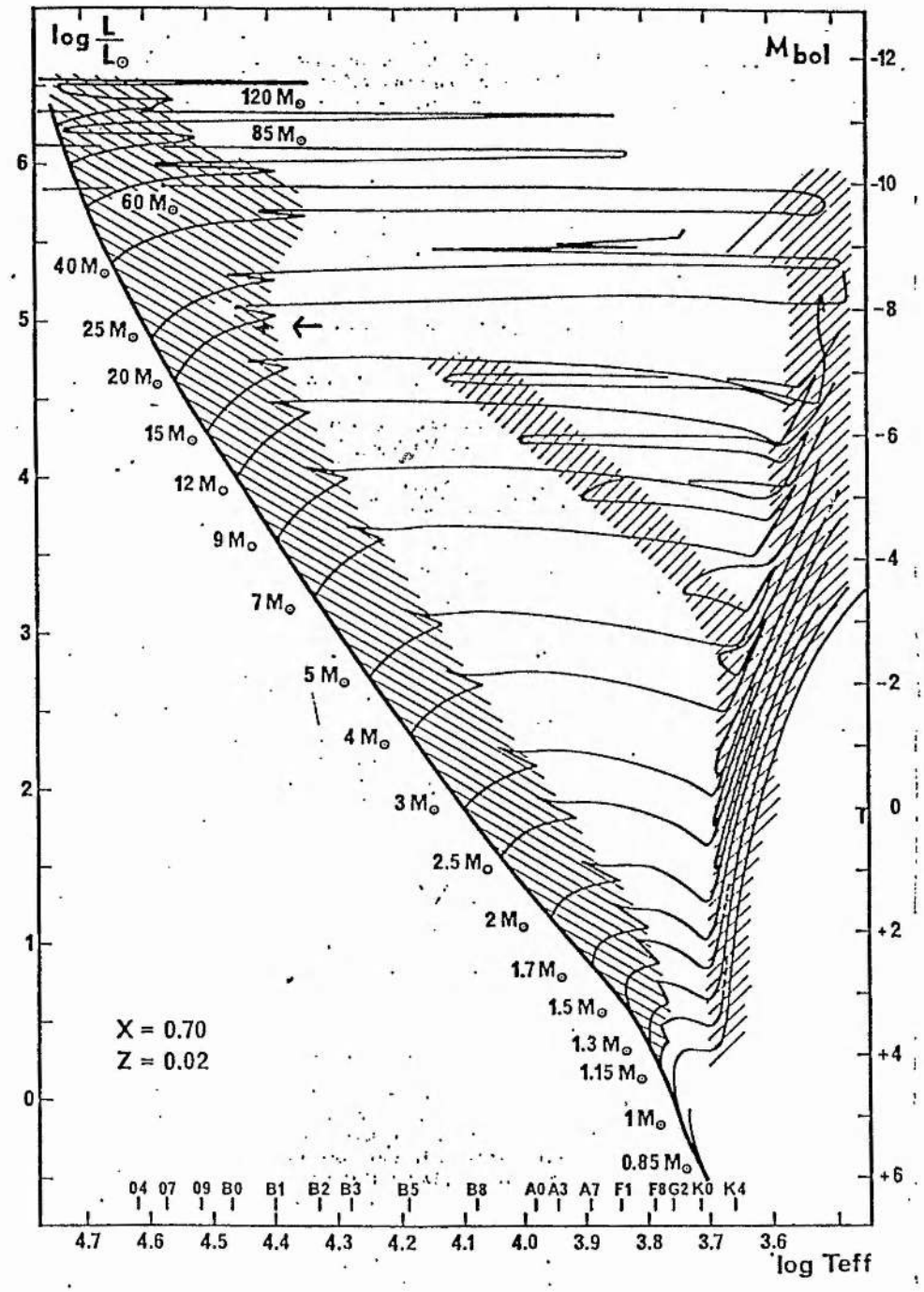

Figure 3.9: SMC X-1 on the HR diagram of Maeder and Meynet (1989)

in the line of sight. Extended dust shells around HMXRBs have been argued for, but not in the case of SMC X-1. The observational evidence for this would be an infrared excess, as seen in the case of several of the Be/x-ray transients (White, 1989). However, a perusal of the data used by Balona and Crampton (1974) shows that there are large residuals in the calculated absolute magnitudes, with the largest being for supergiant systems showing narrow lines. (O-C)s in excess of one magnitude are seen, which therefore limit the accuracy of the distance modulus to much better than $\pm$ 1.0 magnitude. With this in mind, the true distance modulus could be as low as 18.8, leading to a distance of 58 kpc. This is nearer to the value of 45 $\pm$ kpc arrived at by Howarth (1982) but is emphatically a lower limit. The distance modulus derived on the basis of the phase-averaged widths is therefore 19.99 $\pm$ 1.0, giving a range of distances from 63 to 158 kpc. Therefore, on the basis of the equivalent width estimate, the system is still somewhat further away than would be expected from the x-ray characteristics, but is found to be much closer if the T_{eff} luminosity estimate is employed. The latter estimate is however, sensitive to the choice of temperature and bolometric correction, and should be regarded with caution.

3.6 Discussion

The extreme distance of the primary implied by the EW calibration discussed above is clearly problematic from the point of view of adopting a realistic x-ray luminosity for the pulsar. Even the work in this chapter has been based on largely canonical values for L_x; if the above distance calculations are taken into account, substantially larger values of L_x would need to be used. The apparent weakness of the heating effect would then have to be explained.

For the simplistic case of spherical accretion, the limiting luminosity for steady flow is $L_E \approx 1.3{\times}10^{38}\ (M/M_\odot)\,\mathrm{erg\,s^{-1}}$; for a solid columnar flow, this factor must, in very approximate terms, be multiplied by the accretion column's cross-sectional area as a fraction of the surface area of the accreting object (Frank et al 1985, pp2,157), a factor smaller than one half.

The only known parameter is the mass, hence even L_E is uncertain. At 65 Kpc,

over the spectral range 1-40 KeV, Howarth (1982) gives $L_x = 1 \times 10^{39}$ erg s^{-1}; for a distance of 94 Kpc (this study), this would need to be raised by about a factor of two. This is therefore almost reconcilable with symmetric spherical accretion onto a 1.6 $M_\odot$ neutron star, but totally untenable for columnar accretion even if the column impacts over all of one hemisphere (ruled out from the pulse structure). Obviously the problem becomes less extreme if the closer distance estimates are considered, and of course, the above estimates for limiting luminosity are decidedly crude.

This study has therefore found that the orbital solution of HCCO was basically correct, although the above authors found a lower mass for the secondary. Neither work found a value for the neutron star that was either unacceptably high or low according to theory, and the undermassiveness of the primary is confirmed by this study. The remaining problem would seem to be one of correctly interpreting the distance of the system. If this was achieved, the inter-related difficulties of the accretion process and the x-ray heating influence would become much more tractable.

3.7 References

Balona, L.A., Crampton, D., 1974. *Mon. Not. R. astr. Soc.*, **166**, 203.

Basko, M.M., Sunyayev, R.A., Totarchuk, L.G., 1974. *Astr. Astrophys.*, **31**, 249.

Corbet, R.H.D., 1984. *The Evolution of Galactic X-Ray Binaries, eds. Truemper, Lewin and Brinkman (Dordrecht:Reidel), p63.*

Erhorn, G.D., Groote, D., Kaufmann, J.P., 1984. *Astr. Astrophys.*, **131**, 390.

Frank, J., King, A.R., Raine, D.J., 1985. *Accretion power in astrophysics (Cambridge University Press).*

Hammerschlag-Hensberg, G., Kallman, R.T., Howarth, I.D., 1984. *Astrophys. J.*, **283**, 249.

Hill, G., Fisher, W.A., Poeckert, R., 1982. Publs. Dom. Astrophys. Obs., **16**, 27.

Howarth, I.D., 1982. *Mon. Not. R. astr. Soc.*, **198**, 289.

Hutchings, J. B., 1982. *Astrophys. J.*, **255**, 70.

Hutchings, J.B., Crampton. D., Cowley, A.P., Osmer, P.S., 1977. *Astrophys. J.*, **217**, 186.

Joss, P.C., Rappaport, S.A., 1984. *Ann. Rev. Astr. Astrophys.*, **22**, 537.

Kamp, L.W., 1978. *Astrophys. J. Suppl.*, **36**, 143.

Khruzina, T.S., Cherepashchuk, A.M., 1983. *Soviet astr.*, **27**, 1.

Maeder, A., Meynet, G., 1989. *Astr. Astrophys.*, **210**, 155.

Paradijs, J. van., Zuiderwijk, E., 1977. *Astr. Astrophys.*, **61**, L19.

Paradijs, J. van., Kuiper, L., 1984. *Astr. Astrophys.*, **138**, 71.

Primini, F., Rappaport, S., Joss, P.,C., 1977. *Astrophys. J.*, **217**, 543.

Sanduleak, N., 1968. *Astr. J.*, **167**, 293.

Shortridge, K., 1983. *Figaro Users Manual (Starlink Project)*

Underhill, A., Doazan, V., 1982. *B Stars with and without emission lines (NASA Monograph)*

Westerlund, B.F., 1990. A&A Rev., **2**, 29.

White, N.E., Swank, J.H., Holt, S.S., 1983. *Astrophys. J.*, **270**, 711.

White, N.E., 1989. A&A Rev., **1**, 85.

Chapter 4

A spectroscopic study of QV Nor

4.1 The status of QV Nor

Parkes, Murdin and Mason (1978) identified a heavily reddened OB star as the optical companion to the pulsating x-ray source 4U 1538-52. This identification was confirmed by Crampton, Hutchings and Cowley (1978, hereafter CHC) who detected spectroscopic variations in phase with the x-ray pulse orbit.

Superficially, this system was similar to other studied x-ray binaries like SMC X-1, in which an accreting compact object followed a close circular orbit around a tidally distorted early star. Because of the proximity of the stars, eclipses are likely, and in the case of 4U 1538-52, optical and x-ray modulations were observed early on (Pakull et al, 1983, and references therein). However, the optical light curve of the identified early star QV Nor is basically ellipsoidal with no significant filling-in of the phase 0.5 minimum, indicating that x-ray heating is much less apparent than in the case of SMC X-1. Ilovaisky et al (1979) concluded that the depth of the phase 0.0 minimum could only be explained by the eclipse of a luminous accretion disk or some other light source associated with the secondary. This finding was not echoed in the study by Pakull et al, who concluded that the data (and their own) was of insufficient quality

to disprove the ellipsoidal model. The general consensus is that the wind-fed x-ray binaries, of which 4U 1538-52 is a member (Corbet, 1984) may be prevented from forming disks due to the low angular momentum of the wind. Evidence for the lack of a disk also comes from the history of the pulse period, which tends to show a random walk rather than the regular spin-up episodes characteristic of the known disk-fed systems (Makishima et al, 1987). There is also no clear evidence for long-term optical variations, as might be seen if the disk was precessing, though this is also the case with SMC X-1. The x-ray brightness, assuming a distance of 5.5 - 6 kpc is also very low by comparison with the disk-fed systems, consistent with the lack of observed heating.

Ours is only the second spectroscopic study of this system since its discovery. The extreme redness and faintness of the star has obviously contributed to this lack of data. CHC's velocity curve, though demonstrating the correctness of the stellar identification, gave only crude estimates of the orbital parameters, based as it was on only eleven spectrograms taken on photographic plates. At the time of their paper, there was only one estimate of the neutron-star secondary's semi-amplitude, K_x, from pulse timing (see CHC) which was only accurate to 8 %, naturally limiting the reliability of the derived parameters. Fortunately, Makishima et al (1987) give a revised estimate of K_x accurate to 3.5 %, together with a relatively recent period determination.

4.2 Observations and Reduction

25 spectra of QV Nor were obtained between 4-10 March 1991 by Dr S.A. Bell and the author, using the RGO spectrograph on the AAT in conjunction with the 25cm camera and the 1200B grating, with the GEC CCD detector. The spectral range chosen covered 6290-6710 Å, with a dispersion of 33 Å mm^{-1}, giving a wavelength on pixel of 0.7 Å. The red spectral region was chosen to maximise the count-rate from this heavily reddened star (B-V $\approx$ 2). This spectral region allowed us to also study variations of the H_α profile with orbital phase, and to test the value of observing the deep 6678 HeI line, on which the velocities are based.

The exposure times were 1800 seconds, giving a typical s/n (stable from night to night) of $\approx$ 40. The reduction and measurement was performed in the same manner

as SMC X-1, using the previously mentioned FIGARO and DAO software packages. A variety of standard stars observed in the blue and red spectral regions established that the velocities were on the standard system.

The adopted template for cross-correlation purposes was a co-added spectrum of QV Nor utilising all the data and sharpened once. The systemic velocity was then measured by cross-correlation against a B-type standard, HD133955, observed on the same run, and by measurement of the HeI line using the REDUCE (Hill et al, 1982) program VELMEAS; these results agreed to within 1 $km\,s^{-1}$.

For cross-correlation purposes, the whole of H_α was windowed out, as were various interstellar features (the band shortward of H_α and the sharp line at 6614 Å, plus an unidentified pair of lines at around 6375 Å). The CCFs were well-defined, enabling measurements to be made of the top 50% of the profile, although the sensitivity of the derived velocities to changes in the placements was small.

Due to the excellent observing conditions of the run, no spectra were discarded prior to measurement, and none were excluded from any of the velocity solutions. The measured velocities, with the derived systemic velocity for the template of -138.7 ± 2.4 $km\,s^{-1}$, are shown in Table 1.

Table 2 shows the parameters derived from the raw data, with no corrections for non-keplerian velocities. The adopted period is from Makishima et al (1987). Because the data are from one cycle, small errors in the period will not greatly affect the derived parameters. Conversely, our data does not cover a sufficiently long series of epochs to be useful in period determination, and all subsequent calculations are computed with the above period value.

The systemic velocity and time of maximum positive velocity can be compared with the values found in the literature. CHC found V_{opt} = -173 ± 4 $km\,s^{-1}$, which is a very much higher approach velocity than is found by this study. The residual systemic velocity, once solar and galactic motion has been taken into account, is roughly -76 $km\,s^{-1}$, which is less problematic than the high velocity found by CHC.

There is no evidence for any change in the period of the system since it was first

Table 4.1: Radial velocity data for QV Nor

H.J.D	Phasing	Observed Velocity	O-C Residuals
2447000+	T_{+ve}	Km s^{-1}	Km s^{-1}
957.229	0.937	-123.9	+5.1
958.181	0.192	-137.2	+2.7
958.204	0.198	-136.3	+4.3
958.228	0.205	-132.4	+8.9
958.250	0.211	-144.3	-2.3
959.144	0.450	-160.7	+4.2
959.166	0.456	-170.0	-4.9
959.189	0.462	-169.3	-4.0
959.211	0.468	-167.2	-1.7
959.233	0.474	-168.3	-2.7
959.256	0.480	-165.0	+0.7
959.279	0.486	-165.8	+0.0
960.167	0.725	-152.1	-2.4
960.189	0.731	-152.8	-3.8
960.212	0.737	-149.1	-0.8
960.233	0.742	-143.4	+4.2
960.255	0.748	-142.8	+4.1
960.277	0.754	-140.0	+6.2
961.152	0.989	-124.0	+3.6
961.174	0.995	-128.4	-0.8
961.203	0.003	-133.5	-7.9
961.218	0.006	-136.2	-8.6
961.240	0.012	-125.6	+2.0
961.262	0.018	-126.9	+0.8
961.284	0.024	-134.8	-7.0

Table 4.2: Orbital Parameters for QV Nor

V_{opt}	-146.7 ± 0.9 km s^{-1}
K_{opt}	19.2 ± 1.2 km s^{-1}
e	0.000†
Ω	0.000†
P_{orb}	3.72854†
T_{+ve}	47957.4653 ± 0.0440

† — adopted value

monitored by Davison, Watson and Pye (1977). An examination of the literature reveals four independent ephemerides, based on x-ray eclipse, pulse-timing and spectroscopy (including this study). In each case the observed time of maximum positive velocity appears to have occurred within the standard error of the expected time calculated from the ephemeris of the above authors. Some confusion has arisen over the adoption of the earliest ephemeris, since the Modified Julian Day number of the x-ray eclipse quoted by the above authors has been reproduced later in the literature (eg CHC) as an uncorrected Julian Day number (in other words in error by half a day).

The semi-amplitude of the system is much less than the value of 33 ± 5 km sec^{-1} found by CHC. This discrepancy is probably explicable in terms of the improved quality of our data. Our residuals are very much smaller; we also have better phase-coverage, the curve of CHC not being well constrained at either quadrature. As will be demonstrated in the next section, the true semi-amplitude is almost certainly larger than this value, owing to the effect of tidal distortion.

The x-ray data of Makishima et al (1987), taken over several contiguous cycles of the orbit in 1983, gives improved pulse-timing parameters. The authors quote figures for the solutions with and and without a constant period increase term in the pulsation times, concluding that the best fit to the data is achieved in the latter case. No significant evidence for eccentricity was found. Wherever we have adopted their parameters, it has been for the case of increasing pulsation times (ie Makishima et al include a spin-down term). K_x is found to be 309 ± 11 km s^{-1}, giving $q = 16.1 \pm 1.2$. The mass

function $f(m)$ is therefore $0.0027 \pm 0.0005\ M_{\odot}$. From eclipse duration data, the half angle is $25° \pm 5°$. If the primary is assumed to fill its Roche lobe, then from Primini, Rappaport and Joss (1977) the mean radius of the Roche lobe is 0.622 of the component separation. This then gives a value for the inclination of $60° \pm 5$, somwhat lower than found by previous workers. If the primary underfills its Roche lobe by 10 % in radius, the inclination angle is raised by $\approx 6°$. The probable lack of an accretion-disk does allow the primary to underfill the Roche lobe. The primary can underfill by as much as 20 %, on the basis of the x-ray eclipse data alone, but the remaining data does not support such a high inclination. The amplitude of the ellipsoidal light variations is one such constraint: Pakull et al (1982), for instance, suggested that the relative depths of the minima were explicable in terms of the standard tidally-distorted, corotating model (see below). In view of the uncertainties, i may well be $\approx 60°$. In the following section, however, the derived velocity corrections are based on a canonical value of 70°. The derived masses will be discussed in section 4.

Based on the derived value of q, an assumed i and mean radius of the primary, it is possible to generate theoretical light-curves which can be compared with the published data. As was also reported by Pakull et al, the standard model gives a secondary minimum which is too deep in comparison with the data (by ≈ 0.014 in V). In this study, the primary minimum was found to be too deep by approximately the same amount, whereas Pakull found that the model fitted the observations at this point. Considering the limited quality of the photometry, and the non-repeatability from cycle to cycle, it is probably unwise to infer too much from such a discrepancy. However, if i is lowered to 60°, the depths of both minima agree with the data to within 0.005 in V. The simple model fails to account for the slight phase-shift of the secondary minimum with respect to x-ray eclipse. Only when more detailed, longer-term photometry has been performed will it be possible to make strong quantitative deductions.

Figure 1 and Figure 2 display groups of generated light-curves for various inclinations and degrees of filling. The orbital parameters used to construct these solutions are uncorrected for tidal-distortion. As is clear, the underfilling models fail to account for the large amplitude of the light-curve (see Figure 3). Adopting a lower effective temperature for the primary (Pakull et al, 1983) serves only to decrease the amplitude of the theoretical curve.

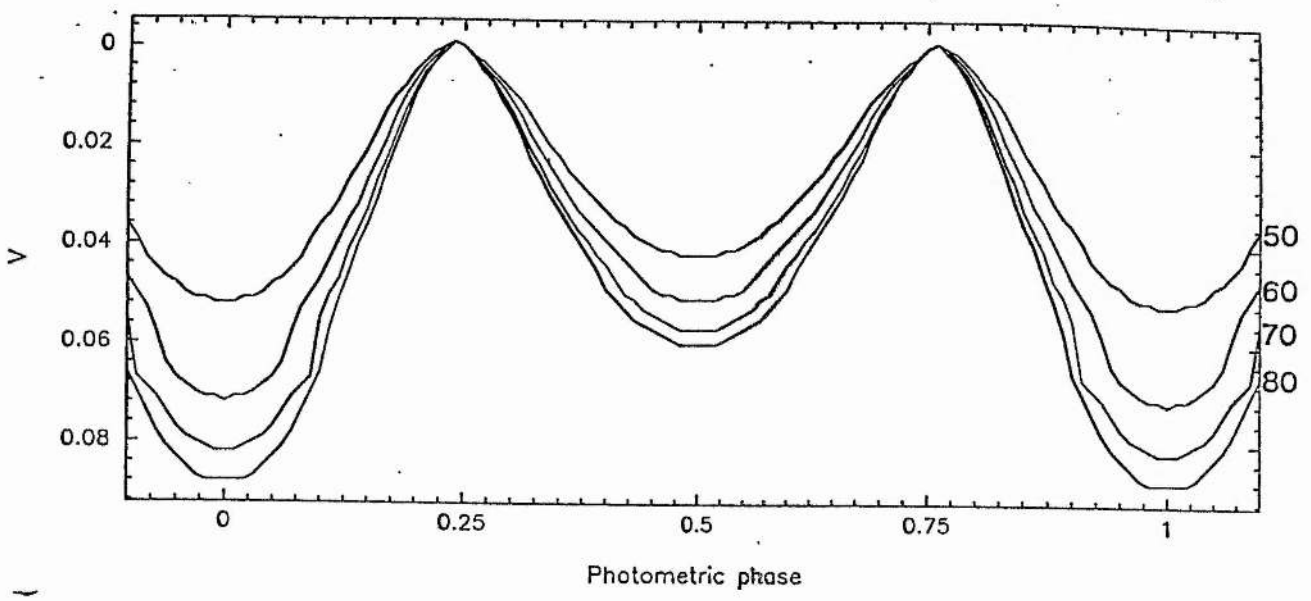

Figure 4.1: Light curves for QV Nor, with i running from 50 to 80

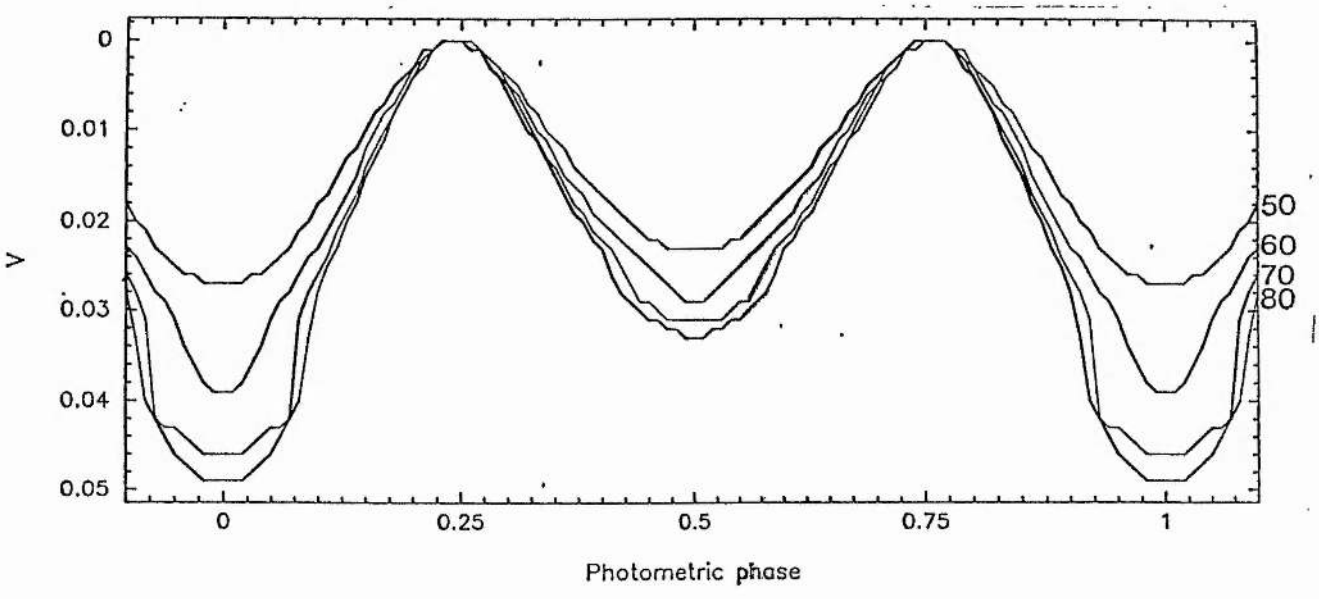

Figure 4.2: Light curves for QV Nor, with 10% underfilling by radius

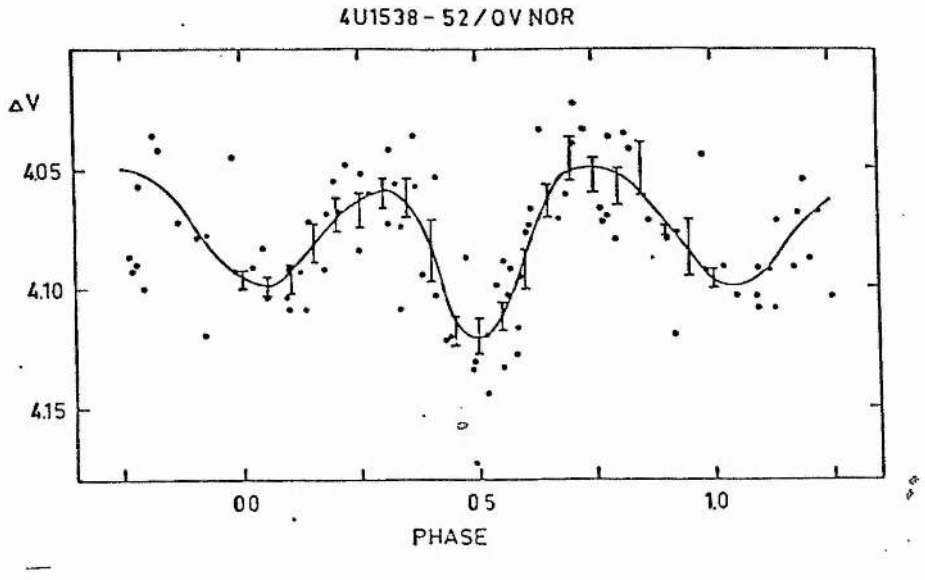

Figure 4.3: V-band photometry from Pakull et al (1983)

4.3 Corrections for the distorted star

4.3.1 Modelling the geometry of QV Nor

As was discussed in the previous chapter, deviations away from keplerian motion in the velocity curves of circular-orbit x-ray binaries can be large, owing to the so-called reflection-effect. As was also seen, the non-keplerian components can be quite large even if there is no heating from the secondary, due to the highly distorted profile of the optical star (even though the substellar point of the star may be substantially cooler than the polar temperature due to gravity darkening). As has been discussed in the previous sections, there is little evidence for x-ray heating in QV Nor on the basis of the photometric data, since the relative depths of the minima are close to what would be seen in ellipsoidal variations. Furthermore, the observed brightness of the 4U 1538-42 x-ray source is very low compared to the known Roche-lobe overflow driven systems which it resembles from a geometric standpoint. SMC X-1, for instance, has L_x at least equal to $4\times\ 10^{38}$ erg s^{-1}. Makishima et al (1987) and Parkes, Murdin and Mason (1978) found L_x for 4U 1538-42 to be $\approx 2\times\ 10^{36}$ erg s^{-1}. The influence of the heating

effect will therefore be negligible compared to the effect of tidal distortion, and has therefore been ignored in the models (though the secondary had to have a miminum temperature of 1000 K).

The methodology behind the models was identical to that considered for SMC X-1, with some simplifications. The luminosity of the secondary was kept low and constant (polar temperature kept at 1000 K), with a constant radius of 0.05 times the component separation. Since the luminosity is comparitively well-known, only two sets of solutions were run, the first of which was essentially equivalent to the "no heating" model of SMC X-1.

The polar temperature of the primary was fixed at 30000 K, and the star was assumed to fill its Roche-lobe, since there is no overwhelming evidence against this simplest case model. The system inclination was fixed at $i = 70°$, with $K_x = 309 \pm 11$ km s^{-1}, from the Makishima study. The initial value of K_{opt} was that derived from the above analysis of our raw data, 19.2 km s^{-1}. The corrections were derived from computed profiles, based on gaussian measurements of the lower 50 % of the line. This was adopted owing to the well-defined CCFs obtained during measurement of the spectrograms. The difference between using the lower 33 % and the half line depth was only significant around optical phase 0.94, (ie transit of the x-ray source across the inner hemisphere of the B-star, when the half-line depth corrections exceeded the 33% corrections by nearly 3 km s^{-1}. This was a positive correction to be applied (subtracted from) a velocity near the systemic velocity of the system, and would appear to represent the obscuration of the blueshifted limb of the B-star (ie the Rossiter effect). A model was then run to examine the generated velocity corrections from phase 0.8 to 0.2, confirming that there was also a negative correction to be applied when the secondary occulted the redshifted limb, although there were no observations at this phase. Assuming that the secondary has no accretion disk, its angular size in the real system would be infinitesimally small; hence the corrections evaluated around this point may be spurious; they have not however been rejected.

Based on the revised velocity data, a second set of corrections was generated using a new estimate of the mass-ratio. This then led to a third set of velocity corrections and a third (final) estimate of the mass-ratio. The difference between these iterations was

very small. The net effect was to increase the semi-amplitude, ie the tidal distortion acted in the same sense as x-ray heating. K_{opt} was found to be 19.8 ± 1.1 km s^{-1}, with V_{opt} = -148.1 ± 0.8 km s^{-1}.

It can be seen that the corrected semi-amplitude does not differ greatly from the initial value, both values overlapping within their respective error margins.

A second set of solutions was run to investigate the effect of the B-star underfilling its Roche-lobe by 10 % in radius. The mean radius of the star inputted in the program was then 0.9 × the value given by the adopted q. Since the rotational velocity of the star will be less, and the effect of gravity darkening and changing profile less severe, these corrections were smaller in magnitude (although the Rossiter effect again produced relatively large corrections during x-ray transit). The models converged very rapidly, with K_{opt} becoming 19.3 ± 1.1 km s^{-1} after the first solution and not changing thereafter. V_{opt} was found to be -147.4 ± 0.8 km s^{-1}

Because the sampling of the velocity curve around phase 0.0 is not symmetrical, the spurious Rossiter effect at one transit of the limb is not cancelled out by a correction of equal magnitude (but opposite sign) as the star traverses the other limb. This means that the systemic velocity will be biassed away from the value given by the raw velocities. As can be seen, however, the difference is very small.

The derived corrections from the three calculations are shown in Table 3.

The adopted velocities, residuals and derived orbital parameters are shown in table 4 and table 5. Figure 4 displays the velocity curve for the revised data.

4.4 Masses of the component stars

The data without corrections for tidal distortion gives $f(m) = 0.0027 \pm 0.0005\ M_{\odot}$. Based on $q = 15.61$, we have $f(m) = 0.0030 \pm 0.0005\ M_{\odot}$. The slight decrease in q has only a very small influence on i, raising it from $\approx 58°$ to 60°. Because of the large uncertainty in the x-ray eclipse duration, there is an intrinsic error in the inclination

Table 4.3: Corrected velocities

Phasing	Observed Velocity	Correction †	Correction
$\Phi_0 = T_{max}$	$Km\,s^{-1}$	$Km\,s^{-1}$	$km\,s^{-1}$
		Roche-lobe filled	10% underfilling
0.937	-123.9	-1.8	-0.8
0.192	-137.2	+9.4	+4.6
0.198	-136.3	+8.9	+4.5
0.205	-132.4	+8.3	+4.2
0.211	-144.3	+7.5	+3.9
0.450	-160.7	-0.2	-0.2
0.456	-170.0	+0.1	-0.2
0.462	-169.3	+0.4	+0.0
0.468	-167.2	+0.6	+0.1
0.474	-168.3	+0.8	+0.4
0.480	-165.0	+1.0	+0.6
0.486	-165.8	+1.2	+0.7
0.725	-152.1	+0.4	+0.1
0.731	-152.8	+0.4	+0.0
0.737	-149.1	+0.3	+0.0
0.742	-143.4	+0.3	+0.0
0.748	-142.8	+0.3	+0.0
0.754	-140.0	+0.3	+0.0
0.989	-124.0	-1.6	-0.6
0.995	-128.4	-1.5	-0.6
0.003	-135.5	-1.3	-0.5
0.006	-136.2	-1.3	-0.4
0.012	-125.6	-1.1	-0.3
0.018	-126.9	-0.9	-0.2
0.024	-134.8	-0.7	-0.1

† = adopted correction (subtracted from raw data)

Table 4.4: Corrected velocity data for QV Nor

H.J.D	Phasing	Corrected velocity	O-C Residuals
2447000+	T_{+ve}	$Km\,s^{-1}$	$Km\,s^{-1}$
957.22931	0.963	-122.1	+6.6
958.18148	0.219	-146.6	-2.4
958.20370	0.225	-145.1	-0.2
958.22801	0.231	-140.6	+5.1
958.25023	0.237	-151.8	-5.3
959.14406	0.477	-160.5	+7.2
959.16559	0.483	-170.1	-2.3
959.18851	0.489	-169.6	-1.9
959.21073	0.495	-167.8	+0.0
959.23295	0.501	-169.1	-1.3
959.25587	0.507	-166.0	+1.8
959.27879	0.513	-167.0	+0.8
960.16706	0.751	-152.5	-4.6
960.18928	0.757	-153.1	-6.0
960.21151	0.763	-149.4	-3.0
960.23304	0.769	-143.7	+2.0
960.25526	0.775	-142.5	+2.4
960.27749	0.781	-140.2	+4.0
961.15186	0.015	-122.1	+6.2
961.17409	0.021	-126.9	+1.5
961.20326	0.029	-134.2	-5.6
961.21784	0.033	-134.9	-6.3
961.24007	0.039	-124.5	+4.3
961.26160	0.045	-126.0	+3.0
961.28382	0.051	-135.5	-6.2

Table 4.5: Corrected Orbital Parameters for QV Nor

V_{opt}	-148.1 ± 0.9 km s^{-1}
K_{opt}	19.8 ± 1.1 km s^{-1}
e	0.000†
Ω	0.000†
P_{orb}	3.72854†
T_{+ve}	47957.3656 ± 0.0395

† — adopted value

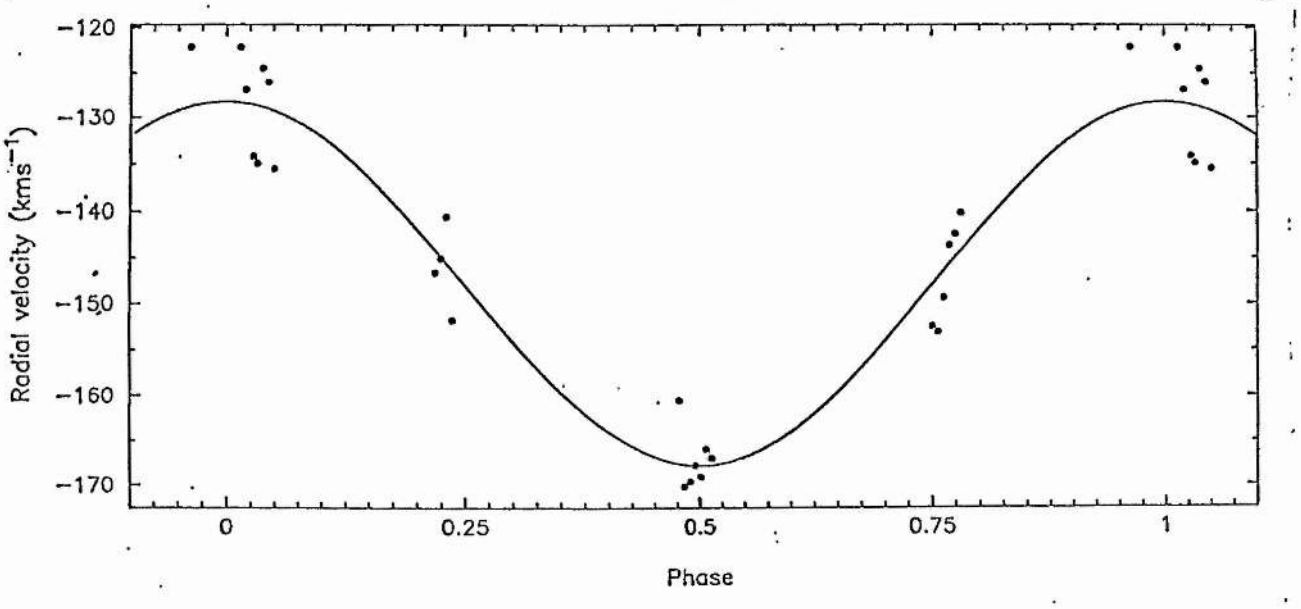

Figure 4.4: The velocity curve of QV Nor, corrected for tidal-distortion

of $\approx 5°$, which naturally limits the accuracy of any subsequent mass-determinations.

For $q = 16.13$, $M_x = 1.2 \pm 0.2\ M_\odot$, $M_{opt} = 19.8 \pm 3.3\ M_\odot$. For $q = 15.61$, $M_x = 1.3 \pm 0.2\ M_\odot$, $M_{opt} = 19.8 \pm 3.3\ M_\odot$.

Although these errors are large, they are somewhat smaller than those obtained by CHC, who found $M_{opt} = 20 \pm 4\ M_\odot$, $M_x = 2.0 \pm 0.5\ M_\odot$. This study has therefore found slightly lower masses for both of the stars, although (as was seen in SMC X-1), the values for the primary star overlap. One factor which would further reduce our errors would be the adoption of the same eclipse duration and inclination angle values as CHC, which show smaller uncertainties.

Since previous workers have adopted a higher value of i than the value deduced from this study (combined with the data of Makishima et al), it was considered worthwhile to solve the parameters for this "canonical" i. The inclination was therefore set at $70° \pm 5°$. Based on the corrected data, it was found that $M_{opt} = 15.6 \pm 2.0\ M_\odot$, $M_x = 1.0 \pm 0.13\ M_\odot$.

The errors in θ_e (eclipse duration half-angle), the x-ray mass function, and the range over which the star may be permitted to underfill its Roche-lobe can be visualised as the "box" constrained by the curves of solution-families in the Mass-Radius plane, (see Figure 5), as shown by Makishima et al. One family of relations is that given by eliminating i from the mass-function equation and the equation relating θ_e with the size of the stellar radius (solid lines). The other family of relations is obtained by eliminating i from the mass-function equation and the empirical equation for the critical size of the Roche-lobe, to which a parameter β may be multiplied, β being the extent to which the lobe is filled by radius (dashed lines). The dashed lines are insensitive to the error in the mass-function, and the error in the mass-ratio has been assumed negligible.

Within the allowed errors of the parameters, the star can underfill by a large extent, but values of β much less than ≈ 0.9 do not seem very likely on the grounds of the light-curve (see earlier section).

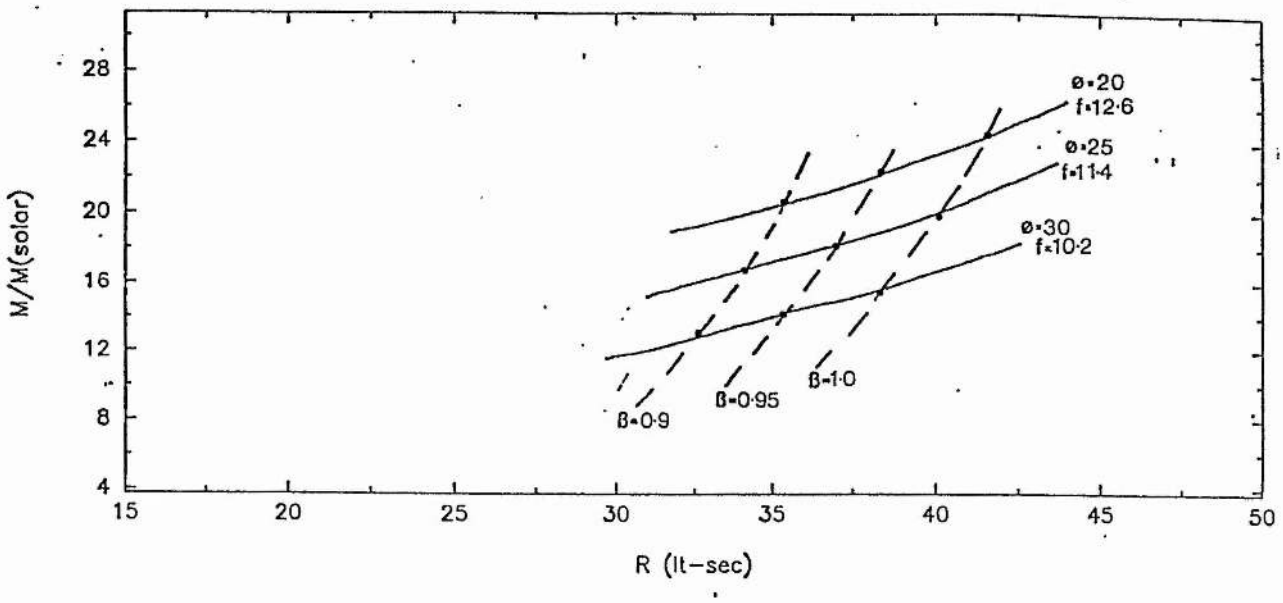

Figure 4.5: M-R constraints in QV Nor - see text for explanation

4.5 Line variations in the spectrum of QV Nor

Line measurements were made on several features in the spectrograms of QV Nor. The method was as described in the previous chapter; ie the fitting of gaussian profiles to obtain line depth, equivalent width and central wavelength measurements. Owing to the relative blandness of the spectrum between 6300 Åand 6700 Å, the choice of measurable features was rather limited. The first line to be measured was the HeI line at 6678 Å, on which the velocities are based. In all the spectra this was a deep, well-defined feature extending to about 15-20 % of the continuum height. The line was strongly broadened rotationally, compared with the neighbouring interstellar line at 6614 Å.

The profile of H_α is complex and shows strong variation between spectrograms. The general profile is apparently an absorption line superimposed on a wide emission feature (such that prominent V and R peaks are seen), at about 10% above the continuum height. Sometimes the absorption core extends below the continuum level. The V/R ratio is not constant, with each peak stronger than the other at certain phases.

Measuring the profile was difficult, owing to the double-peaked nature of each of the individual emission features, and the asymmetry of the central absorption line. In addition, the continuum height was very difficult to establish, partly due to the blueward interstellar absorption band.

Gaussian profiles were fitted to the central absorption feature, using the whole of the profile, irrespective of the true continuum height. The derived velocities are strongly blueshifted, and show pronounced variation from spectrum to spectrum. The centre of the line was often noisy, and hence these velocities should be regarded with caution. Gaussians were also fitted to the redward emission feature, this profile being in general stronger and better defined than the blueward component. The adopted rest wavelength for the H_α measurements was 6562.790 Å.

The blueward component was measured in 6 of the spectrograms, where the V/R ratio was closest to unity.

The V and R heights were measured by hand from intensity tracings, based on an estimated continuum level. Since the V/R ratios do not depend on an absolute height of the continuum, they are assumed to be meaningful, especially since the variation is over such a large range.

Figure 6 and Figure 7 display a co-added spectrum of QV Nor and a stack-plot of the H_α profile through all the spectrograms.

Widths and depths for the HeI line are given in Table 6, with H_α measurements in Table 7 (absorption line and V/R), Table 8 (Redward emission), and Table 9 (Blueward emission).

4.5.1 Changes through phase

The HeI depths and EW measurements show an unambiguous phase dependency. The widths and depths are greatest at spectroscopic phases 0.25 and 0.75, ie photometric phases 0.0 and 0.5. Since HeI reaches a maximum at B2, this clearly shows that the inner and averted hemispheres of QV Nor are cooler than the rest of the star, as

Table 4.6: HeI line measurements for QV Nor

H.J.D	Phasing	HeI 6678 EW	HeI 6678 depths
2447000+	T_{+ve}	Å	
957.22931	0.963	0.827	0.153
958.18148	0.219	0.997	0.185
958.20370	0.225	0.937	0.180
958.22801	0.231	0.986	0.185
958.25023	0.237	1.008	0.186
959.14406	0.477	0.770	0.145
959.16559	0.483	0.723	0.145
959.18851	0.489	0.699	0.138
959.21073	0.495	0.759	0.145
959.23295	0.501	0.691	0.141
959.25587	0.507	0.694	0.148
959.27879	0.513	0.761	0.154
960.16706	0.751	0.882	0.178
960.18928	0.757	0.907	0.188
960.21151	0.763	0.926	0.186
960.23304	0.769	0.920	0.185
960.25526	0.775	0.923	0.180
960.27749	0.781	0.863	0.175
961.15186	0.015	0.772	0.150
961.17409	0.021	0.752	0.157
961.20326	0.029	0.682	0.151
961.21784	0.033	0.708	0.153
961.24007	0.039	0.800	0.160
961.26160	0.045	0.710	0.159
961.28382	0.051	0.772	0.167

Table 4.7: H_α measurements for QV Nor - 1

H.J.D	Phasing	RV	error	V/R
2447000+	T_{+ve}	km s^{-1}	km s^{-1}	
957.22931	0.963	-151.4	29.2	0.26
958.18148	0.219	-149.7	3.7	0.55
958.20370	0.225	-167.9	15.3	0.63
958.22801	0.231	-166.0	2.6	0.67
958.25023	0.237	-154.1	6.8	0.53
959.14406	0.477	-217.3	6.6	0.44
959.16559	0.483	-223.0	5.1	0.38
959.18851	0.489	-211.8	5.1	0.40
959.21073	0.495	-214.0	6.5	0.38
959.23295	0.501	-218.5	7.7	0.32
959.25587	0.507	-203.9	6.0	0.31
959.27879	0.513	-202.1	12.5	0.29
960.16706	0.751	-187.6	6.5	0.32
960.18928	0.757	-195.0	5.6	0.55
960.21151	0.763	-192.8	4.3	0.49
960.23304	0.769	-190.7	4.4	0.53
960.25526	0.775	-184.5	4.2	0.58
960.27749	0.781	-192.6	3.4	0.52
961.15186	0.015	-140.7	111.9†	0.72
961.17409	0.021	-209.9	116.5†	0.77
961.20326	0.029	-239.3	532.0†	0.90
961.21784	0.033	-230.7	378.1†	0.89
961.24007	0.039	-168.8	20.7	1.10
961.26160	0.045	-192.1	122.9†	1.00
961.28382	0.051	-201.9	32.3	1.20

Table 4.8: H_α measurements for QV Nor - 2

H.J.D	Phasing	RV	error	EW	Depth
2447000+	T_{+ve}	km s^{-1}	km s^{-1}	Angstroms	
957.22931	0.963	125	13	0.699	-0.149
958.18148	0.219	64†	134	4.098	-0.348
958.20370	0.225	49†	251	6.476	-0.444
958.22801	0.231	77†	103	2.845	-0.265
958.25023	0.237	49†	186	4.861	-0.403
959.14406	0.477	-106†	16 1	23.36	-1.631
959.16559	0.483	-64†	137	7.137	-0.548
959.18851	0.489	-100†	575	0.142	-7.980
959.21073	0.495	-14	27	1.636	-0.220
959.23295	0.501	-7	44	1.535	-0.188
959.25587	0.507	-7	39	1.860	-0.218
959.27879	0.513	-4	26	1.322	-0.207
960.16706	0.751	67	7	0.536	-0.157
960.18928	0.757	33	10	1.220	-0.205
960.21151	0.763	62	6	0.517	-0.121
960.23304	0.769	63	11	0.799	-0.143
960.25526	0.775	48	5	0.681	-0.138
960.27749	0.781	43	37	4.695	-0.430
961.15186	0.015	97	45	1.394	-0.168
961.17409	0.021	33†	127	3.463	-0.317
961.20326	0.029	46†	150	5.293	-0.411
961.21784	0.033	112	9	0.440	-0.091
961.24007	0.039	95	12	0.623	-0.105
961.26160	0.045	96	10	0.643	-0.101
961.28382	0.051	118	9	0.525	-0.093

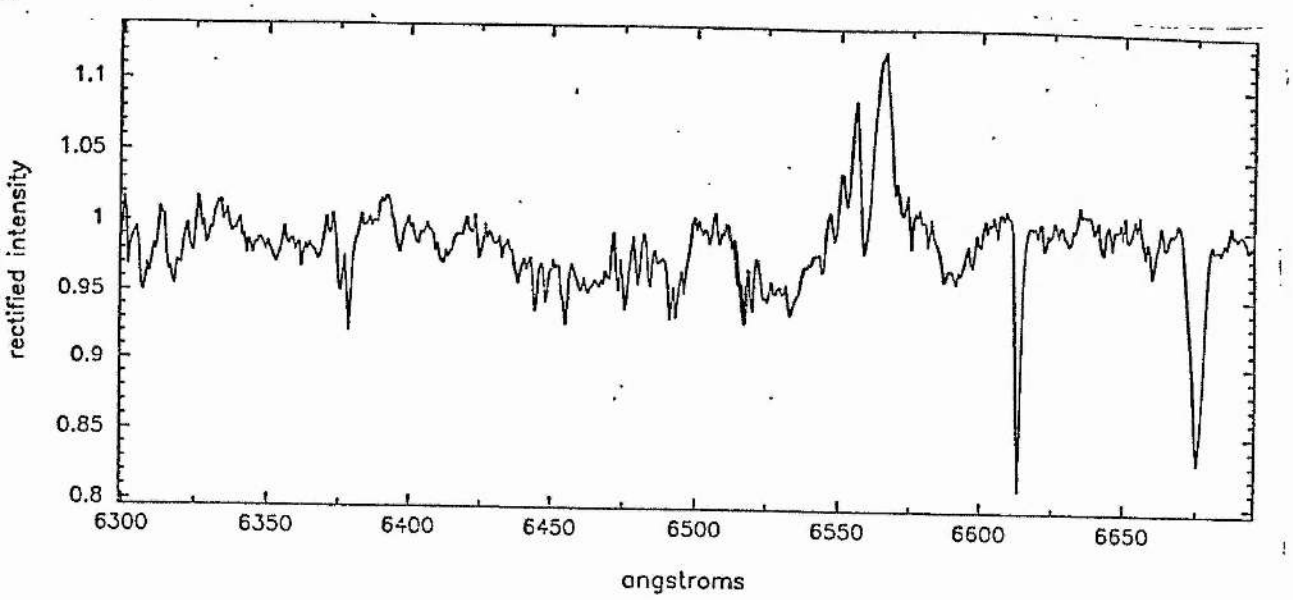

Figure 4.6: Rectified spectrum of QV Nor from all the spectrograms

Table 4.9: H_α measurements for QV Nor - 3

H.J.D	Phasing	RV	error
2447000+	T_{+ve}	Å	
961.17409	0.021	-324	12
961.20326	0.029	-323	11
961.21784	0.033	-319	10
961.24007	0.039	-319	10
961.26160	0.045	-308	29
961.28382	0.051	-318	3

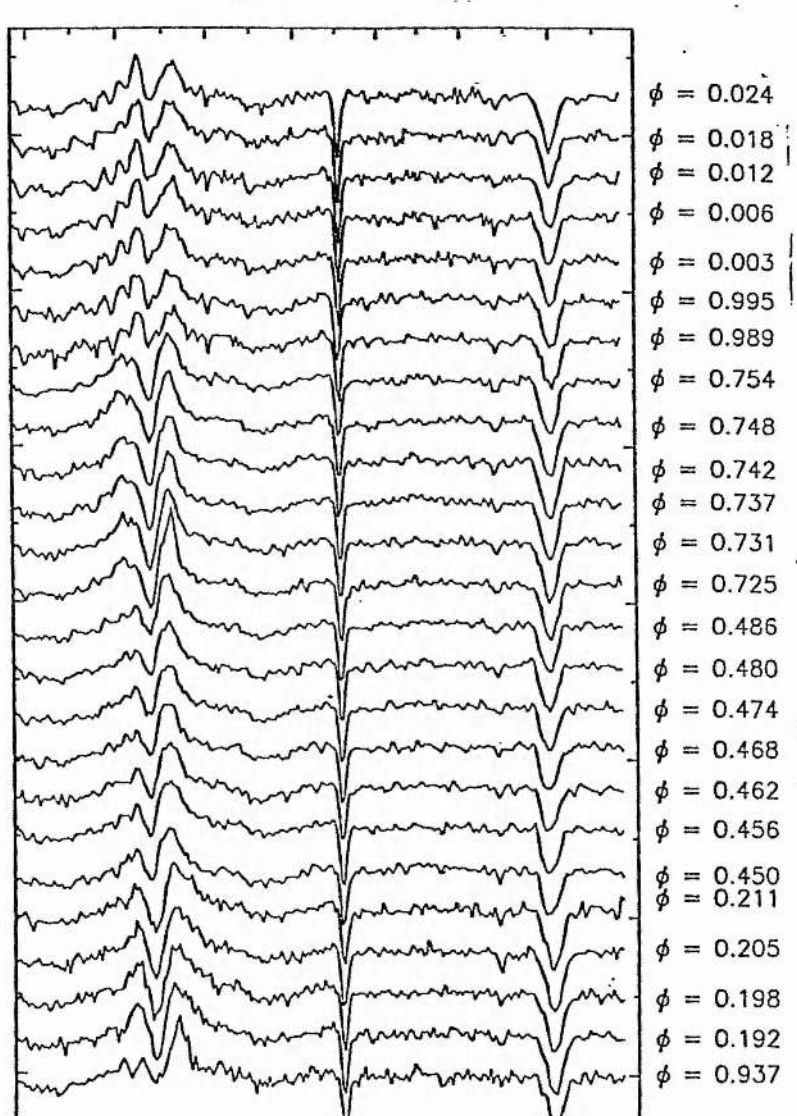

Figure 4.7: The changing profile of H_α

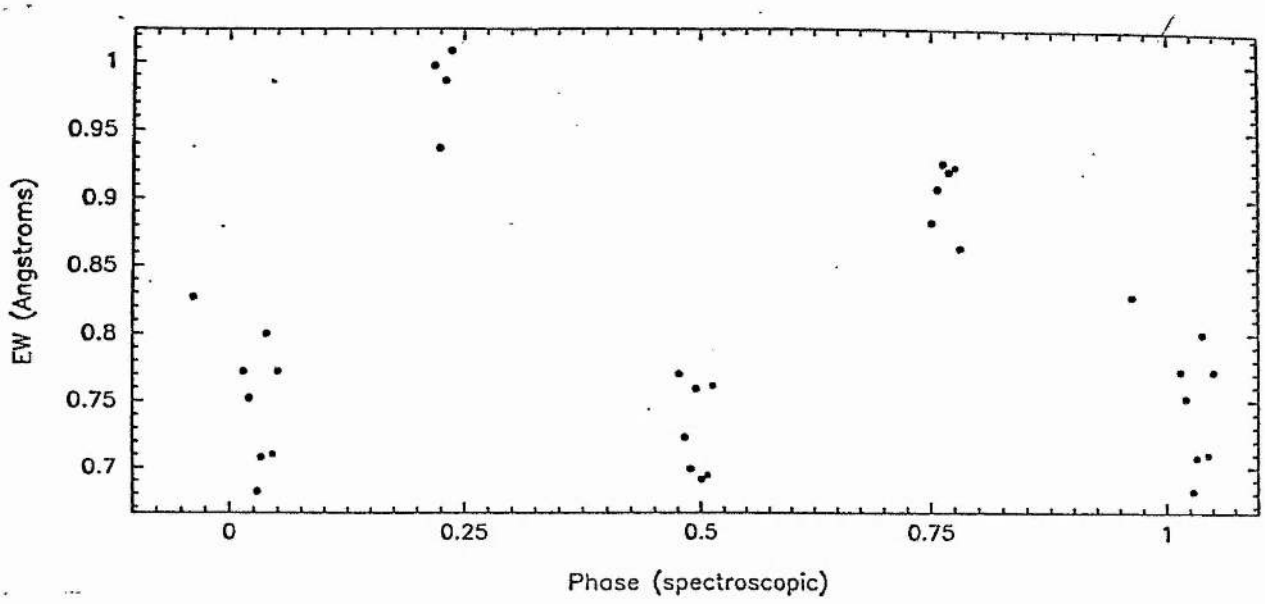

Figure 4.8: HeI 6678 EW measurements

expected in the case of a tidally distorted system with little heating effect. The EW at phase 0.25 is noticeably higher than at 0.75, though this is not reflected in the depth measurements. The reason for this is not clear. If both hemispheres of the star are on average hotter than $\approx 25000\,\mathrm{K}$, then the inner hemisphere is the cooler.

These results are displayed in Figure 8 and Figure 9.

The measured H_α velocities are plotted in Figure 10 and Figure 11.

The data points marked with a dagger in the previous 2 tables have been rejected on the basis of their large associated errors. As can be seen, the absorption profile varies in phase with the HeI line, with a similar semi-amplitude. There is therefore no strong evidence that the "wind" is formed nearer the compact object than the photospheric lines. The very large difference in systemic velocities ($\approx 40\,\mathrm{km\,s^{-1}}$) can presumably be interpreted in terms of the outflow velocity of material (eg Underhill and Doazan, 1982, and references therein). H_α would be expected to show the most negative velocity of the Balmer series. In fact this apparent outflow velocity is rather low, much less than the escape velocity of a typical B-type supergiant, whereas typical wind velocities in

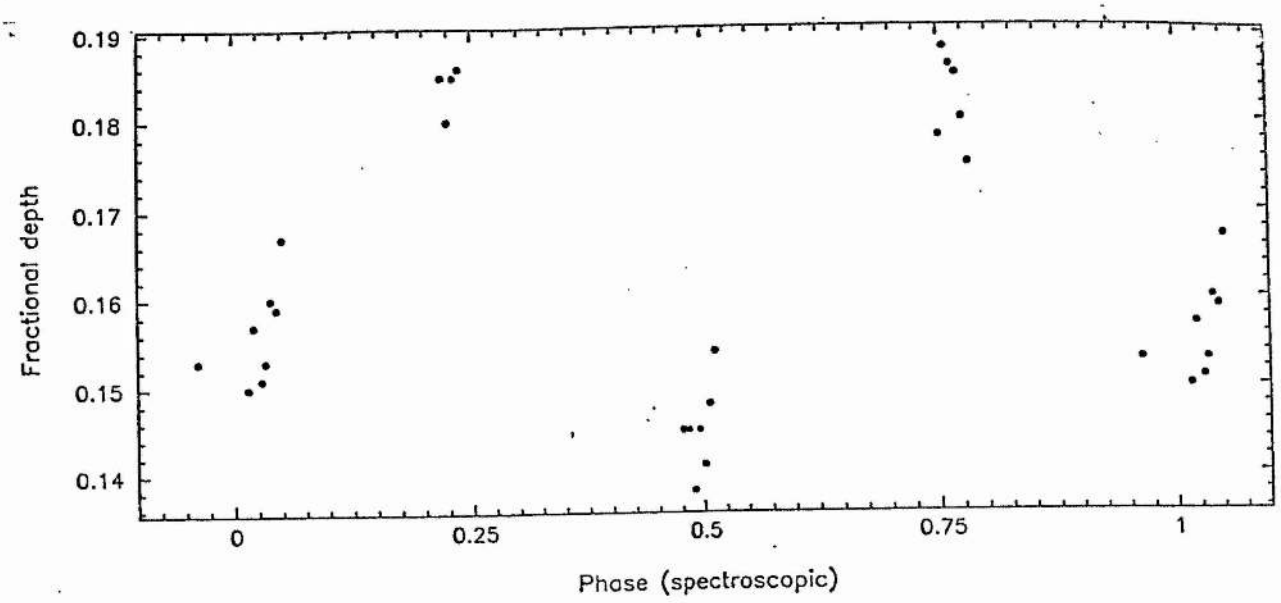

Figure 4.9: HeI 6678 depth measurements

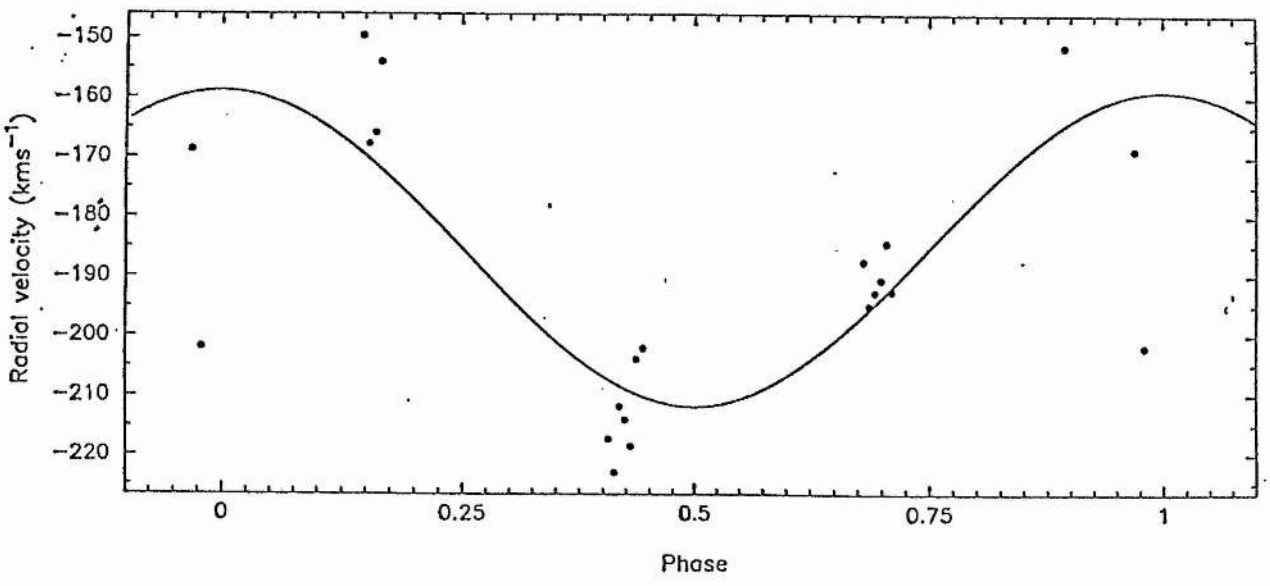

Figure 4.10: H_α central absorption velocities

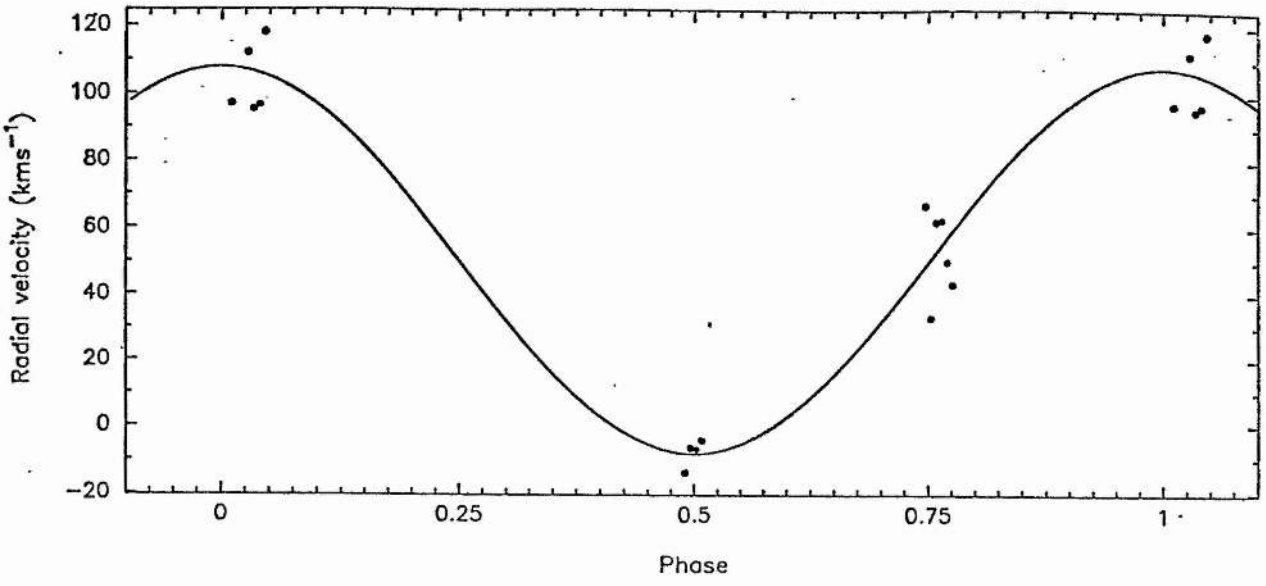

Figure 4.11: H_α redward emission velocities

these systems are usually much higher (Abott, 1978).

Underhill and Doazan suggest that the absorption component characterises mass leaving the star at approximately 2 stellar radii, while Hutchings (1968) suggested that the emission was formed at about 1.5 stellar radii. Both these features therefore arise in the B-star "mantle", a region not yet well modelled. The observed shape did not match exactly any of the profiles described by Rosenthal (1973), although the general profile was reminiscent of a B5 supergiant, HD4841. Visual inspection of the QV Nor profiles showed that, under Rosenthal's criterion, the net EW of the profile would generally be negative (emission was stronger than absorption), as would be expected for an early supergiant under Rosenthal's calibration scheme.

The central absorption feature is deepest at spectroscopic phases 0.25 and 0.75. If this line arises close to the photosphere, this deepening could be attributed to gravity darkening, or due to a increase in opacity of the outflow region along the line of centres. Wind models, however, predict that there will be a high anisotropy along this axis, due to the wind being focussed by the gravitational field of the secondary (Ho and Arons, 1986).

CHC found a value for this line close to the value they derived for the systemic velocity of QV Nor, -173 km^{-1}, which is not therefore in contradiction with the above results.

The redward emission line velocities also vary in phase with the photospheric lines, though the systemic velocity is much higher, at 50 $km\,s^{-1}$, and the semi-amplitude also higher, at 58 $km\,s^{-1}$. It is difficult to interpret this motion without knowing the origin of the emission profile. If however, the profile is simply the "remnant" of a broader emission feature which has been filled in by absorption, the velocity of any peak may have no particular relevance. To investigate this, it is necessary to fit a function to the whole of the profile, after somehow masking the absorption line so that it does not bias the fitting parameters. This proved impossible, so, as mentioned above, gaussians were also fitted to some of the blueward components, in 6 spectrograms taken close together where the blueward feature was deemed sufficiently strong relative to the redward feature.

The velocities derived from 4 of these 6 measurements were then averaged with the corresponding redward velocities (2 of the redward velocities were unavailable, having already been discarded). The average blueward velocity was -316 $\pm$ 3 $km\,s^{-1}$, compared with an average redward velocity of 118 $\pm$ 8 $km\,s^{-1}$. The average of the mean between each red and blue component was -105 $\pm$ 2 km^{-1}. The average photospheric velocity for the star was -131 $\pm$ 3 $km\,s^{-1}$. It would therefore seem that the emission component as a whole (on which the absorption is superimposed) is redshifted by $\approx$ 26 $km\,s^{-1}$ with respect to the photospheric motion. One interpretation would be that the emission feature is caused by inflowing material below the level of the outflow characterised by the absorption.

The weakening of the emission line strength at x-ray eclipse, reported by CHC, is not seen in our study.

4.5.2 Rotational velocity measurements

As described in the previous chapter with regard to the HeI 4026 Åline, the gaussian profile measurements of HeI 6678 Åyield estimates of the FWHM. These results are given in Table 4.10 . The mean FWHM is 4.7 Å. Currently, Hilditch and Reynolds are in the process of deriving an empirical calibration for this line based on Reticon observations of bright $V \sin i$ standard stars. Since this calibration does not yet cover the desired FWHM value, we are forced to adopt the calibration of Hill (private communication) discussed in the previous chapter. The observed FWHM then implies $V \sin i \approx 160$ km s^{-1}. The actual value is expected to be about 217 km s^{-1} for the parameters derived after the inclusion of non-keplerian motion, with no underfilling. CHC reported visual estimates of the rotation of 200 km s^{-1}. The underestimate is attributed to the broadening of the 4471 Åline due to the presence of a forbidden component at 4469 Åwhich is present in main-sequence stars. This will broaden the measured FWHM of the calibration star (provided it is not a supergiant) such that $V \sin i$ implied by the FWHM of the 6678 Åline will be an underestimate.

If the implied rotation is taken as real, which is considered unlikely, a filling parameter β of ≈ 0.73 is required. This is permissible within the eclipse geometry, since, the *lower* value of the eclipse duration is adopted, the filling parameter may be relaxed down to 0.55. QV Nor is not of course obliged to fill its Roche lobe, since there is no firm evidence for a disk. The adoption of a smaller diameter for the primary will tend to decreased the estimated mass of the secondary.

4.5.3 A temperature calibration for HeI 6678 Å

Observations of a number of Reticon B stars are in progress with the aim of establishing a $V \sin i$ calibration. The HeI line should also be a good temperature indicator close to B2, and the measured EW values (for gaussian profiles) obtained to date have been plotted against spectral class in Figure 4.12. The average EW for all spectrograms was 0.82 ± 0.02 Åwhich is intermediate between the EW expected for a B0Ia and a B1Ib.

Table 4.10: HeI rotational measures for QV Nor

H.J.D	Phasing	HeI 6678 FWHM
2447000+	T_{+ve}	Å
957.22931	0.963	5.08
958.18148	0.219	5.06
958.20370	0.225	4.90
958.22801	0.231	5.01
958.25023	0.237	5.09
959.14406	0.477	5.00
959.16559	0.483	4.70
959.18851	0.489	4.75
959.21073	0.495	4.90
959.23295	0.501	4.61
959.25587	0.507	4.41
959.27879	0.513	4.63
960.16706	0.751	4.64
960.18928	0.757	4.53
960.21151	0.763	4.67
960.23304	0.769	4.67
960.25526	0.775	4.82
960.27749	0.781	4.64
961.15186	0.015	4.82
961.17409	0.021	4.50
961.20326	0.029	4.23
961.21784	0.033	4.35
961.24007	0.039	4.69
961.26160	0.045	4.20
961.28382	0.051	4.35

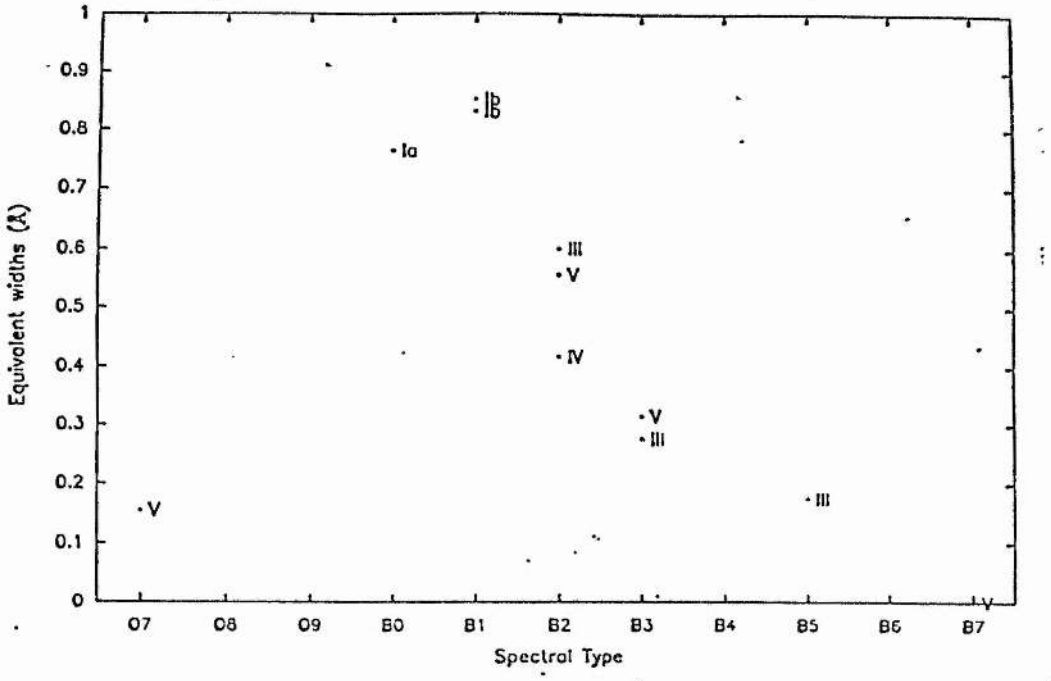

Figure 4.12: HeI 6678 Å EW against spectral type

4.5.4 The absolute magnitude and distance of the system

In principle, the net equivalent width of H_α can be used to determine the absolute magnitude of the system, in the manner described by Rosenthal (1973). Owing to the complicated H_α profile of QV Nor, and its obvious variability, this has not been attempted. The remaining constraint on the distance is the luminosity of the system, derived from its estimated size and temperature. Due to the paucity of temperature-sensitive lines in the red part of the spectrum, the adopted temperature used in this study (see the corrections for non-Keplerian velocities) is a compromise between the value suggested by CHC (31,500 K) and the value reported by Pakull, (25000 K), based on a study by Bohm-Vitense (1981). Since the spectrum shows clear signs of variability, it is evident that there will be a high uncertainty in any temperature derivation.

The detailed velocity analysis yielded a final value for the mass-ratio of 15.61. Assuming again that the star fills its Roche-lobe, a mean radius of 0.614 is derived on the basis of the computed data of Mochnackie (1984). Adopting $i = 70°$, $a \approx 58.7$ lt-secs ($= 1.76 \times 10^{10}$ m), the surface area is 1.47×10^{21} m^2 for a spherical star of the

volume radius as QV Nor.

If T is assumed to be 30000 K, M_{bol} is found to be -8.4. If T is assumed to be 25000K, M_{bol} is found to be -7.6. With E(B-V) = 2.0, A_V = 6.3, which, with the observed m_v = 14.5 gives a distance of $\approx$ 5.8 kpc assuming M_{bol} = -8.3 and BC= 2.8. This is at the lower limit of the generally accepted range for QV Nor. If M_{bol} is taken as -7.6, the star is found to be at $\approx$ 4.0 kpc.

Based on T_{eff}=30000 K, QV Nor is seen to lie near the 25 $M_\odot$ mass tracks on the HR diagram of Maeder and Meynet (1989), as displayed in Figure 14. The location of the star is such that core-hydrogen burning will have ceased. The star will probably have undergone substantial mass-loss, bringing the true value below 25 $M_\odot$.

It is concluded therefore that QV Nor is *not* appreciably over-luminous/sub-massive, as has been repeatedly stated by previous workers (eg Savonije, 1980), and that this apparent discrepancy is probably due to the improved quality of our orbital parameters (smaller semi-amplitude for primary implies smaller radius).

4.6 Discussion

This study has found masses for the component stars in QV Nor which are within normal theoretical mass limits. The large errors on the derived masses can be ascribed to the quality of the x-ray data, which in the case of both the eclipse-timing and pulse-timing is not of a standard comparable to the Roche-lobe overflow driven "bright" sources. The evaluation of improved masses will therefore have to wait until the x-ray data-set is sufficiently reliable. The photometry is also rather inconclusive; although the general picture is one of ellipsoidal variations, some evidence exists for a shift between the heights of successive maxima, perhaps indicative of third-light (accretion disk/vortex?) in the system. The detailed shape of the light-curve is also not well modelled, and this aspect of the system awaits both improved photometry and beter theoretical understanding. This study has found no obvious contradictions in assuming a filled Roche-geometry at a lower inclination than previously adopted. This, in combination with an improved estimate of the size of the primary from the velocity solution,

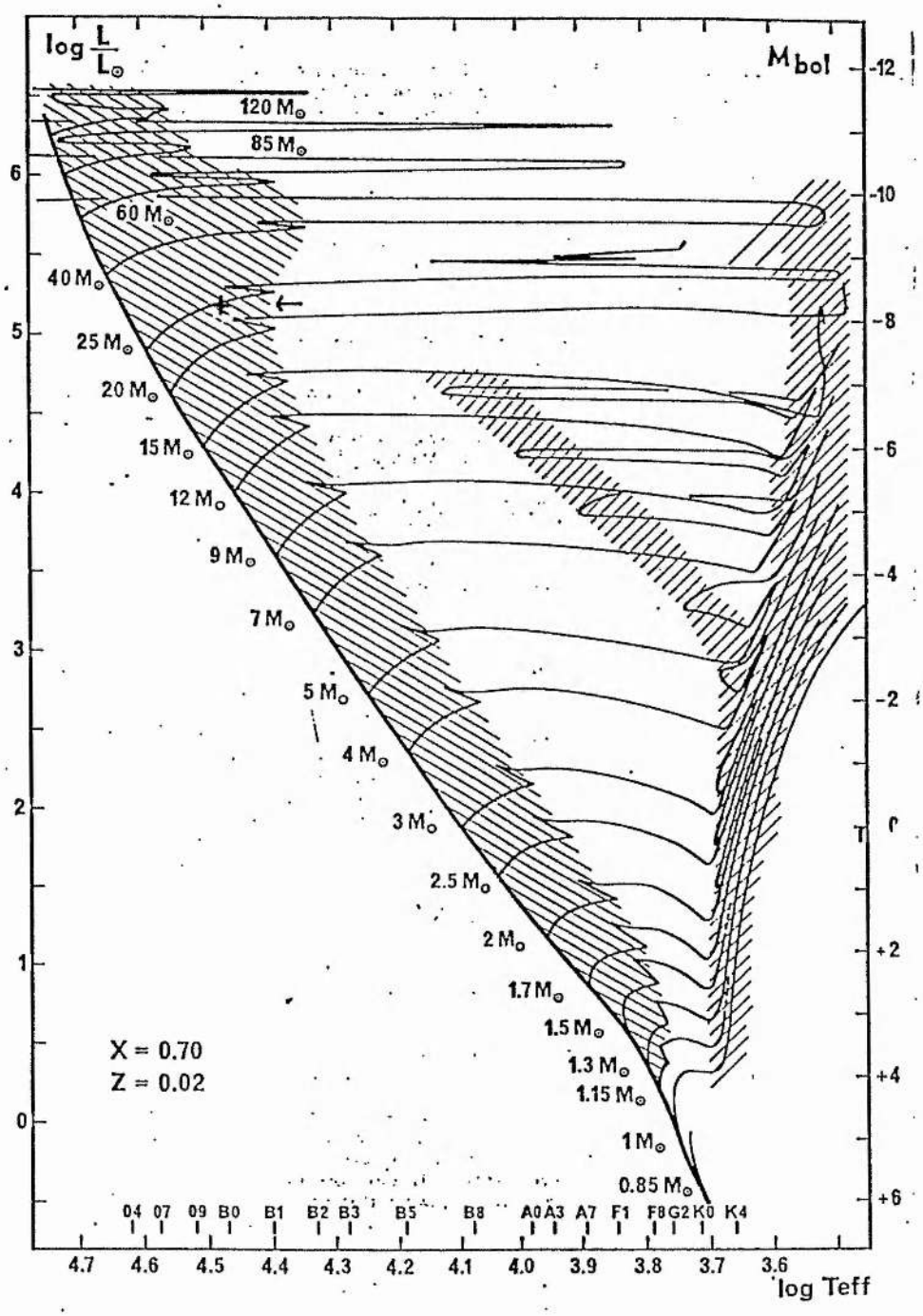

Figure 4.13: QV Nor on the HR diagram of Maeder and Meynet(1989)

predicts the observed depths of the minima to within the accuracy of the photometry. The distance derived for the system is in agreement with previous results. The x-ray luminosity of 4U 1538-42 is more than an order of magnitude less than the Eddington limit (by contrast with SMC X-1); therefore the primary distance constraints are those derived from the optical characteristics of QV Nor.

The spectrum shows marked variability, the photospheric components of which appear to vary in phase with the changing profile of the star. The H_α behaviour is more complex, and does not appear to be strongly linked to the orbital cycle. There is some inconclusive evidence for low velocity inflow and outflow, the outward component of which can be tentatively identified with the wind driving the x-ray source. There does not appear to be any spectroscopic evidence for an accretion disk (eg antiphased emission componenents).

4.7 References

Abott, D.C., 1978. *Astrophys. J.*, **225**, 893.

Corbet, R.H.D., 1984. *The Evolution of Galactic X-Ray Binaries, eds. Truemper, Lewin and Brinkman (Dordrecht:Reidel), p63.*

Crampton, D., Hutchings, J.B., Cowley, A.P., 1978. *Astrophys. Lett.*, **225**, L63.

Hill, G., Fisher, W.A., Poeckert, R., 1982. Publs Dom. Astrophys. Obs, **16**, 27.

Ho, C. and Arons, J., 1987. *Astrophys. J.*, **316**, 283.

Hutchings, J.B., 1968. *Mon. Not. R. astr. Soc.*, **141**, 329.

Ilovaisky, S.A., Chevalier, C., Motch, C., 1979. *Astr. Astrophys.*, **71**, L17.

Maeder, A., Meynet, G., 1989. *Astr. Astrophys.*, **210**, 155.

Makishima, K., Koyama, K., Hayakawa, S., Nagase, F., Astrophys. J.. *314*, **619**,

Mochnaki, S.W., 1984. *Astrophys. J.*, **55**, 551.

Parkes, G.E., Murdin, P.G., Mason, K.O., 1978. *Mon. Not. R. astr. Soc.*, **184**, 73P.

Primini, F., Rappaport, S., Joss, P.C., 1977. *Astrophys. J.*, **217**, 543.

Rosenthal, J.D., 1973. *Astrophys. J.*, **186**, 909.

Savonije, G.J., 1980. *Astr. Astrophys.*, **81**, 25.

Underhill, A., Doazan, V., 1982. *B stars with and without emission lines, (NASA Monograph).*

Chapter 5

Some observations of Cen X-3

5.1 Brief Comment

This chapter presents an incomplete spectroscopic data set of Cen X-3, the principal reason for this incompleteness being that the star was observed off quadrature during the five nights of the study (from which a successful series of observations of QV Nor were drawn). The dates were scheduled according to the ephemeris published in the Eighth Catalogue of the Orbital Elements of Spectroscopic Binary Stars (Batten, Fletcher and McCarthy, 1989) - based on the spectroscopic observations of an earlier group of workers (HCCPW, see below). As is evident, however, that ephemeris had ceased to be useful, partly because of a combination of inherent inaccuracy in the formula and partly because of secular period variations in the system. Lamentably, this author was unaware of a later x-ray ephemeris published in 1984 (Nagase), which would have altered the chosen nights of the observation. Nonetheless, the data are still worthy of interest, in view of the fact that it (by its nature) offers an insight into the long-term periodicity of the system. In addition, the spectroscopic ephemeris is now updated, enabling future workers to schedule their observing with greater confidence (although the period decay should certainly be taken into account).

5.2 The status of Cen X-3

Cen X-3 was the first of the eclipsing pulsating x-ray sources to be linked observationally to an early-type binary, the evolved O-star known as Krzeminski's star (Krzeminski, 1974). Despite the fact that its x-ray parameters are well studied, there has been little spectroscopy performed on the optical star, a fact noted in 1979 by Hutchings, Cowley, Crampton, van Paradijs and White (HCCPW from hereon).

In its broad details, Cen X-3 is similar to SMC X-1 and LMC X-4, and has been tentatively associated with an anti-correlated pulse-period relationship (Corbet, 1984). As was shown in the study of SMC X-1 (chapter 3, this study), this class of system is eminently suited to optical study, since once spectroscopy has been performed, all the information needed to determine the component masses is in place, the proximity of the two stars making eclipses likely and the brightness of the x-ray source allowing accurate pulse-timing. Three spectroscopic studies were published, both based on data accumulated in the early-to-late seventies - Osmer, Hiltner and Whelan (1975), OHW from hereon, published six low dispersion spectrograms which did not permit an orbital solution, HCCPW (1979) published a velocity curve with considerable scatter about the derived sinusoidal solution, while Mouchet, Ilovaisky and Chevalier (1980), MIC from hereon, were only able to demonstrate the *existence* of positive and negative radial velocities, their solution based on just 10 spectrograms. All studies used intermediate to low resolution configurations, using image tube/photocathode spectroscopy and photographic plates. MIC did not derive a semi-amplitude but stated that their observations were consistent with the value of 25 $\mathrm{km\,s^{-1}}$ reported by HCCPW, on the basis of measurements of photospheric HeI lines. Interestingly, the Balmer line measurements performed by HCCPW seem to show only a very marginal radial velocity variation. This is what might be expected from the "classical" picture of tidal-distortion and reflection-effect, where the true orbital variations are suppressed, rather than exaggerated, as would be seen in a heating scenario dominated by a soft x-ray flux. In this respect, HCCPWs observations seem to be similar to those of SMC X-1 reported in this study.

The above authors did however report spectrophotometric evidence for temper-

ature variations of $\approx 3000\,K$ between hemispheres - HeII is stronger relative to HeI during x-ray transit - but these observations were made largely by eye, and are perhaps subject to some reservation, in view of the reported faintness of the x-ray source relative to SMC X-1 (About a factor of ten less luminous, assuming distance estimates are valid).

5.3 Observations and Reduction

40 spectra of Cen X-3 were obtained between 4-10 March 1991 by Dr S A Bell and the author, using the RGO spectrograph on the AAT in conjunction with the 25 cm camera and the 1200B grating, with the GEC CCD detector. These observations were made in the first half of each night, before tilting the grating into the red to perform observations of QV Nor (Chapter 4). The spectral range chosen covered 4290-4710 Å, with a dispersion of $33\,Å\,mm^{-1}$, giving a wavelength on pixel of 0.7 Å. The chosen spectral region yielded several helium lines, as well as some interstellar features, and the HeII emission feature at 4686 Å. Because of the early-type nature of the primary, the helium features are weaker than in QV Nor, and it was decided against using the single line at λ 6678.

The exposure times were 1800 seconds, giving a typical S/N (stable from night to night) of ≈ 40. The reduction and measurement was performed in the same manner as for SMC X-1 and QV Nor, using the previously mentioned FIGARO and DAO software packages. A variety of standard stars observed in the blue and red spectral regions established that the velocities were on the standard system.

The adopted template used for cross-correlation purposes was a co-added spectrum based on all the Cen X-3 data; this was then sharpened once after velocity measurements were obtained. The template was measured by cross-correlation against two Reticon B-star spectra; these gave consistent results to within 2 $km\,s^{-1}$. The value adopted was that with the smallest associated error. The template velocity was then taken to be $57 \pm 1\ km\,s^{-1}$. As a check on the external consistency of these measurements, it is gratifying to see that the derived systemic velocity of the system agrees with the value obtained by HCCPW to within 1 $km\,s^{-1}$ (see later) - a result to be expected

since HCCPW omitted Balmer lines from their estimate. Thus the result is not biassed by the usual velocity progression that might be seen if heating was operational, or if a strong stellar wind was present.

The cross-correlation measurements were made after defining windows across the spectrogram that left out the Balmer lines, He emission features and interstellar bands. The windows included the λ 4471 HeI line and the λ 4541 HeII line. The 4388 HeI line was not used on the grounds of its weakness.

The derived velocities are shown in Table 1 and Table 2, where several spectra have been rejected on the basis of low S/N or very poor cross-correlation profiles.

Table 3 shows the parameters derived from the raw data. As can be seen, the semi-amplitude is poorly defined - a consequence of the fact that that the data are clustered around conjunction, rather than the times of quadrature. Unfortunately, this limits the usefulness of the data in constraining the system masses, although the ephemeris is well defined. As can be seen from Figure 1, however, the sinusoidal fit to the data would clearly be poor if the amplitude was constrained to the HCCPW value. This is difficult to explain, and in the absence of further observations, no attempt will be made to do so; suffice to note that the spread of velocities in the HCCPW data is even larger than the extreme difference observed in this study. Some additional observations at the times of quadrature predicted by this analysis were unfortunately prevented by instrument problems on the nights in question.

It was also not possible to combine the data of HCCPW or MIC with our own, since neither of these authors published their individual velocity measurements. Aslanov and Cherapashchuk (1982) reexamined the data but did not indicate how they obtained the velocities, which again were not tabulated. The low-dispersion (102 $\text{Å}\,\text{mm}^{-1}$) observations by OHW were presented, however, and these have been added to the new data. A second orbital solution was generated, with the systemic velocity, semi-amplitude, period and T_{+ve} as free parameters. The new period differed only slightly from the adopted value used in the first solution (see Table 4), suggesting that the old data does show orbital variation, and is not merely instrumental scatter. The resulting solution is graphed in Figure 2, with the supplementary data represented by

Table 5.1: Radial velocity data for Cen X-3

H.J.D	Phasing	Observed Velocity	O-C Residuals
2447000+	T_{+ve}	$Km\,s^{-1}$	$Km\,s^{-1}$
956.957	0.776	62.1	+12.2
956.979	0.787	55.6	1.7
957.004	0.799	35.4	-22.7
957.025	0.809	49.1	-12.8
957.056	0.824	81.3	14.3
957.945	0.250	15.5	-24.6
957.968	0.261	25.8	-10.0
957.991	0.272	40.8	9.1
958.022	0.287	18.8	-7.3
958.142	0.344	13.2	7.1
958.895	0.705	24.8	1.8
958.918	0.716	36.3	9.3
958.940	0.726	11.4	-19.5
958.963	0.737	31.9	-3.2
959.015	0.762	64.1	19.5
959.038	0.774	62.9	+14.1
959.060	0.784	66.7	+14.0
959.086	0.797	55.4	-1.9
959.109	0.807	68.6	+7.5
959.968	0.219	55.0	+3.2
959.992	0.230	32.0	-15.3

Table 5.2: Radial velocity data for Cen X-3 (continued)

H.J.D	Phasing	Observed Velocity	O-C Residuals
2447000+	T_{+ve}	Km s^{-1}	Km s^{-1}
960.014	0.241	43.1	-0.2
960.037	0.252	46.4	+7.3
960.059	0.263	37.4	+2.3
960.082	0.273	31.3	+0.2
960.110	0.287	30.6	+4.6
959.133	0.298	46.9	+24.9
960.920	0.675	15.3	+2.9
960.943	0.686	5.4	-10.9
960.987	0.707	13.3	-10.5
961.016	0.721	18.8	-10.1
961.038	0.732	37.0	+4.1
961.061	0.743	33.3	-3.8
961.084	0.754	46.2	+4.9
961.105	0.764	33.2	-12.0

Table 5.3: Orbital Parameters for Cen X-3

V_{opt}	$+39.9 \pm 2.1$ km s^{-1}
K_{opt}	61 ± 9 km s^{-1}
e	0.000†
Ω	0.000†
P_{orb}	2.08712†
T_{+ve}	47957.42 ± 0.01

† — adopted value

Table 5.4: Parameters derived with addition of the OHW data

V_{opt}	$+34.2 \pm 3.1$ km s^{-1}
K_{opt}	57 ± 10 km s^{-1}
e	0.000†
Ω	0.000†
P_{orb}	2.08716 ± 0.00002
T_{+ve}	47957.41 ± 0.02

† — adopted value

starred points.

5.4 Orbital decay in Cen X-3

The problem of interpreting the shift in the expected times of maximum positive velocity (T_{+ve}) is by no means simple. What is apparent is that, since the HCCPW ephemeris was first published, the star's relative orbital phase has shifted by about half a day. The elapsed time between these two spectroscopic studies is about 4370 days, requiring a shift of 0.0001 days per day, or 0.0002 days per cycle. This is several orders of magnitude higher than the individual error in any separate estimate of the period, but is of the same order as the reported changes from estimate to estimate. The shift can therefore be ascribed to secular period variations in the system. It is more difficult

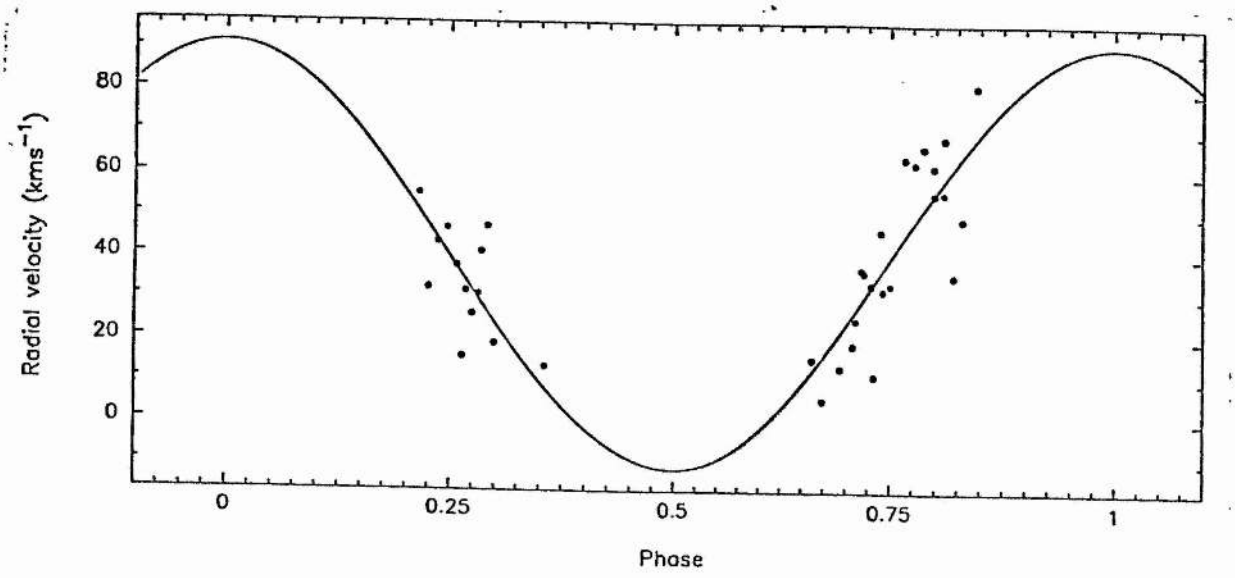

Figure 5.1: The velocity curve of Cen X-3

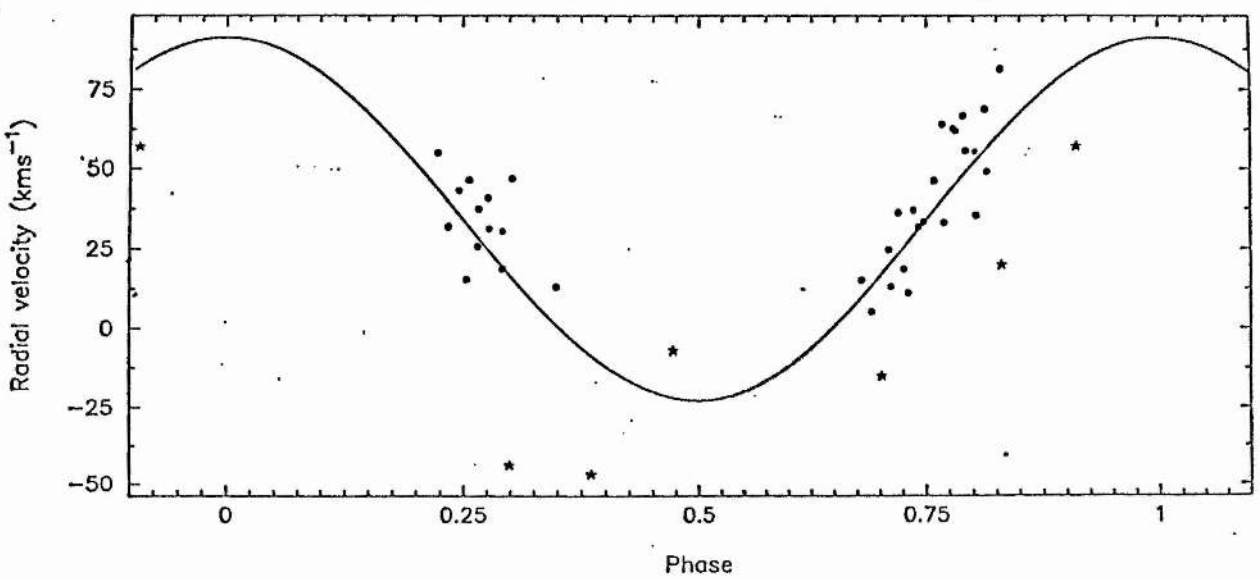

Figure 5.2: The velocity curve including the data of OHW

to relate this observation to a quantitative estimate of the rate of change of the orbital period. The period of Cen X-3 is known to vary haphazardly, with the general trend seeming to be a gradual decrease in the orbital period. All of the x-ray derived epochs published by Kelley (1984) show the system reaching eclipse earlier than expected relative to a given ephemeris. Furthermore, as the x-ray data has accumulated, widely differing estimates of the orbital period change have been published. For instance, Fabbiano and Schreier give $\dot{P}_{orbital}/P_{orbital}$ = -8 ($\pm$ 4) $\times$ 10^{-6} yr^{-1}, while Kelley gives -1.7 ($\pm$ 0.04) $\times$ 10^{-6} yr^{-1}, based on second-order polynomial fits to the eclipse times. The later estimate may be the more meaningful, since it is over a greater time span (the decay rate is known to fluctuate on a monthly time-scale).

All the x-ray epochs published by Kelley are derived from pulse-timing analyses. It is therefore possible to relate these data to the time of maximum positive velocity obtained from this spectroscopic study (whereas true eclipse centres cannot be *exactly* related to spectroscopic phase, since the x-ray minimum may not occur precisely at the time of transit of the optical star, due to complicating effects such as disk precession, etc). Based on the ephemerides of Kelley and the data collated by Kelley et al (1983), as well as the data of Murakami (1983) and Nagase et al (1984), each 'eclipse centre' determined by *pulse timing* was used to determine the O-C (delay in minutes between the event and the prediction), including the 'eclipse centre' determined by spectroscopy (see Table 5 and Figure 3). The time axis covers over 3500 cycles, with data from 1971 - 1990. The data show a large gap between 1983 and our observation, which is unfortunate. The author is not aware of any pulse timing analysis performed during this interval. Assuming equal weighting, zero uncertainty for each point, a second-order polynomial was fitted to the data (solid line in Figure 3). The coefficient of the second order term is then twice the linear period change (see Kelley, 1984, Fabbiano and Schreier, 1977). The epoch quoted by HCCPW is not used, on the basis of its large associated error. It is found that the decay rate, $\dot{P}_{orbital}/P_{orbital}$ = -1.98 ($\pm$ 0.04) $\times$ 10^{-6}, a higher rate of decay than seen by Kelley but still not as large as the earlier result of Fabbiano and Schreier. If the spectroscopic epoch is omitted, and the remaining x-ray data fitted likewise, the derived decay rate is -1.84 ($\pm$ 0.04) $\times$ 10^{-6}. This is equivalent to the Kelley estimate but differs slightly, presumably due to the lack of weighting of the data in this derivation. If the polynomial fit obtained in this manner

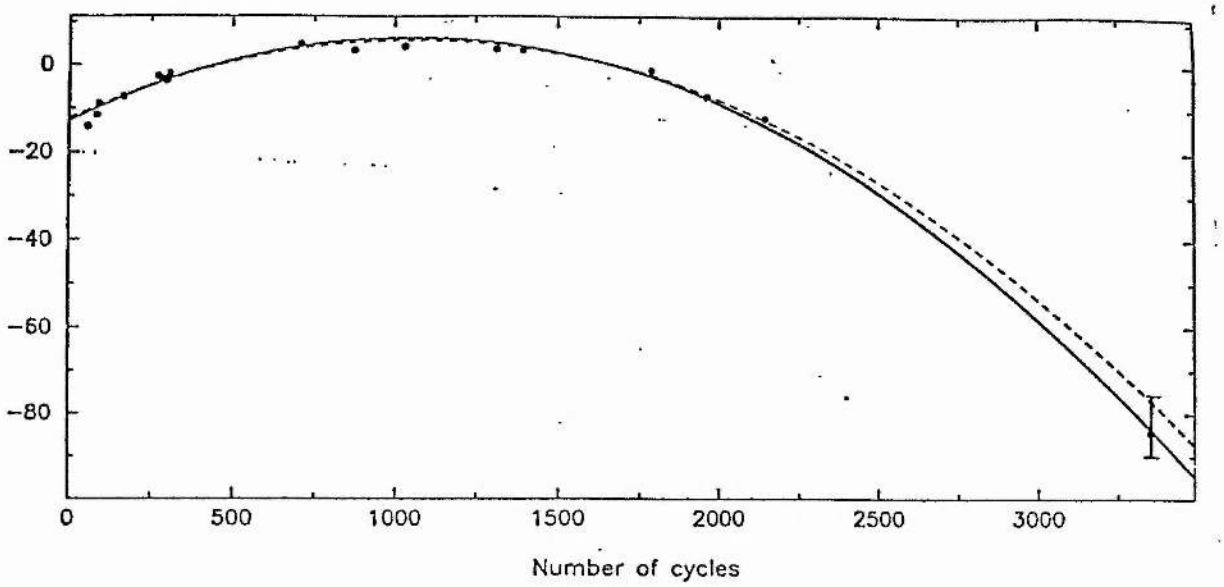

Figure 5.3: Eclipse time O-C diagram for Cen X-3

is extrapolated (dashed line in Figure 3), it predicts that the spectroscopic epoch will occur $\approx$ 5 - 7 mins later. This is however within the uncertainty of the optical epoch ($\approx$ 12 mins), and it thus seems clear that the orbital decay rate of Cen X-3 has stayed constant (to within 10%) since the mid 1970s.

This derived rate of period decay may be discussed in terms of the possible modes of mass-transfer occurring in the system. Evidently (see Kelley, 1984), the observed rate is several orders of magnitude in excess of the expected rate for conservative mass transfer, but it is already known that Cen X-3 is a high wind-loss system, and that only about 0.1 % of the mass in the wind is captured by the pulsar. It is not quantitatively clear what fraction of the observed luminosity is generated by conventional Roche lobe overflow, compared to that fed by the wind (see, for instance, Ho and Arons, 1987). This ambiguity is important since the wind carries less angular momentum than the gas stream, and will thus play a different role in influencing the pulse-period evolution.

Table 5.5: Eclipse delays in Cen X-3

T_e = 958.859144 + 2.08711652n			
Cycle Number	H.J.D	Time delay	Observatory
57	1077.81497	-14.1	Uhuru
83	1132.08181	-11.5	Uhuru
91	1148.78051	-9.0	Uhuru
166	1305.31533	-7.4	Uhuru
273	1528.64010	-2.7	Uhuru
284	1551.59798	-3.3	Uhuru
293	1570.38199	-3.3	Uhuru
295	1574.55610	-3.5	Uhuru
296	1576.64330	-3.4	Uhuru
297	1578.73037	-3.4	Uhuru
298	1580.81722	-3.8	Uhuru
300	1584.99193	-3.1	Uhuru
303	1591.25328	-3.1	Uhuru
304	1593.34025	-3.4	Uhuru
307	1599.60212	-2.6	Uhuru
308	1601.68930	-2.5	Uhuru
309	1603.77671	-2.1	Uhuru
709	2438.628	+4.6	Ariel-V
876	2787.1755	+3.3	OSO-8
1032	3112.76642	+4.3	SAS-3
1314	3701.33275	+3.6	OSO-8
1395	3870.38910	+3.5	SAS-3
1786	4686.4470	-1.6	Hakucho
1960	5049.6025	-7.3	Hakucho
2142	5429.45421	-12.3	Tenma
3353	7956.90	-84.4	St-And

5.5 Spectral variations in Cen X-3

In view of the restricted phase coverage of the data, the analysis of individual line profiles will yield little information about the temperature distribution of primary. It was however considered worthwhile considering the λ 4686 HeII emission feature for phase-related velocity variations, since this spectral component is generally assumed to arise in the vicinity of the secondary (in the disk or the gas-stream/disk impact hot-spot). MIC found an apparently well-defined anti-correlation (based as it was on only six points), with an amplitude of $\approx$ 800 km s^{-1}. As was evident from a cursory examination of our spectra, the emission peak was not always well-defined, and was highly variable from spectrum to spectrum (ie on a time-scale of hours or less).

The general profile was crudely similar to the H_α profile seen in QV Nor, but with a substantially weaker central absorption, and with a tendency for the redward peak to be much broader than the blueward (when the blueward was visible at all). Assuming that the emission feature is located on the edge of the disk, and assuming that the absorption is photospheric, the emission feature would be expected to exhibit a sinusoidal variation from blue to red (unlike the case in QV Nor where the feature appeared to be associated with the photospheric motion of the primary). However, whereas the night 4 data clearly shows the blue peak dominating, the night 2 data does not, in contradiction with the $\approx$ 2 day period of the system. It was therefore decided to measure the emission features in the red and the blue, on every spectrogram, where the features were sufficiently strong.

The measurements are shown in Table 6 and displayed against the previously determined phases in Figure 4, the redward measures shown in filled circles, the blueward in open circles, with a sinusoidal variation of amplitude 400 km s^{-1} graphed through, in antiphase with the photospheric motion of the primary component. Starred points represent the average velocities on images where both peaks were measured. There is no obvious correlation with the theoretical curve, hence the result of MIC is not confirmed. HCCPW also failed to find any such correlation. We conclude, therefore, that there is no conclusive spectroscopic evidence for the hot-spot on the disk, although it might be more apparent at quadrature. Note that the phasing need not be shifted by

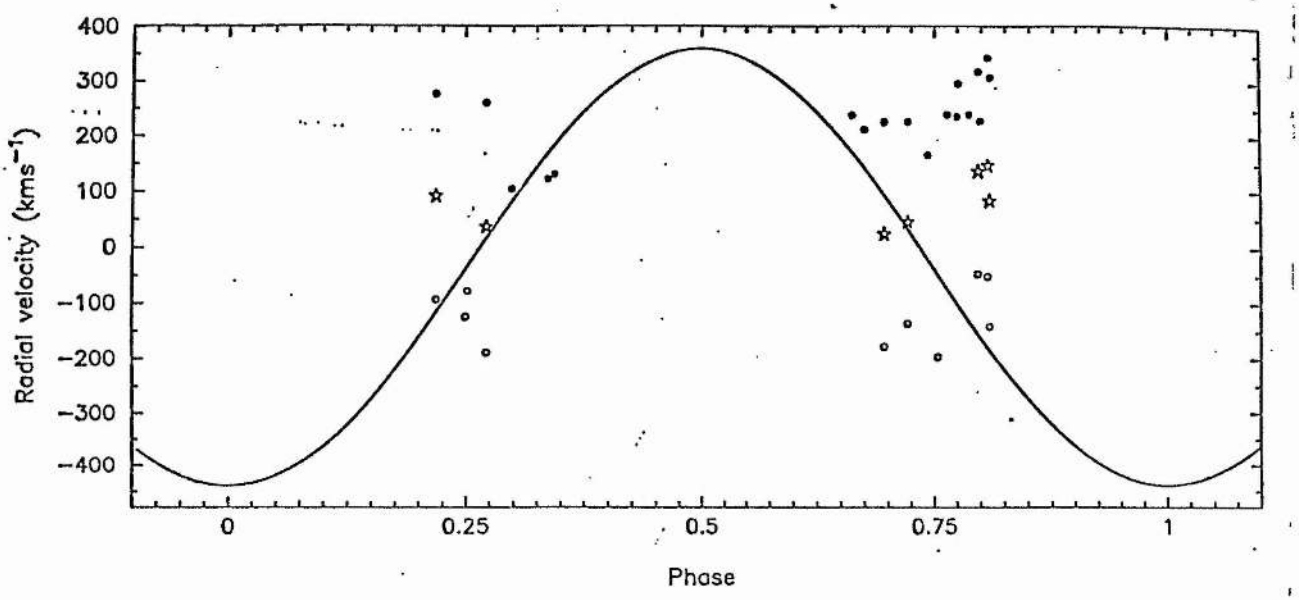

Figure 5.4: HeII velocities with a sinusoid of amplitude 800 km s^{-1}

exactly 0.5, since the hotspot would probably lie off-axis of the line of centres, the exact distance depending on whether or not the disk fills its available space (see Hutchings et al, 1977).

5.6 Comments

Clearly Cen X-3 warrants further study, not least to complete the spectroscopic phase coverage. It will be interesting to see whether other observers deduce a large value for the semi-amplitude, as may be hinted at by our data; such a result would be difficult to reconcile with the current picture of HMXRBs, and would presumably indicate that some velocity-distorting mechanism was functioning. Since K_x is reasonably well determined, 415 km s^{-1} (Schreier et al, 1972), the observed semi-amplitude of this study implies a mass ratio M_{opt}/M_x of at most ≈ 8.8. For a 1.4 $M_\odot$ neutron star, therefore, the mass of the optical component would have to be as low as 12 $M_\odot$. Assuming a Roche geometry, (see Chapter 1 for details of this discussion), the optical star would have an effective radius of $\approx 0.57 \times a$. Taking the known eclipse half-angle, 39°, the

Table 5.6: HeII emission velocities

H.J.D	Phasing	Redward Velocity	error	Blueward Velocity	error
2447000+	T_{+ve}	Km s^{-1}	km s^{-1}	km s^{-1}	Km s^{-1}
956.957	0.776	296.74	75.4	—	—
956.979	0.787	240.42	8.2	—	—
957.004	0.799	229.74	10.1	—	—
957.025	0.809	309.11	25.2	-140.84	7.2
957.056	0.824	240.70	117.8 *	—	—
957.945	0.250	252.14	141.0 *	-124.82	1.4
958.048	0.299	104.27	32.3	—	—
958.127	0.337	122.57	19.3	—	—
958.142	0.344	130.50	55.3	—	—
958.895	0.705	139.34	401.6 *	—	—
958.940	0.726	260.13	260.13*	—	—
959.015	0.762	177.67	178.9 *	—	—
959.038	0.774	237.52	87.5	—	—
959.086	0.797	319.29	10.0	-45.89	3.2
959.109	0.807	344.03	30.4	-50.29	6.8
959.968	0.219	277.25	20.0	-94.43	13.1
959.992	0.230	—	—	-126.13	93.7 *
960.037	0.252	—	—	-78.37	14.5
960.081	0.272	261.5	—	-189.10	24.5
960.897	0.662	239.49	11.3	—	—
960.920	0.675	213.25	52.6	—	—
960.943	0.686	127.97	145.1 *	—	—
960.965	0.696	226.96	8.4	-178.39	3.7
961.016	0.721	227.27	4.4	-136.16	43.4
961.061	0.743	166.89	80.5	—	—
961.084	0.754	217.71	163.4 *	-196.44	15.3
961.105	0.764	241.08	3.4	—	—

* — rejected measurement

equation for i *cannot* be solved. If we take the upper limit whereby $\sin i = 1$, this requires that the sine of the eclipse half-angle be equal to the fractional size of the primary, 0.57. The eclipse duration would then have to be 34°, outside the quoted error of 2°. This may however be a permissible assumption (see below). The limited nature of these data is nonetheless stressed.

Cen X-3 was the star which was first described as being "undermassive", a status subsequently accorded to most of the observed optical candidates of the x-ray pulsars, though (see Chapters 3 and 4) perhaps not justified in the light of new results. With Cen X-3, however, the question is still open, and the possibility that Krzeminski's star is in some way abnormal should not be ruled out. Future workers should take into account the findings of Clark, Minato and Mi (1988), that the reported eclipse-duration is an inappropriate estimator of the geometric size of Cen X-3 (ie the eclipse defines a region wider than the photospheric radius, owing to attenuation by the wind or extended atmosphere of the star), and should take into account the faint possibility that the system may be in a tidal, rather than a Roche configuration (rotation may not be synchronous). In concluding, the Cen X-3 system *can* be understood in the light of these observations, so long as the inclination angle is very close to 90° and the eclipse duration is reinterpreted. Van den Heuvel (1983) expects that the mass of the helium star in an HMXB progenitor system would have been around 10 $M_{\odot}$, so the system would have avoided disruption during the supernova.

5.7 References

Aslanov, A.A, Cherepashchuk, A.M., 1982. *Soviet astr.*, **26**, 177.

Batten, Fletcher, McCarthy, 1989. *Eight Catalogue of the Orbital Elements of Spectroscopic Binary Stars, (DAO publication)*

Clark, G.W., Minato, J.R., Mi, G., 1988. *Astrophys. J.*, **324**, 974.

Corbet, R.H.D., 1984. *The Evolution of Galactic X-Ray Binaries, eds. Truemper, Lewin and Brinkman (Dordrecht:Reidel), p63.*

Fabbiano, G., Schreier, E.J., 1977. *Astrophys. J.*, **214**, 235.

Ho, C., Arons, J., 1987. *Astrophys. J.*, **316**, 283.

Hutchings, J.B., Crampton, D., Cowley, A.P., Osmer, P.S., 1977. *Astrophys. J.*, **217**, 186.

Hutchings, J.B., Cowley, A.P., Crampton, D., van Paradijs, J., White, N., E., 1979. *Astrophys. J.*, **229**, 1079.

Kelley R.L., Clark, G.W., Petro, L.D., Rappaport, S., 1983. *Astrophys. J.*, **268**, 790.

Kelley, R.L., 1984. *The Evolution of Galactic X-Ray Binaries, eds. Truemper, Lewin and Brinkman (Dordrecht:Reidel), p75.*

Krzeminski, W., 1974. *Astrophys. Lett.*, **192**, L138.

Murakami, T., Inoue, H., Kawai, N., Koyama, K., Makishima, K., Matsuoka, M., Oda, M., Ogawara, Y., Ohashi, T., Shibazaki, N., Tanaka, Y., Hayakawa, S., Kunieda, H., Makino, F., Masai, K., Nagase, F., Tawara, Y., Miyamoto, S., Tsunemi, H., Yamashita, K., 1983. *Astrophys. J.*, **264**, 563.

Mouchet, M., Ilovaisky, S.A., Chevalier, C., 1980. *Astr. Astrophys.*, **90**, 113.

Nagase, F., Hayakawa, S., K II Tsuneo, Sata, N., Ikegami, T., Kawai, N., Makishima, K., Matsuoka, M., Mitani, K., Murakami, T., Oda, M., Ohashi, T., Tanaka, Y., 1984. *Publs astr. Soc. Japan*, **36**, 667.

Osmer, P. S., Hiltner, W. A., Whelan, J.A.J., 1975. *Astrophys. J.*, **195**, 703.

Schreier,E., Levinson, R., Gursky, H., Kellog, E., Tananbaum, H., Giacconi, R., 1972. *Astrophys. J.*, **172**, L79.

Van den Heuvel, E.P.J., 1983. *Accretion driven stellar x-ray sources, eds Lewin and van den Heuvel (Cambridge University Press).*

Chapter 6

A long-term spectroscopic study of X Per

6.1 The enigma that is X Persei...

X Per is the brightest x-ray binary in the northern hemisphere (at its brightest, just within the range for naked-eye detection), yet also one of the most poorly understood of all the systems in the category. Only in the last few years has a basic model arisen which can encompass the various observational facts that have been uncovered in recent decades, yet it is still far from canonical, in the sense that one might use the term with reference to QV Nor or SMC X-1. In 1988, it was decided to embark on a 3-year observational program using the telescope facilities in St Andrews, in order to obtain a longer and more frequently sampled data set than had been obtained to date. The principal aim was to search for velocity variations, but the data would also show spectral variations in the star on a timescale ranging from days to years. Interestingly, during the period of study, X Per underwent a pronounced photometric decline, which may be interpretable as the loss of its disk. This is probably the only detailed spectroscopic study conducted around the time of the event in question (see later).

6.2 The status of X Persei

X Persei is known as a variable ($\approx$ 0.6 mag) Be star of spectral type around O9.5IIIe, but subject to considerable uncertainty. It has long been associated with the transient pulsating x-ray source 4U 0352+30 (Braes and Miley, 1972, van den Bergh, 1972), which undergoes semi-regular flare-ups on a timescale of around 580 days. Most authors ascribe this to a 580 day orbital period, in which the flare-ups are due to the periastron passage of the compact object through the circumstellar environment of the Be star. Such transient events are known among other Be/x-ray systems, and in some cases the velocity variations do appear to share the same periodicity. There are, however, problems in extending this model to encompass the longer period transients. Hutchings et al, (1974, HCCR hereafter) published parameters indicative of very large amplitude Balmer line variations which at the time meant that X Per had the highest mass-function of any known binary system, and was thus proposed as a black-hole candidate, assuming a "normal" mass for the optical star. Hutchings, (1977), published supplementary velocity measures which showed that there were in fact no detectable velocity variations in the HeI lines above the 5 $\mathrm{km\,s^{-1}}$ level, although the published data were rather sparse with regard to time resolution. Milgrom (1975) and Penrod and Vogt (1985) have both discussed this discrepancy in terms of emission components contaminating the photospheric Balmer lines, such as to render the impression of high-amplitude orbital variations, while other workers have invoked putative hierarchical triple systems involving black-holes *and* neutron stars, or apsidal motion in a close binary. It is perhaps too early to dismiss any one model in favour of another, but it is an unavoidable fact that almost all the other black-hole candidates pegged in the mid seventies turned out to have more prosaic explanations, and that, bearing in mind the welter of evidence from X Per which plainly contradicts such a hypothesis, it would be suprising indeed if the black-hole model were correct.

That said, the cause of the emission contamination is still a mystery; Penrod and Vogt discuss the possibility of tidal distortions in the Be "disk" (in this discussion, use of the term disk will be taken to refer to any extended circumstellar structure), which would act on an orbital timescale. Unfortunately, the environments of Be stars are still highly conjectural; ironically, the most advantageous probes of these stars have been

the x-ray sources themselves.

Corbet (1984) points out that the Be/x-ray systems show a pulse-period correlation, apparently due to the pulsars' Alfven and corotation radii being on average equal. Since the size of the Alfven radius depends on the accretion rate, and hence the density of the surrounding medium, the spin-rate will depend on the distance of the pulsar from the Be star. This relationship is only borne out if the 580 day period is explicitly taken to be orbital. It is interesting to note that, on Corbet's diagram (reproduced in Chapter 1), X Per lies well to the right of the correlation. To bring it in line requires that the true period be $\approx$ 300 days (assuming P_{pulse} = 835 seconds).

Penrod and Vogt (1985) obtained two spectra of X Per eight months apart in 1983, using a Reticon system, at 0.5 Åresolution and high S/N, covering the same spectral region as HCCR. By stripping away emission profiles from the Balmer lines, they were able to show that the underlying absorption profiles were consistent with the low amplitude (ie unseen) variations in the neutral helium lines, and that there were no large shifts between the observations. However, their two observations, scheduled according to HCCR's ephemeris, did not enable the period or geometry of the system to be estimated with greater certainty than before - all that was now clear was that the Balmer velocities were spurious. There was still need for a saturation-coverage study of the star over a period in excess of two years, with observations taken as frequently as possible in view of the fact that the system might well be highly eccentric (indeed, the nature of the transient flare-ups clearly suggested that eccentricity was present.)

6.3 Observations and Reduction

Between February 1989 and March 1991, around 130 Reticon spectra of X Per were gathered on the 0.5 m Leslie Rose Telescope (LRT). The spectrograph, mounted at the Cassegrain focus, has been in service since 1988 (Edwin, 1989). During the two full seasons of the program, observations were made on every available (ie clear) night between early September and late March. The LRT was largely given over to this project for the period involved, although supplementary spectra for other programs were obtained during periods of the year (or night) when X Per was inaccessible. A

typical night's observing would involve the taking of two or three 3000+ second exposures on X Per , the observation of radial velocity standard stars, plus the observation of a number of early stars for the purposes of compiling a high S/N template against which to cross-correlate the program spectra. Most of the X Per spectra were taken in the blue, covering 3930 - 4570 Å, at a dispersion of 25 Å mm^{-1}, with a resolution of $\approx$ 0.5 Å. One spectrogram was obtained in the H_α region to investigate the possibility of using the 6678 ÅHeI line for a velocity determination (as in Chapter 4 of this study). Presumably because of the relative earliness of X Per in relation to QV Nor, the line was not usable, being broad and shallow in the examined spectrogram.

An additional sixteen CCD spectra at a variety of dispersions and central wavelengths were obtained as service observations on the 2.5m Isaac Newton Telescope (INT) on La Palma. These spectra were taken at irregular times between February and December 1990. In some instances the spectra could not be used for radial velocity determinations, owing to the absence of useful features around high dispersion spectra of H_α. The reduction and analysis of these INT frames was performed in the same manner as the observations discussed in the preceding three chapters. Radial velocities had to be determined on an individual line basis by fitting gaussian profiles, since there were no suitable templates available for cross-correlation.

Throughout the course of the X Per program, radial velocity standard stars had been observed as a matter of course. These established that the spectrograph velocities were on the IAU system. Over the two winters, 1988-1989 and 1989-1990, the mean difference between observed and standard velocities for F-K standard stars was (O-S) = -0.3 $\pm$ 2.2 $km\,s^{-1}$ (Hilditch et al, 1991). For the winter 1990-1991, the mean (O-S) for 55 F-K standards was 0.9 $\pm$ 1.0 $km\,s^{-1}$.

The observed B-type templates proved unsatisfactory for cross-correlation against the X Per spectra, many of which were exceptionally noisy. It was decided to form a single template from 5 spectra taken on one night (HJD = 2447857), giving a S/N in excess of 50. The cross-correlation window was then defined so as to pick up only the most reliable HeI lines: 4026, 4387, 4471 Å, omitting Balmer, metal and continuum features. The template velocity was fixed at -21 $km\,s^{-1}$ - a somewhat arbitrary value (see below). As was immediately evident during the measuring procedure, the derived

velocities showed large scatter, with a range between successive spectra on a given night of up to 20 km s^{-1}. This is quite characteristic of Be-stars, even when the S/N is much improved, and convinced us that only a very large data set would serve to reveal any systematic variations.

The derived velocities are shown in Tables 1 - 4.

The spectra measured against the template had an average velocity close to zero, indicating that the template's adopted velocity should be close to the systemic velocity of X Per . Four high S/N early-star templates were available. Correlation against an O9.5V secondary standard gave a template velocity of -25 $\pm$ 2 km s^{-1}. A B3V star gave a template velocity of -21 $\pm$ 2 km s^{-1}. A B2IV star gave -10 $\pm$ 2 km s^{-1}, while a B1I gave -11 $\pm$ 2 km s^{-1}. It was decided to adopt a value of -21 km s^{-1} in view of the fact that the later dwarf B-type may be a better spectral match to X Per in terms of line widths than either of the earlier B-types (see Chapter 3 for a similar argument). The value was also reasonably close to that given by the O-type.

Interestingly, the average of all the INT velocities was found to be -21 $\pm$ 4 km s^{-1}, though as this data set is less well distributed in time, this may not be significant. However, it is noted that the adopted systemic velocity is entirely consistent with the HeI velocities published by Penrod and Vogt (1985), as well as the velocities in Hutchings (1977). It therefore seems satisfactory to merge the INT data set with the Reticon observations before proceeding with any further analysis, with the caveat that the Reticon velocities may be systematically in error (blueshifted) by up to 10 km s^{-1}. The mean of this data set is -22 $\pm$ 2 (s.e) km s^{-1}.

To investigate the Balmer contamination problem already mentioned, all the Reticon spectra were remeasured, using a different CCF window that also included H_δ and H_γ. It was already obvious from a visual inspection of the data that emission of some sort was present in many of the spectra, though there did not seem to be any smooth progression with time. The Balmer lines alone yielded noisy, unmeasurable CCFs in even the best S/N spectrograms. The mean of this data set was 0 $\pm$ 4 (s.e) km^{-1}. The results are displayed in Tables 5 - 7.

Table 6.1: Reticon velocities for X Per - 1

H.J.D	Velocity	H.J.D	Velocity
2440000+	Km s^{-1}	2440000+	Km s^{-1}
7568.377	-10	7864.562	-26
7570.353	-5	7864.644	-18
7574.433	+48	7865.512	-41
7596.354	-71	7866.507	-51
7957.378	-17	7866.569	-18
7957.433	-67	7866.629	-25
7601.357	+18	7883.411	+4
7603.402	-48	7898.410	-16
7607.366	-65	7904.403	-26
7840.619	-24	7920.328	-11
7853.520	-23	7920.379	-33
7853.580	-15	7920.415	-32
7855.575	-24	7926.389	-22
7855.630	-20	7931.365	-12
7857.534	-25	7931.401	-39
7857.570	-16	7931.466	-41
7857.623	-32	7935.373	-21
7857.667	-3	7935.425	-17
7857.704	-15	7935.484	-37
7864.503	-23	7938.417	-14

Table 6.2: Reticon velocities for X Per - 2

H.J.D	Velocity	H.J.D	Velocity
2440000+	$Km\,s^{-1}$	2440000+	$Km\,s^{-1}$
7938.410	-22	8215.581	-33
7938.417	-15	8215.617	-16
7938.456	-49	8215.652	-2
7964.446	-32	8223.466	-29
7970.400	-22	8223.516	-5
7978.343	+0	8223.551	-35
8138.663	-39	8224.447	-10
8148.628	-28	8224.483	-35
8198.511	-57	8228.485	-19
8198.554	-26	8228.522	-33
8198.586	-49	8228.561	-31
8199.515	-41	8229.496	-11
8199.550	-34	8230.472	-30
8199.595	-32	8230.530	-28
8199.631	-31	8230.566	-30
8214.571	+4	8237.441	-12
8214.611	-20	8237.482	-9
8215.467	-22	8237.528	-24
8215.508	-36	8239.457	-25
8215.544	-24	8239.507	+0

Table 6.3: Reticon velocities for X Per - 3

H.J.D	Velocity	H.J.D	Velocity
2440000+	$Km\,s^{-1}$	2440000+	$Km\,s^{-1}$
8239.558	-18	8277.427	-12
8240.445	-12	8278.383	-4
8240.484	-11	8279.377	-31
8240.527	-20	8287.469	-76
8271.381	-26	8300.365	-25
8271.430	-47	8300.414	-15
8271.474	-21	8308.408	-21
8272.385	-12	8308.447	-19
8272.431	-4	8312.350	-36
8272.473	-21	8312.395	+30
8273.395	-38	8313.357	-34
8274.405	6	8313.409	-46
8274.441	35	8319.347	-34
8277.387	+6	8321.361	-24

Table 6.4: INT data for X Per

H.J.D	Velocity	Error	Velocity
2440000+	$Km\,s^{-1}$	$km\,s^{-1}$	λ region
7944.378	-48	10	Blue
8136.651	-13	13	Red
8136.684	-31	5	Blue
8175.769	-13	8	Red
8210.653	-23	7	Blue
8210.656	-22	6	Blue
8210.658	-26	7	Blue
8210.671	-10	17	Red
8210.673	-41	30	Red
8210.674	-35	28	Red
8252.617	+5	4	Blue
8252.629	+3	4	Blue

(Note that these measurements are with respect to a zero-velocity template, since it was not intended to merge them with any external data sets.)

6.4 New constraints on the orbital parameters of X Per

The data from Tables 1 to 4 (ie omitting Balmer lines) should contain evidence of the underlying photospheric motion. To investigate this, the data were folded and phased according to the ephemeris of HCCR, ie $T_N = T_{+ve} + 580.5N$, $T_{+ve} = 2442091$. The folded data were subjected to a least squares sinusoidal fit using RVORBIT, in which the period and phase was constrained; the resultant amplitude of the fit, -1.0 $\pm$ 2.1 km s^{-1}, is, lamentably, fully consistent with scatter about the systemic velocity (given as -22 $\pm$ 2 km s^{-1}). While the real amplitude might be correspondingly low, one would at least expect it to be positive (see Figure 1), if the variations reported by HCCR were apparent in these data. Note that the times of quadrature, based on the above ephemeris, would have occurred during the times of observation.

A visual inspection of the plotted Balmer data showed no clear variations superimposed on the scatter. This was unexpected, since modulations with the semi-amplitude reported by HCCR ought to have been particularly prominent. The Balmer data was also phased according to the ephemeris above (Figure 2).

Since the above procedure failed to yield significant variations at the reported period, it was decided to subject the data to a period-searching procedure using several techniques. Extensive use was made of the program PULSAR (Skillen, 1985). The data are in the form of an unevenly spaced time series with noise, and may be multiply periodic (because of non-radial pulsations, disk effects, and so on, which can operate on sub- or super-orbital timescales). Although such additional periodicities may be manifest in the data, they have not been searched for, since the recovery of higher order frequency components requires the unambiguous identification of the principle frequency, which in this case has proved impossible.

Even though the data are not sampled at an absolutely constant frequency, there will nonetheless be enforced regularities, since observations tend to be taken at the same

Table 6.5: Balmer velocities for X Per - 1

H.J.D	Velocity	H.J.D	Velocity
2440000+	Km s^{-1}	2440000+	Km s^{-1}
		7864.503	+12
7568.377	+1	7864.562	+3
7570.353	+25	7864.644	+17
7574.433	+6	7865.512	-34
7596.354	+39	7865.566	-134
7957.378	+29	7865.578	-66
7957.433	-67	7866.507	-6
7601.357	+55	7866.629	-47
7603.402	-83	7883.411	-10
7607.366	+7	7898.410	+40
7840.619	+29	7904.403	+44
7847.530	+46	7920.328	-60
7853.520	-31	7920.379	-31
7853.580	-13	7920.415	-129
7855.575	+50	7926.389	+31
7855.630	-34	7931.365	+4
7857.534	-32	7931.401	+8
7857.570	+18	7931.466	-5
7857.623	-53	7935.373	+18
7857.667	+26	7935.425	+11
7857.704	+18	7935.484	-45

Table 6.6: Reticon Balmer velocities for X Per - 2

H.J.D	Velocity	H.J.D	Velocity
2440000+	Km s^{-1}	2440000+	Km s^{-1}
7938.365	-15	8215.544	44
7938.410	-2	8215.581	-15
7938.417	-10	8215.617	+23
7938.456	+30	8215.652	-27
7964.446	+20	8223.466	-6
7970.400	+88	8223.516	-20
7978.343	+16	8223.551	-10
8138.663	+13	8224.447	+56
8148.628	+14	8228.483	-8
8198.511	-12	8228.485	-20
8198.554	+0	8228.522	+16
8198.586	+16	8228.561	-26
8199.515	+49	8229.496	-61
8199.550	+47	8230.566	-6
8199.595	+0	8230.530	+50
8199.631	+50	8230.566	+30
8214.508	-26	8237.441	+24
8214.611	+36	8237.481	-13
8215.467	-45	8237.528	+43
8215.501	-45	8239.457	+25

Table 6.7: Reticon Balmer velocities for X Per - 3

H.J.D	Velocity	H.J.D	Velocity
2440000+	$Km\,s^{-1}$	2440000+	$Km\,s^{-1}$
8239.507	+60	8277.427	-57
8239.558	+18	8278.383	-26
8240.445	-33	8279.377	52
8240.484	-9	8287.469	-27
8240.527	+13	8300.365	+82
8271.381	+29	8300.414	+89
8271.430	+3	8308.408	-31
8271.474	+19	8308.447	+77
8272.385	+48	8312.350	-59
8272.431	-34	8312.395	-63
8272.473	-17	8313.357	-26
8273.395	+21	8313.409	-4
8274.405	-33	8319.347	-54
8274.441	-76	8321.361	+18
8277.387	+51		

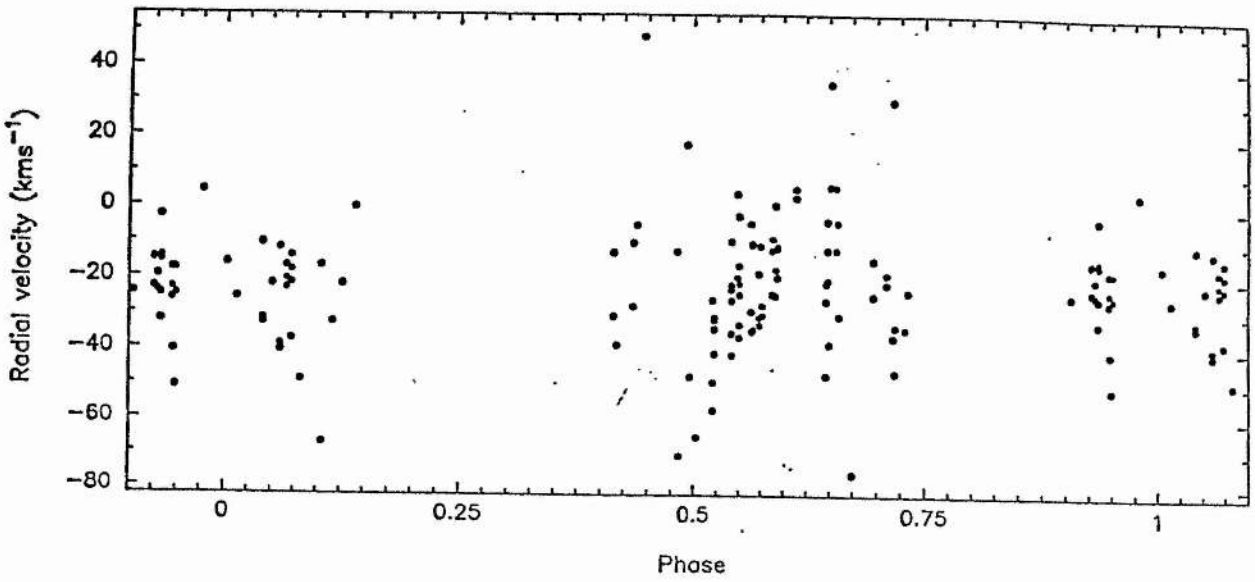

Figure 6.1: The data folded about 580.5 days (see text)

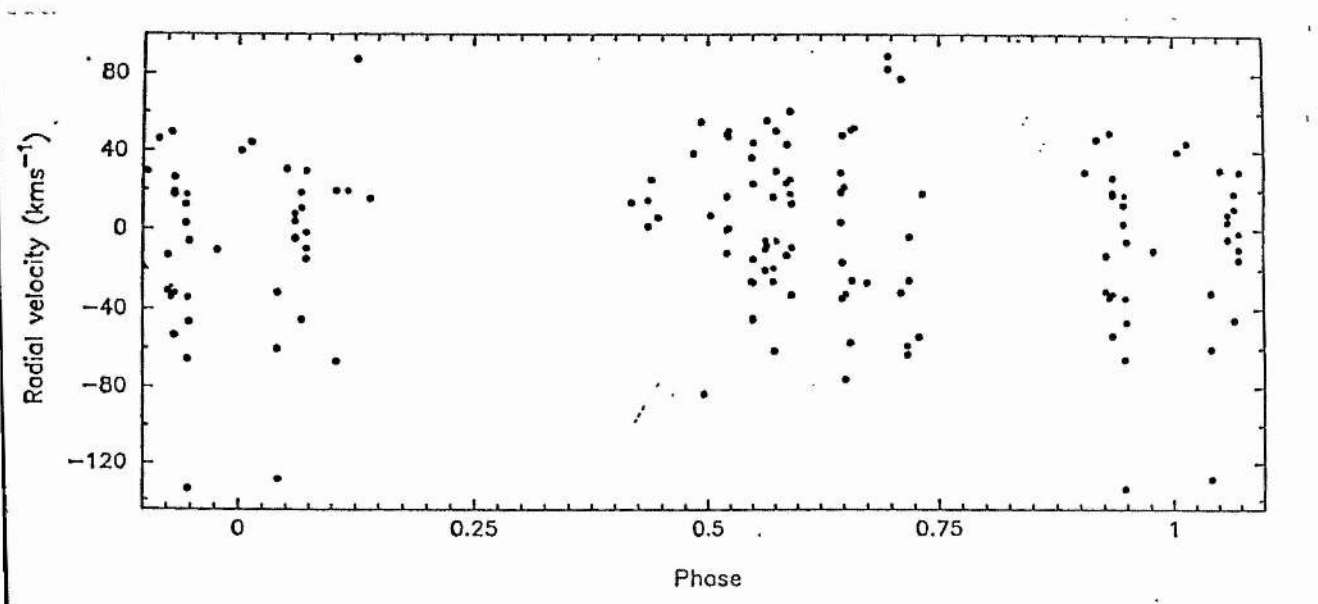

Figure 6.2: The Balmer data folded as above (see text)

time each night, same month each year, and so on. This will result in distant sidelobes in the power spectrum (quasi-aliases) which may be mistaken for actual periodicities, particularly when their amplitude is large. In order to highlight genuine periodicities, "window" spectra can be generated. The window spectrum probes the sampling function's influence on the power spectrum, being the particular power spectrum where each data point on a given time is constant (as if a noise-free radial velocity standard star had been observed), and where features in the power spectrum are entirely a consequence of the sampling interval. The noise spectrum is related, but replaces each observation by a computed point of gaussian noise (or adds additional noise to the observations already made). Broadly speaking (see Skillen), if there is a distinct peak, and if there is no other peak of comparable height, it is most likely that the peak in question is genuine.

The period search was initially confined to the interval spanning 10-600 days (0.0016 - 0.1 in the frequency domain), computing a grid of transforms at a frequency spacing of 0.0005. The search was restricted to frequencies short of 0.1 in the interests of efficiency, since any periods in the data shorter than 10 days were very unlikely to be genuine.

The data window spans over 700 days, longer than the anticipated period. Within a data-block, say one night's observing, the average spacing between observations is far shorter than the minimum period of interest that is being probed for. Conventional aliasing, therefore, is very unlikely, but quasi-aliasing will in general always be present in astronomical observations. This arises because the bandwidth of the noise may be considerably higher than the band-limit of any variations, and will thus behave as undersampled "signal".

Power spectra (equivalent to periodograms in the frequency domain) were made of the entire data set, and also of subsets comprising the observations from the first two seasons and the third season. The power spectrum of the whole program is notable for the appearance of a pronounced peak at a frequency corresponding to approximately 30 days, with more than half the power again of any other feature seen (see Figure 3). This peak has distinct sidelobes which seem to correspond to the sidelobes seen in the power window, indicative of quasi-aliasing at around 250 days, for which there is no

immediately obvious physical reason. Interestingly, the power window (Figure 4) is largely devoid of other aliases at frequencies shorter than 0.1 days^{-1}. When evaluated over a sufficiently long frequency axis, strong one day sidelobes are seen; these are to be expected in this form of data set, for reasons mentioned above.

The 30-day periodicity is completely absent in the subset of data covering the first two seasons (Figure 5). Based on this alone, it would be unwise to identify the 30 day feature with a genuine periodicity, since it would surely be apparent in the earlier data set. Although some of these early spectra are exceptionally noisy, the s/n for the winter 89-90 is probably no worse on average than that for 90-91. In fact, the periodogram from the first two seasons contains a peak and associated sidelobes feature centered on around 0.075 in the frequency domain (13 days). This peak is still seen in the full set of data, but is swamped by the "noise" in the spectrum to the extent that it does not obtrude as a significant feature. The power window for the first two seasons shows strong pairs of sidelobes at around 2 days (Figure 6), which give rise to quasi-aliases spaced by 0.5 in the frequency domain. The power spectra are too noisy to ascertain the identity of true generating peaks and their aliases, and no periodicity is thus inferred.

The data from the final season (Figure 7) largely dictate the relative significance of the peaks in the full set of data, but are far less noisy. No periodicity is suggested at 13 days, and this is therefore not likely to be astrophysical.

It is possible that the feature at 30 days (and indeed that at 13) arises as a consequence of a distant sidelobe *spilling over* from the negative frequency domain, or as the conventional sidelobe of a generating peak in the positive domain. To investigate this, the third-season power spectrum was recomputed between 0.8 to 1.2 (where the central peak generating such a sidelobe would lie in the positive frequency domain). A very strong peak was found at around 0.968 to 0.97 (see Figure 8). This was approximately 3.5 times the power of the peak located at 1.03. Since 1-0.97 is 0.03, it is concluded that the 30 day feature *is* spurious. For the sake of completeness, the power spectrum was also evaluated out to a frequency limit of 2 (Figure 9), using a coarser grid, to identify the relative strengths of the various components. This revealed a strong feature short of 0.5 days, believed to be the other quasi-alias. Other features were also evident, none

of which appeared real. The power window for the final (third) season is shown in Figure 10. The spectrum shows a strong one-day sidelobe.

A perusal of the literature has failed to find evidence for any *other* reported periodicity in X Per on or around 30 days, whereas one would presumably be expected if there was spectroscopic motion on this timescale (neither is there any reported periodicity around 13 days). The INT observations can be exempted from blame since the periodograms were broadly similar in shape before the La Palma data were added to the data set. A periodicity in the x-ray flux at 22.5 hours has been reported by several authors (see Penrod and Vogt), but this is not thought to be associated with the aforementioned one-day signal in the 90-91 data.

A Lafler-Kinman period search was also implemented from within PULSAR. Simply put, this procedure evaluates a parameter, theta, which is related to the sum of the squares of the distance between the ordinates of each data point when they are arranged in phase-space (ie in the time domain). The period which minimises theta is then the "best". In general, if theta is ≈ 2, the data contain no periodic components. As can be seen (Figure 11), the resulting variation of theta is not greatly suggestive of any particular period, nor is it substantially less than 2 at any point. However, the Lafler-Kinman technique is best at searching for periodicities in sharply discontinous data (light curves, etc), and may thus not be best suited where the underlying variations are likely to be very smooth (in the case of a long period binary).

A string-search algorithm was also utilised, based on the formula discussed by Dworetsky (1983), and run using a code supplied by Hill (private communication). This is conceptually similar to the Lafler-Kinman technique, but evaluates the string-length between co-ordinates after they have been phased, rather than just the differences in the ordinates. Again, the period is indicated by the smallest string length. The expectation value of the parameter is, also, strongly conditioned by the random errors in the sample. The resulting variation in string-length is graphed in Figure 12. Interestingly, the two deepest dips are seen at ≈ 0.031 and ≈ 0.078 - close to the two frequencies highlighted above.

The mean of the variation is clearly around 9.4. For a purely sinusoidal underlying

variation, this implies that the additional string length due to random noise is ≈ 8, since the noise-free string length of a sinusoid is ≈ 1.4. Dworetsky gives an empirical formula for estimating this term based on assumed random errors in the sample. Working backward, one can infer that, if variations are present, Dworetsky's error parameter *epsilon* must be in the range 0.2 - 0.25. Then, if we adopt a tentative value for the underlying motion's semi-amplitude of 5 km s^{-1}, this implies an internal standard error of an observation of $2 \times 5 \times 0.2$, ie a value of 2 km s^{-1}. One rough estimate of the actual internal standard error can be gained from considering the statistics of a single night's observing. For the night running from 2447857.534 to 7857.704, the standard deviation for the five derived velocities is 5.3, giving a standard error of 2.4 km s^{-1}. If there are sinusoidal variations present, therefore, they are constrained (approximately) such that $K_{opt} \times epsilon = 2.5$. Of course, the real variations may not be sinusoidal, in which case, *epsilon* can be reduced.

As an aside, no periodicity near a year has been detected in any of these procedures, which is itself a check on the internal consistency of the data reduction with regards to the derivation of the heliocentric velocities (see Margoni et al, 1988). The one-day periodicity in the third season is not thought to be related to the sidereal day, since it clearly lies at a slightly *longer* period than a day.

At the risk of seeming over-cautious, therefore, it is concluded that this study has yielded no evidence for spectroscopic motion in the X Per system. The implications of this are now considered.

6.4.1 The orbit of X Persei

The absence of observable variations in the helium lines, as observed over a 2 year period, is consistent with the results of Hutchings (1978) and supports the conclusions of Penrod and Vogt (1985). The failure to detect any variations in the Balmer lines is less easy to explain, since the large amplitude motions reported by HCCR would certainly have been detected in this study. One possibility may be that (see following section) the Be "disk" itself has dissipated during the interval of this program. The disk was mentioned by Penrod and Vogt as a possible origin for their purported 580

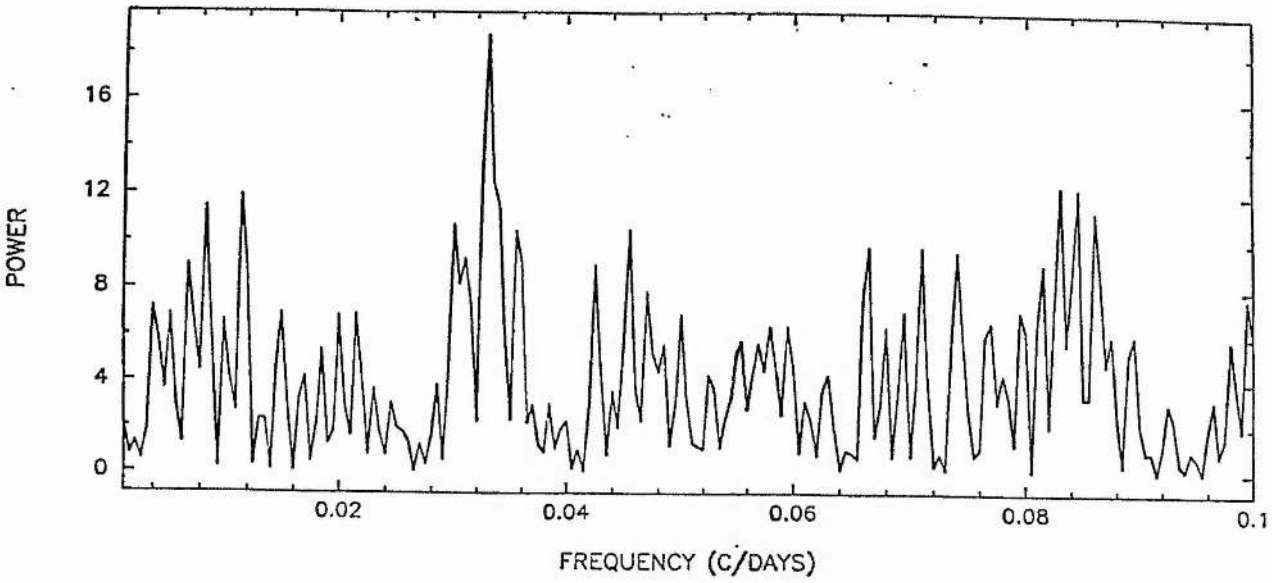

Figure 6.3: X Per power spectrum (see text)

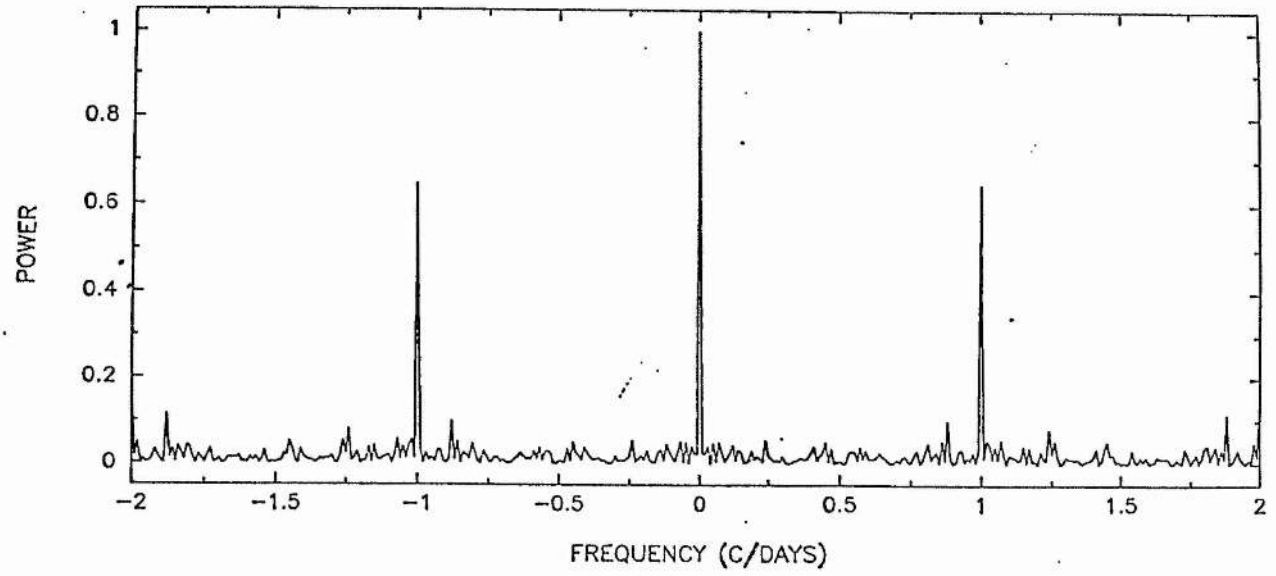

Figure 6.4: Power window for whole program (see text)

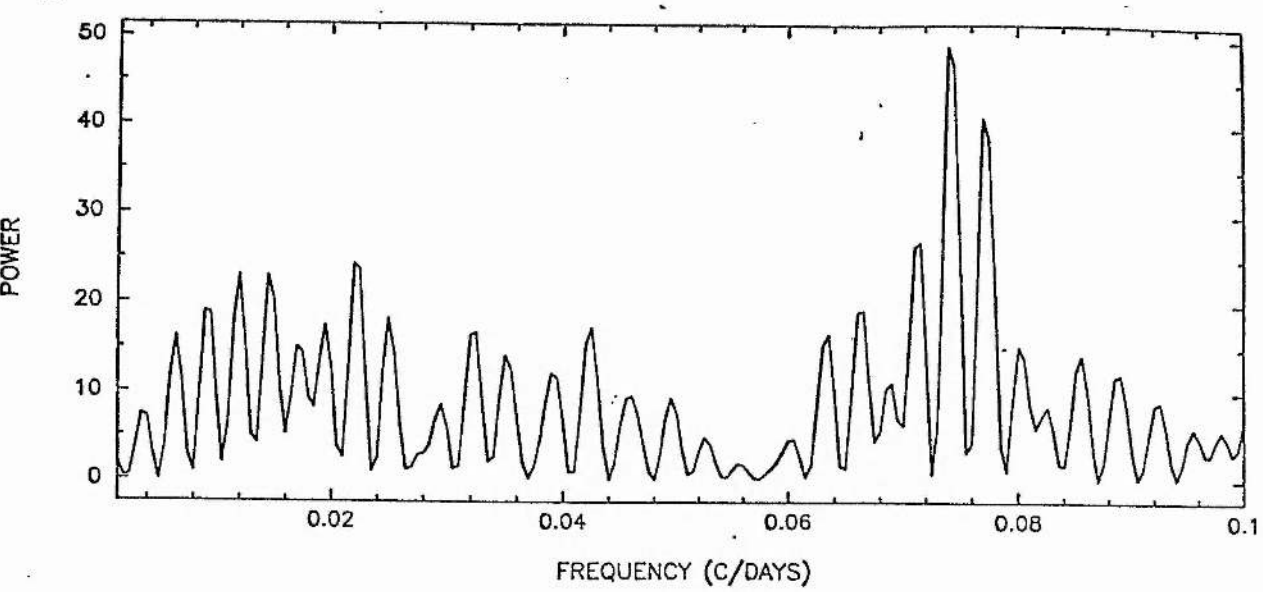

Figure 6.5: Power spectrum for first two seasons (see text)

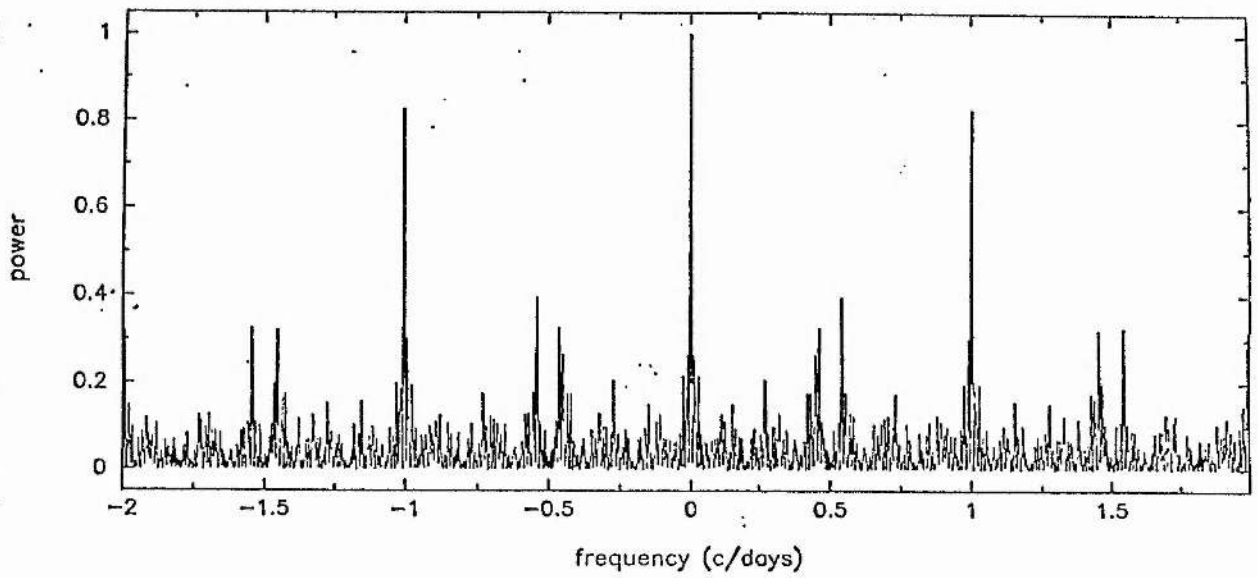

Figure 6.6: Power window for first two seasons (see text)

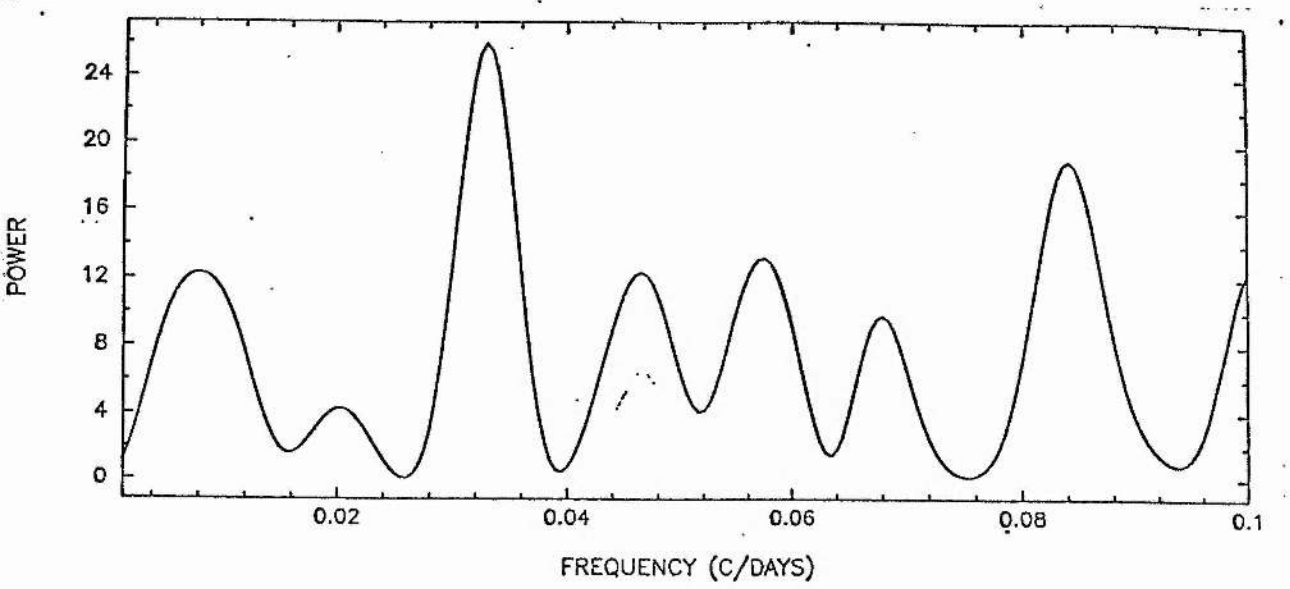

Figure 6.7: Power spectrum for third season (see text)

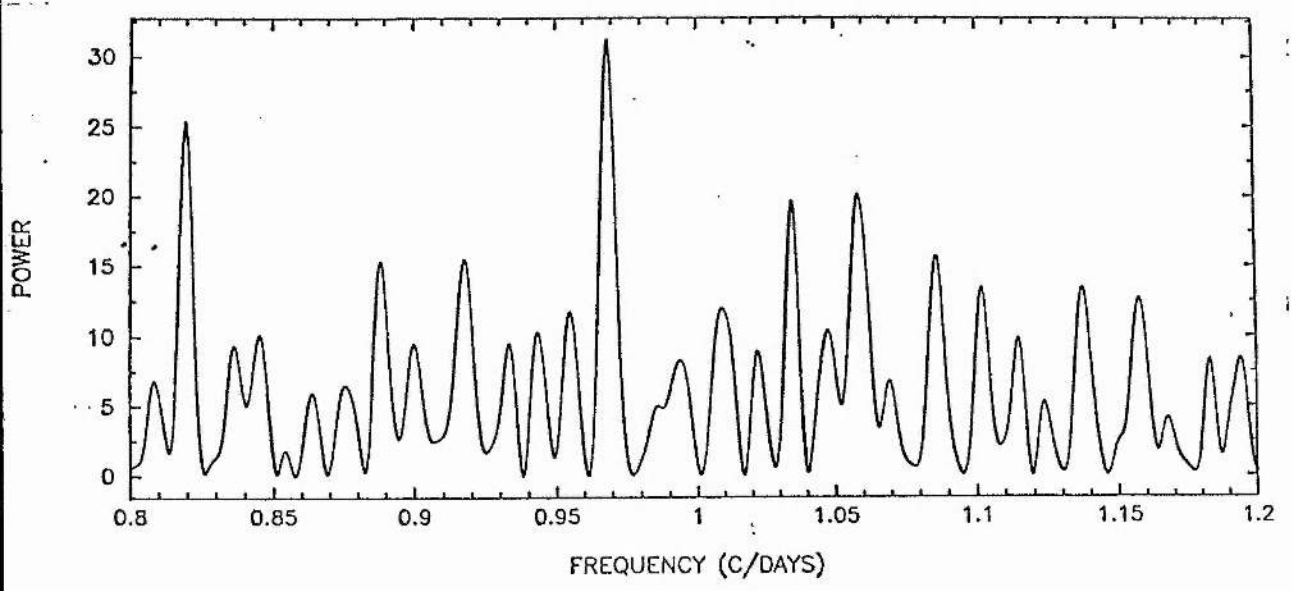

Figure 6.8: As above, in 0.8 to 1.2 frequency range (see text)

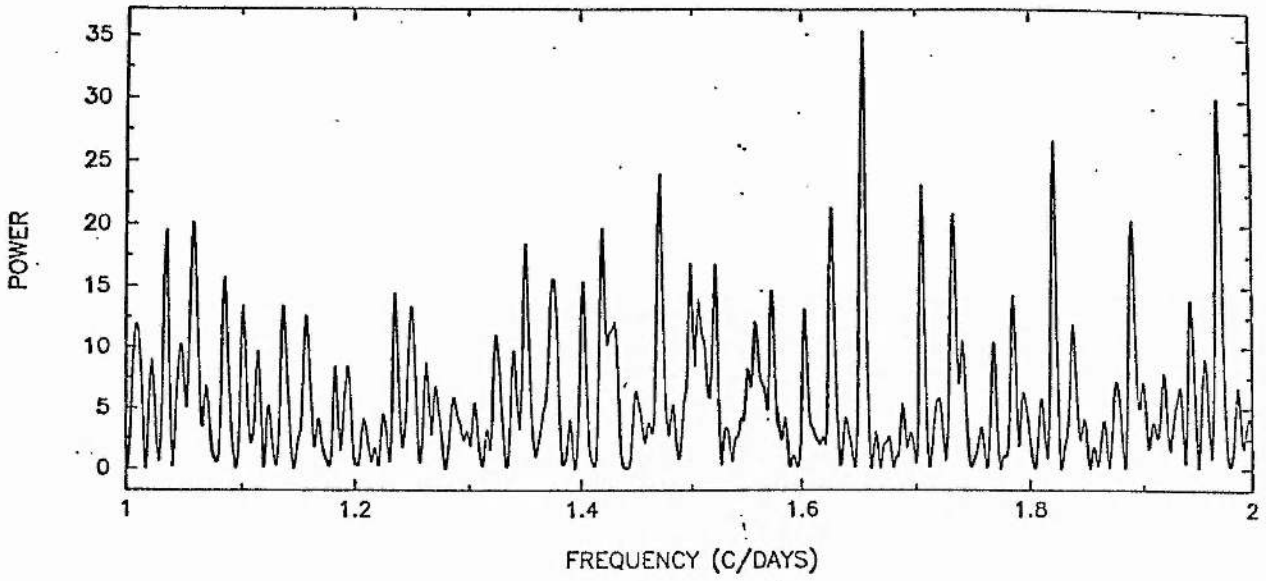

Figure 6.9: As above, out to 2 with a coarser grid (see text)

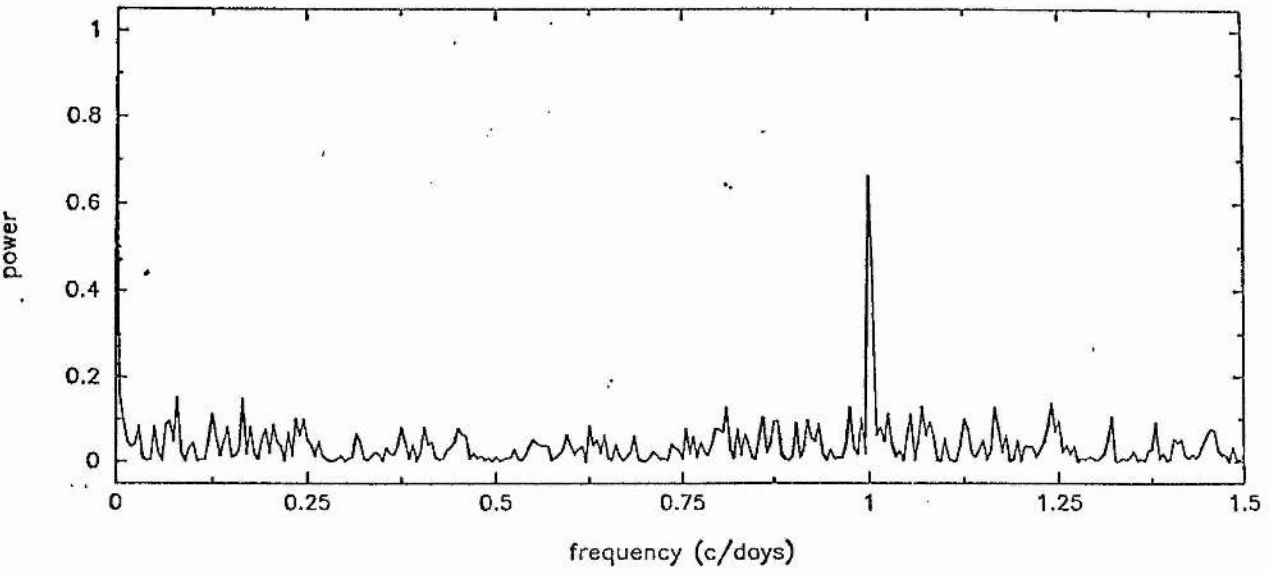

Figure 6.10: Power window for third season (see text)

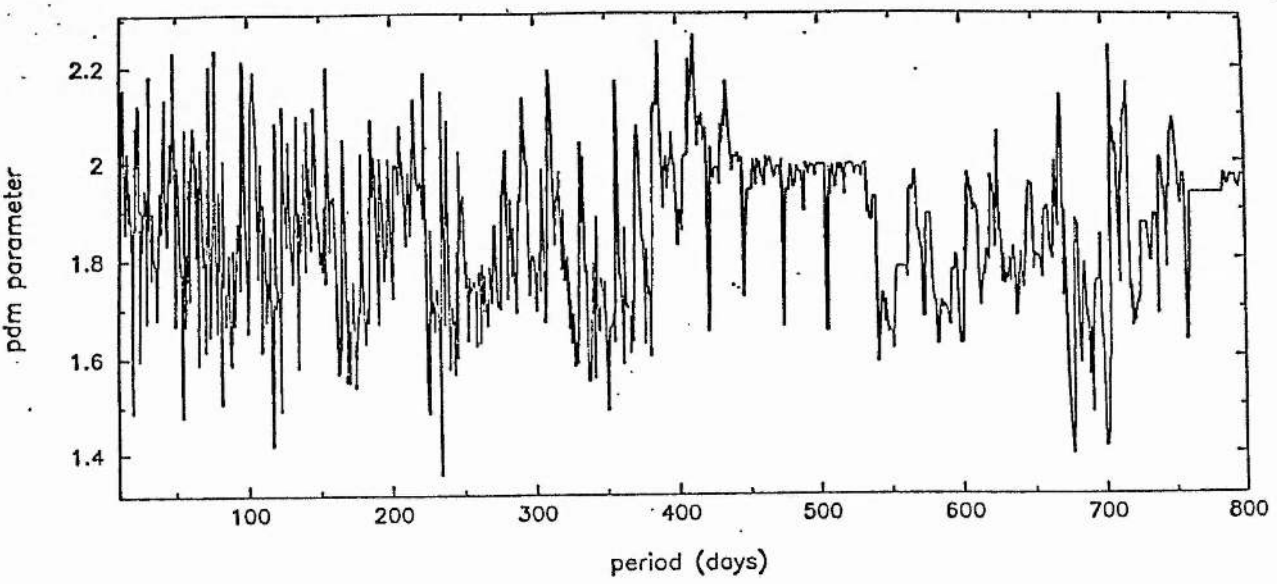

Figure 6.11: Lafler-Kinman periodogram (see text)

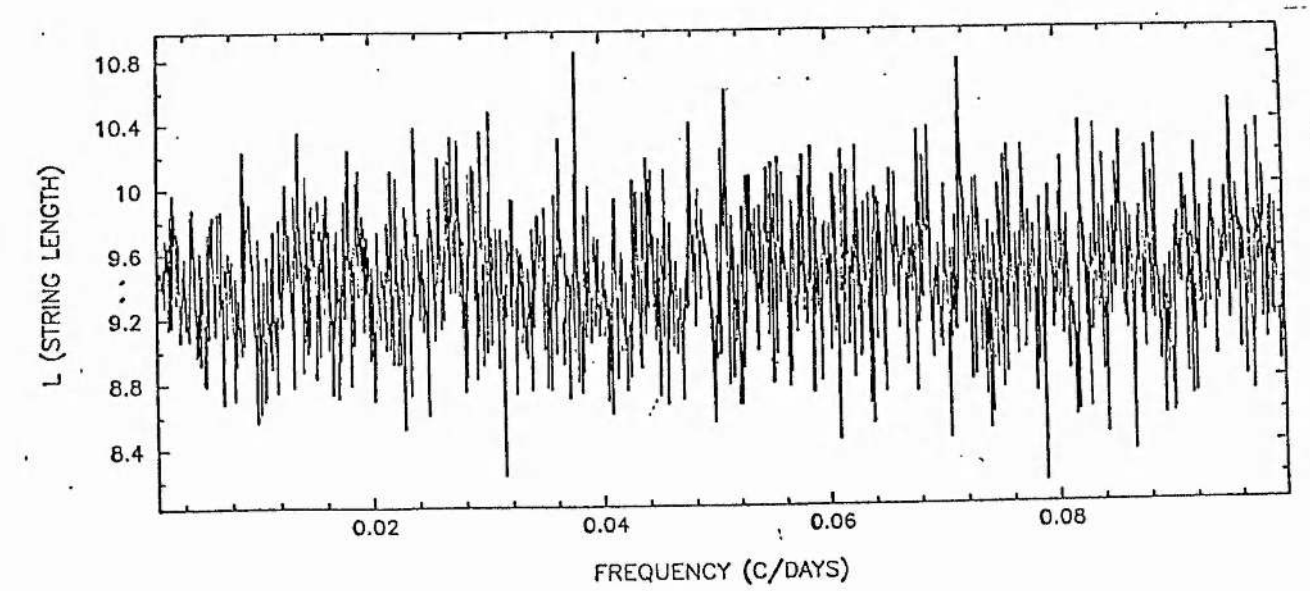

Figure 6.12: String-length periodogram (see text)

day emission contamination, and its absence would therefore leave the Balmer lines undistorted, and thus offering velocities not significantly different from those of the helium lines.

X Per may therefore be a binary system of long period, viewed at low inclination, or with a high eccentricity orbit; or it may be a single star (perhaps unlikely!).

6.5 Line Profile changes in X Per

Reticon spectra from each night were co-added to give the highest s/n prior to measurement of a variety of line profiles. In view of the largeness of the data set, and the limited time at the disposal of the measurer, it was not feasible to assign a measurement to every identifiable feature in the spectrum. As a compromise, it was decided to pick out lines not just on their intrinsic merit as spectral signifiers, but by virtue of how easily they could be defined with respect to continuum height, etc, in what were still rather noisy tracings. This limited the choice to the two Balmer lines H_δ and H_γ, plus the two strong helium lines at 4471 Å and 4026 Å. In some spectra, no lines at all could be measured, while others yielded only one or two measurements. One factor that should be mentioned is that the intrinsic weakness of a line may mitigate against its succesful measurement, even though the S/N may be no worse than the average.

The measurements were made in the manner described in previous chapters, by the fitting of gaussian profiles to rectified spectra, using REDUCE. The results are summarised in Tables 8 - 11.

The Balmer widths and depths are displayed against date in Figure 13 and Figure 14, with the corresponding Helium measures shown in Figure 15 and Figure 16. A visual inspection of the Balmer data shows an apparent difference between the relative strengths of the two lines from season 89-90 to 90-91. There is insufficient data to comment on the trend in the previous season. Whether this is significant or not is open to argument, since it might simply reflect the S/N in the spectra. However, the two seasons' data are of similar S/N level on average, and any observed differences presumably reflect actual spectral variations. The overall pattern, reflected in both

Table 6.8: Balmer line profile changes in X Per -1

H.J.D	H_γ depth	H_γ EW	H_δ depth	H_δ EW
2440000+		Å		Å
7568	—	—	—	—
7570	—	—	—	—
7574	—	—	—	—
7581	0.270	0.884	—	—
7584	—	—	—	—
7596	—	—	—	—
7597	—	—	0.059	0.062
7561	—	—	—	—
7603	—	—	—	—
7607	—	—	—	—
7841	—	—	0.061	0.048
7853	0.078	0.630	0.135	1.888
7856	0.227	3.241	0.226	3.634
7858	0.114	0.965	0.075	0.376
7864	0.215	1.375	0.406	9.835
7866	0.090	0.677	0.121	1.037
7867	0.113	1.051	0.127	1.295
7883	—	—	0.329	8.712
7898	0.132	1.316	0.184	1.972
7904	0.118	1.078	0.142	1.151
7920	0.156	1.705	0.325	6.281
7926	0.142	1.253	0.216	3.088
7931	0.133	1.140	0.144	1.578
7935	0.116	1.072	0.131	1.083
7938	0.129	1.369	0.144	1.356

Table 6.9: Balmer line profile changes in X Per -2

H.J.D	H_γ depth	H_γ EW	H_δ depth	H_δ EW
2440000+		Å		Å
7938	0.115	0.934	0.148	1.493
8149	0.155	1.071	0.136	1.166
8199	0.177	0.688	0.127	1.113
8200	0.141	0.799	0.137	0.984
8215	0.149	1.080	0.154	1.181
8216	0.136	0.910	0.146	1.219
8224	0.139	0.964	0.141	0.867
8225	0.105	0.651	0.134	0.912
8229	0.171	1.486	0.194	1.979
8230	0.123	0.754	0.126	1.005
8231	0.144	0.969	0.160	1.513
8238	0.157	1.027	0.152	1.455
8240	0.148	0.866	0.153	1.272
8241	0.130	0.801	0.145	1.213
8271	0.142	0.912	0.134	0.868
8272	0.122	0.738	0.172	1.710
8274	0.130	0.757	0.119	0.859
8277	0.136	0.822	0.118	0.997
8278	0.178	1.262	0.138	1.080
8279	0.146	1.064	0.137	1.078
8288	0.197	1.328	0.188	1.082
8300	0.151	0.951	0.145	0.925
8308	0.135	0.852	0.132	1.097
8312	0.170	1.019	0.186	2.740
8313	0.173	1.364	0.139	0.833
8319	0.119	0.766	0.148	1.427

Table 6.10: He1 line profile measurements in X Per -1

H.J.D	HeI 4471 Å depth	He1 4471 Å EW	HeI 4026 Å depth	HeI 4026 Å EW
2440000+		Å		Å
7568	0.058	0.177	0.069	0.299
7570	0.059	0.074	—	—
7574	0.037	0.122	—	—
7581	0.071	0.279	—	—
7584	—	—	—	—
7596	0.051	0.077	0.047	0.085
7597	0.160	1.262	—	—
7561	0.290	2.033	0.095	0.247
7603	—	—	—	—
7607	0.069	0.167	0.116	0.408
7841	0.046	0.039	—	—
7853	0.083	0.537	—	—
7856	0.122	0.949	0.075	0.349
7858	0.178	2.189	—	—
7864	0.100	0.440	0.098	0.590
7866	0.111	0.949	0.240	3.346
7867	0.121	0.876	0.087	0.456
7883	0.046	0.102	—	—
7898	0.118	0.613	0.137	0.748
7904	0.098	0.669	0.111	0.512
7920	0.105	0.586	—	—
7926	0.120	0.687	0.121	0.607
7931	0.092	0.484	0.131	0.913
7935	0.097	0.669	0.112	0.462
7938	0.121	0.839	0.102	0.351

Table 6.11: HeI line profile measurements in X Per -2

H.J.D	HeI 4471 Å depth	HeI 4471 Å EW	HeI 4026 Å depth	HeI 4026 Å EW
2440000+		Å		Å
7938	0.108	0.644	0.115	0.659
8149	0.110	0.667	0.096	0.455
8199	0.093	0.562	0.147	1.017
8200	0.101	0.543	—	—
8215	0.132	0.894	0.113	0.795
8216	0.131	0.932	—	—
8224	—	—	—	—
8225	0.105	0.651	—	—
8229	0.098	0.645	0.109	0.845
8230	0.078	0.396	—	—
8231	0.110	0.622	0.095	0.442
8238	0.107	0.615	0.118	0.794
8240	0.113	0.566	0.145	1.024
8241	0.149	1.313	0.214	2.605
8271	0.147	1.180	0.105	0.553
8272	0.116	0.691	—	—
8274	0.142	1.292	0.061	0.294
8277	0.113	1.074	—	—
8278	0.164	1.908	0.112	0.690
8279	0.119	0.713	0.205	2.510
8288	—	—	—	—
8300	0.205	1.970	—	—
8308	0.111	0.747	0.148	1.465
8312	0.130	0.825	—	—
8313	0.107	0.748	—	—
8319	0.089	0.667	—	—

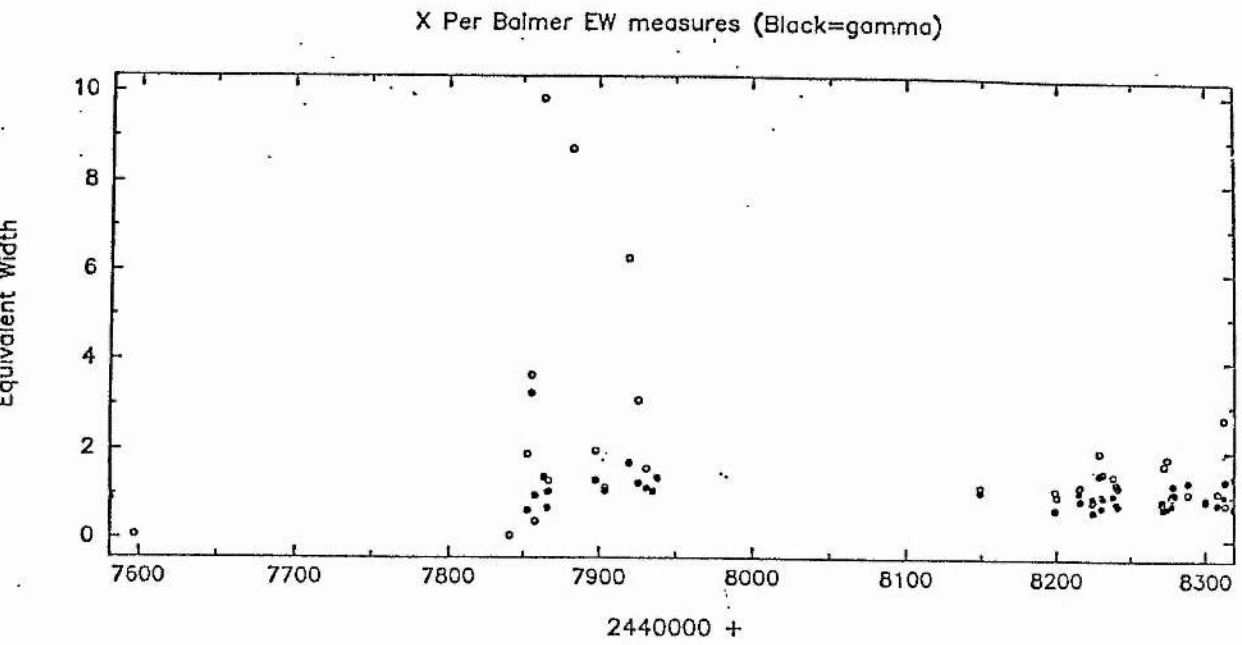

Figure 6.13: X Per Balmer widths against Julian day number

the depth and equivalent width estimates, is of approximate constancy in H_γ between 89-90 to 90-91, with an clear tendency for H_δ to become weaker by the third season. This is difficult to interpret; had there been variable degrees of emission contamination present, the effect would have been more pronounced at H_γ, falling off with increasing quantum number so that H_δ would have been less perturbed. In other words, had this source of contamination been dissipated, the change would have been more evident in H_γ than H_δ. The changes are therefore of interest, but do not shed useful light on the topical question of the dissipation of the disk (see next subsection).

The Helium line measurements display no obvious pattern, showing approximately equal depth and equivalent width ranges for the entirety of the program. A very slight tendency toward increasing strength *may* just be evident. No major changes would be expected, however, since even if the star is differentially heated, its fast rotation would mean that real changes would occur on too short a time-scale to be resolved in these co-added spectra.

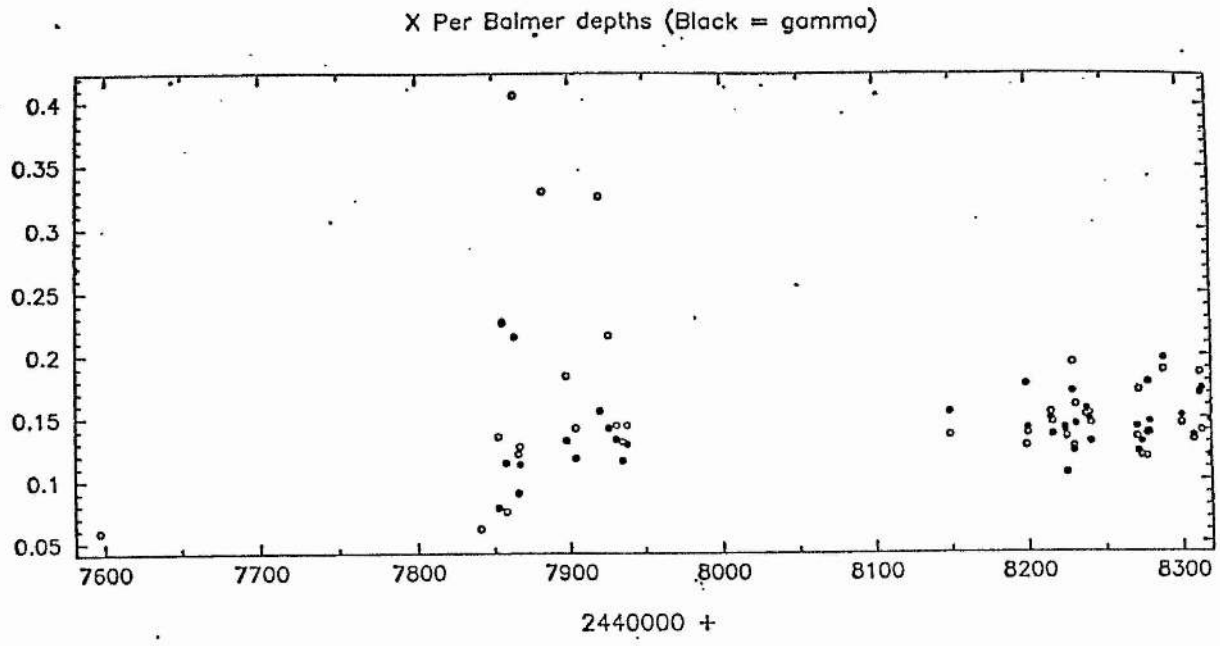

Figure 6.14: X Per Balmer depths against Julian day number

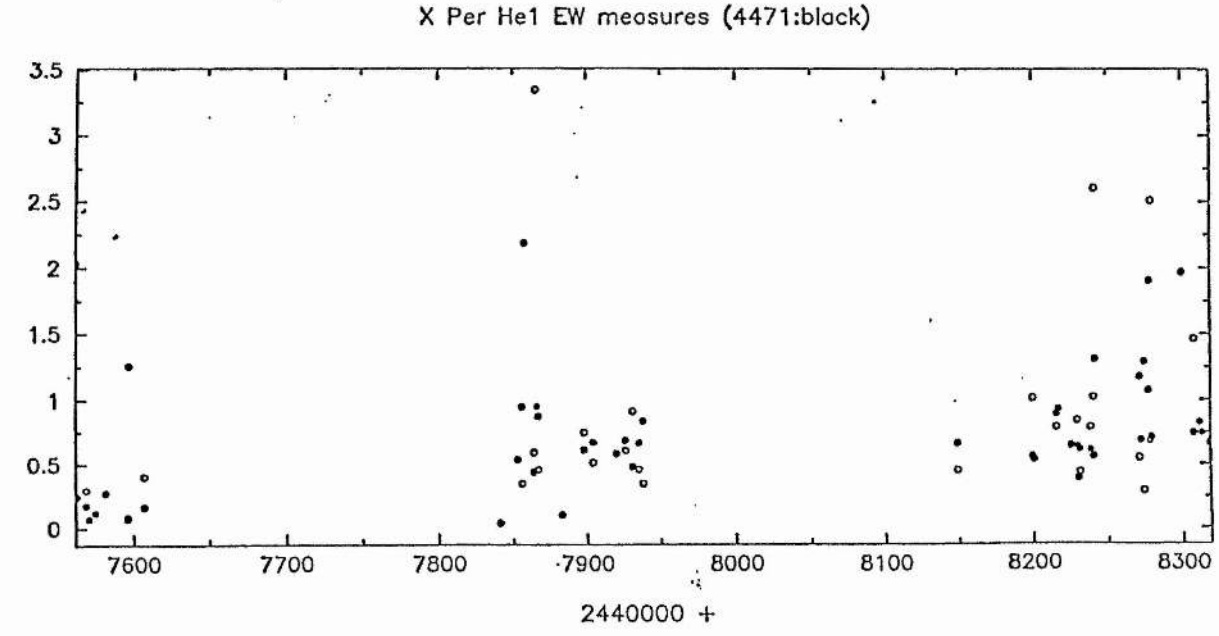

Figure 6.15: X Per HeI widths against Julian day number

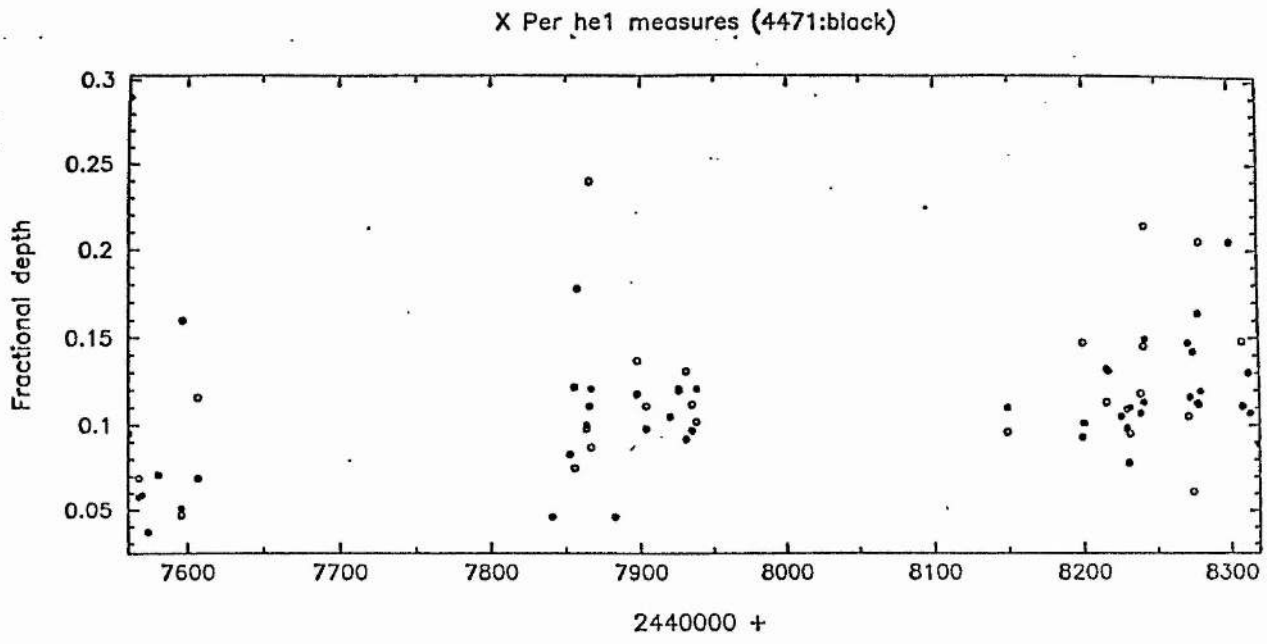

Figure 6.16: X Per HeI depths against Julian day number

6.5.1 A decline in X Per ?

As is generally accepted, stars exhibiting Be spectra may be expected to show, at various times, shell spectra (absorption lines with deep, narrow cores), emission lines and "normal" early-type spectra. These switches are generally termed *phase variations*, and are virtually unpredictable. As discussed in Underhill and Doazan, (1982), Be stars have been seen to switch almost arbitrarily from one state to another, with no apparent regard for order. Such changes, however, have not been reported for the Be/x-ray systems, perhaps owing to the relatively short periods over which they have been studied in sufficient detail. (For instance, Pleione's last two shell phases before 1982 were spaced by 35 years). Interestingly, our attention was drawn (Coe et al, private communication), to a pronounced reversal in the emission of X Per at H_α, sometime between 1988 and 1990. This seemed to indicate the switch over from classical Be star to a normal O9 or even shell spectra. Fortunately, our recently reduced INT data enable the period of reversal to be pinned down to between February and September 1990. It is frustrating that such an event chose to manifest itself during the period when X Per was not observable.

The red INT frame of February 21 1990 (Figure 17) shows a typical H_α profile. Because of the lack of emission in any of the other Balmer lines in the blue spectra from around this time, and the non-supergiant spectral classification, X Per is clearly in the Be-phase at this time. The feature shows a well-defined double peak, V slightly stronger than R, at about 1.4 times the continuum flux. There is almost certainly sub-structure not resolved at the frame's dispersion. The double peak structure argues against a low inclination.

By September 2 1990, the emission feature has gone, leaving a shallow absorption line (Figure 18). This is verified by Reticon observations taken later in the season, and can be ruled out as being due to misidentification of the star, or a scale error in the CCD data. Insofar as this feature is concerned, X Per would be identified as a routine B or O star. Spectra taken later in the season, not portrayed here, seem to show the possible reemergence of emission as a weak feature in the core of the absorption line.

Though this change is clearly of significance, evidence for it elsewhere in the spectrum has not been found (see above). Possibly there *were* marked changes which were not observed because of the star's inaccessibility over the summer. Underhill and Doazan (1982) refer to a velocity progression observed during shell-ejections, this however would probably only have been seen in the low quantum number lines.

6.5.2 Rotational velocity measures

Each of the line measurements performed above also automatically generated an estimate of $V \sin i$ the observed component of the rotational velocity of the star. Since X Per is a Be star, the rotation might be expected to lie in the higher range of values for early stars. In Be stars, $V \sin i$ has been observed to be as high as 450 $\mathrm{km\,s^{-1}}$ (Jaschek and Jaschek, 1987). X Per is however the O-type counterpart of a Be star, and, furthermore, the binarity will presumably result in an atypical rotation rate, since synchronisation may have been forced at some point in the binary's history. In the case of non-Be O stars, Slettebak (1956) concluded that part of the line broadening effect arises due to macroturbulence, in addition to rotational broadening. From a survey of O stars, Jaschek and Jaschek quote an observed upper limit on $V \sin i$ of around

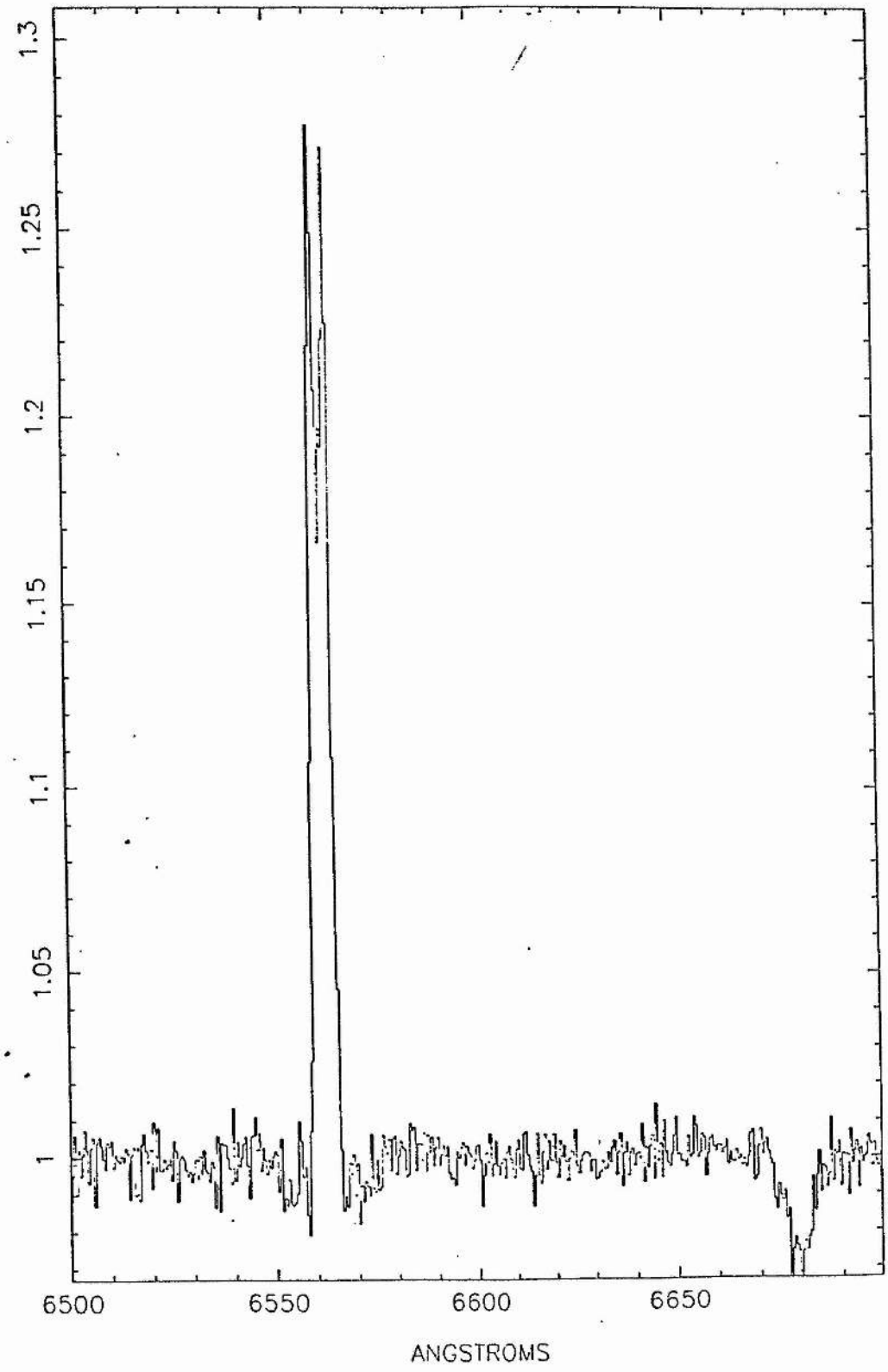

Figure 6.17: Sky-subtracted CCD image of X Per , wavelength in normal sense

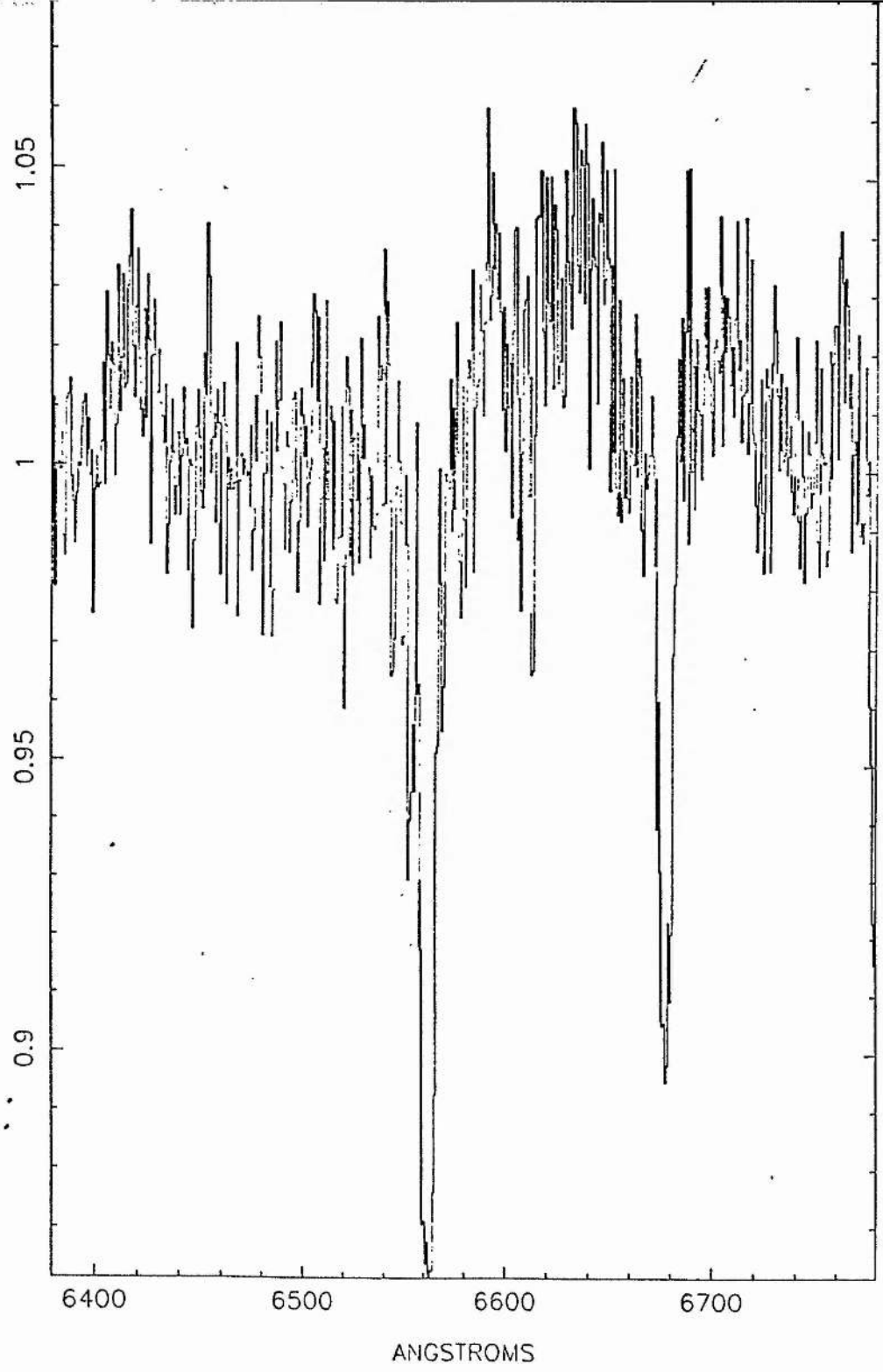

Figure 6.18: As above, but several months later, with feature now absorbed

220 km s^{-1}, assuming that macroturbulence contributes nothing to the broadening. If it is present, which seems at least conceivable, then the broadening function of the line is more complicated, and the rotational velocity will have been overestimated in the measurements. Other sources of error in Be stars arise because the star may be appreciably oblate, with a different limb-darkening law. The overestimate *without* the problem of macroturbulence may be as high as 15 %.

The HeI observations sample the star's rotation curve closest to the photosphere, and these have been tabulated in Table 12. They may *still* suffer from contamination from the envelope, and, in addition, Underhill and Doazan (1982) report that, though these lines are the pair most frequently adopted for rotational studies, they may nonetheless suffer from harsh blending effects. As the plate factor for the X Per observations is even lower than the moderate values usually used, such effects are definitely present. The measurements are clearly variable. It is obvious that a component of this variability is imposed by the subjectivity of the measuring process, while the varying quality of the spectra themselves clearly have some effect. The mean FWHM for the 4471 Åmeasures was 5.8 $\pm$ 0.3 km s^{-1}, while that for the 4026 Åmeasures was 5.8 $\pm$ 0.5 km s^{-1}. Based on the FWHM versus calibration of Hill (private communication) used in Chapters 3 and 4, this suggests a $V \sin i$ of $\approx$ 200 km s^{-1}.

This suggests a rotational velocity, which, even though overestimated, is still well below the critical velocity for such a star (Underhill and Doazan, quoting Slettebak, show that the critical velocity would be in excess of 600 km s^{-1}), even for a B0 type). Once again, therefore, the Struve model has been shown to be deficient.

6.6 Comments

A lengthy study of X Persei has failed to find substantive evidence for orbital motion, between periods of 10 - 600 days. The true orbital period is probably close to the upper limit of this range, since one must account for the quasi-periodicity of the x-ray flares, but the semi-amplitude may be so low as to preclude detection. The rotational velocity measurements found a value of around 200 km s^{-1}, which is somewhat low for a Be star, and may suggest a low value for i, and hence a correspondingly low expected

Table 6.12: HeI $V \sin i$ measurements

H.J.D	HeI 4471 Å	HeI 4026 Å	HJD	HeI 4471 Å	HeI 4026 Å
2440000+	FWHM (Å)	FWHM (Å)	2440000+	FWHM (Å)	FWHM (Å)
7568	2.90	4.07	8149	5.71	4.43
7570	1.18	—	8199	5.67	6.52
7574	3.08	—	8200	5.05	—
7581	3.71	—	8215	6.36	6.62
7584	—	—	8216	6.68	—
7596	1.41	1.71	8224	—	—
7597	7.42	—	8225	5.83	—
7561	6.59	2.43	8229	6.19	7.31
7603	—	—	8230	4.74	—
7607	2.28	3.31	8231	5.30	4.40
7841	0.79	—	8238	5.39	6.31
7853	6.09	—	8240	4.71	6.65
7856	7.30	4.39	8241	8.26	11.45
7858	11.58	—	8271	7.57	4.96
7864	4.15	5.66	8272	5.61	—
7866	8.00	13.08	8274	8.52	4.52
7867	6.81	4.92	8277	8.89	—
7883	2.09	—	8278	10.93	5.79
7898	4.87	5.13	8279	5.63	11.50
7904	6.44	4.32	8288	—	—
7920	5.25	—	8300	9.04	—
7926	5.39	4.71	8308	6.33	9.33
7931	4.93	6.56	8312	5.95	—
7935	6.49	3.88	8313	6.58	—
7938	6.50	3.24	8319	7.01	—

semi-amplitude. Two other periodicities were hinted at, but as neither repeated itself from season to season, and as neither had any astrophysical counterpart, they are not believed real.

Studies of line-profile variations showed a peculiar variation between the Balmer line strengths which was opposite to the expected behaviour, had the emission forming region been dissipated. No explanation for this has been advanced.

To conclude, the X Per picture is still rather murky, and future studies of the orbital period based on spectroscopy may be forlorn, unless the spectral resolution, spectral coverage, time-resolution, observational bandwidth and signal to noise ratio can all be markedly improved. Short of the dedication of a large telescope to this sole aim, the best avenue for understanding the system may lie in a more detailed coverage of the X-ray and polarimetric behaviour, the former to probe the flare cycles, the latter to study the circumstellar environment in the necessary detail.

6.7 References

Braes, L.L.E., Miley, G.K., 1972. *Astrophys. J.*, **173**, L105.

Corbet, R.H.D., 1984. *The Evolution of Galactic X-Ray Binaries, eds. Truemper, Lewin and Brinkman (Dordrecht:Reidel).*

Dworetsky, M.M., 1983. *Mon. Not. R. astr. Soc.*, **203**, 917.

Edwin, R.P., 1989. The Observatory, **109**, 173.

Hilditch, R.W., Reynolds, A.P., Bell, S.A., Pollacco, D.L., Edwin, R.P., 1991. The Observatory, *Vol III*, **1100**, 14.

Hutchings, J.B., 1977. *Mon. Not. R. astr. Soc.*, **181**, 619.

Hutchings, J.B., Cowley, A.P., Crampton, D., Redman, R.O., 1974. *Astrophys. J.*, **191**, L101.

Jaschek, C., Jaschek, M, The Classification of Stars.

Margoni, R., Ciatti, F., Mammano, A., Vittone, A., 1988. *Astr. Astrophys.*, **148**, .

Penrod, G. Vogt, S.S, 1985. *Astr. Astrophys.*, , .

Skillen, W.I, 1985. *PhD Thesis, Univ. St Andrews.*

Slettebak, A., 1956. *Astrophys. J.*, **124**, 173.

Underhill, A., Doazan, V., 1982. *B Stars with and without emission lines, (NASA monograph).*

van den Bergh, S., 1972. Nature, **235**, 273.

Chapter 7

Conclusions

7.1 Summary

The aim of this study was to improve on the spectroscopic observations of high-mass x-ray binaries which had been published by previous authors, mainly in the nineteen seventies. It was known that a spectroscopic analysis of these systems, coupled with extant data from x-ray observations, offered the possibility of determining the masses of the component stars to an accuracy better than 10 %. The spectroscopy that had been performed earlier was, however, arguably the weak link in the chain, since the observations invariably had large random (and possibly systematic) errors. Based on studies of faint binaries already performed at St Andrews and elsewhere, using the new generation detectors on large telescopes, and the more sophisticated techniques of velocity measurement now available, it was thought likely that the spectroscopy could be improved. To this end, observations of all three types of HMXB were made, using CCD and Reticon detectors, over timescales ranging from four days to more than two years. The theory and practice of determining the masses is discussed in Chapters 1 and 2, where it is stressed that the number of external assumptions that need be made is remarkably small (and can usually be justified by recourse to other observational properties).

However, the observer is still at the mercy of the observing conditions, even

when all else is optimised. In Chapter 3, for instance, our observations of SMC X-1 were compromised by low signal to noise, such that the omission of the Balmer lines in the velocity derivation was not possible. In Chapter 5, observations of the star Cen X-3 were hampered by the unreliability of a first-order ephemeris, with the effect that the crucial quadratures were not observed. In Chapter 6, a detailed reexamination of the long-period system X Persei failed to reproduce any systematic velocity variations at all. The last mentioned case apart, all the studies of binaries in this study were made over only one or two (consecutive) orbital cycles. If observations had been made over a longer time-base, confidence concerning subtle variations would grow. For instance, in SMC X-1 and QV Nor, there is evidence for temperature variations around the primary, which, if real, contain information on the degree of distortion of the star and the intensity of the x-ray heating effect. Because these variations were only seen in one cycle, one cannot ascribe too much significance to them. If on the other hand the star had been observed over several cycles, during which time the x-ray flux was also monitored, one would have a valuable insight into the luminosity and beaming characteristics of the pulsar.

Despite the difficulties encountered, we were able to determine relatively precise masses for two of the short-period systems. This represents a success rate of about 50 % - observations were also attempted of the RLOF system LMC X-4, but were scuppered by poor weather, while the afore- mentioned phasing error in the observations of Cen X-3 precluded the mass determination (although a range of possibilities are discussed). There is no intrinsic reason why future observations of LMC X-4 and Cen X-3 should not also yield improved masses.

As discussed in Chapter 1, there is a suspicion that the masses of the secondary components should lie in the $1.4 \pm 0.2\ M_{\odot}$ range. Although the existing estimates were certainly not in conflict with this, they were in general subject to very large errors. Interestingly, the highest and lowest estimated masses prior to our study were for QV Nor's pulsar and that of SMC X-1 respectively (see the relevant chapters for the quoted masses of previous authors). It is gratifying that our derived masses bring both pulsars within the permitted mass range, as depicted in Fig 7.1, adapted from Joss and Rappaport (1983). The central bar in each new estimate is the spread of masses between the adopted non-keplerian solution and the uncorrected masses, with the appropriate

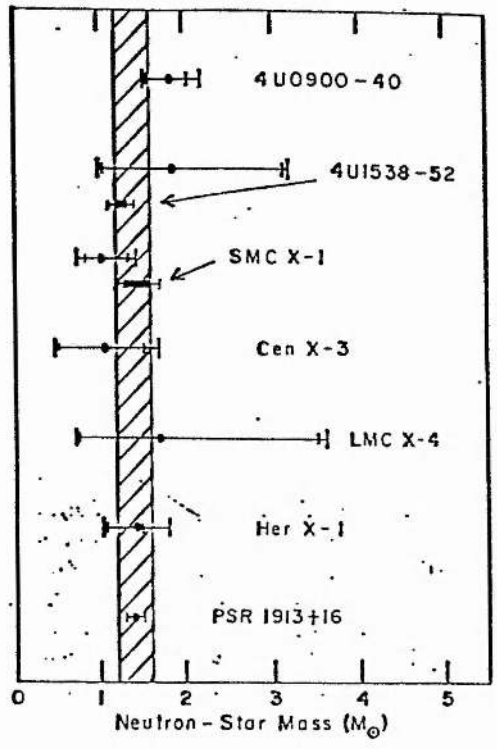

Figure 7.1: Masses for neutron-stars, including estimates from this study

error bars. The only other estimate of comparable accuracy mentioned in Joss and Rappaport's study was the binary pulsar PSR 1913+16. These results therefore lend credence to the standard model for the formation of HMXBs, as discussed in Chapter 1.

Concerning the masses of the primary components, there seems little reason to suppose that they are anything but ordinary B stars. A slight tendency toward under-massiveness may be apparent when the derived parameters are compared with evolutionary models, but this may simply represent the outcome of mass-loss in the originally heavier star (the 20 $M_\odot$ star's luminosity puts it on the 25 $M_\odot$ mass track). Although our masses are similar to those already derived, the luminosities are less since we have arrived at smaller Roche volumes for the primaries (The adopted temperatures are those employed by previous workers since we do not have access to better spectral classifications).

The distances to the two systems for which we have the best mass estimates have also been determined. In SMC X-1, the distance is rather critical, since the x-ray source is close to its Eddington limit. Using a canonical temperature for the primary and its newly estimated surface area, the M_v gives a distance estimate of 47 kpc, which,

while placing the system nearer to us than the SMC, is valid from the standpoint of the observed x-ray flux. Using an equivalent width calibration, a higher but very much less certain range of distances is implied (for which the source is moderately or strongly super-Eddington). The other system, QV Nor, is not strongly constrained by its x-ray properties since it appears an intrinsically weak source. In the absence of a published distance calibration, the M_v has again been estimated from the temperature/size of the star, giving a distance of similar size to that estimated by previous authors.

Observations were also made on X Persei, to investigate the validity of its implied 580-day orbital period. Data taken over more than 2 years, around 130 spectrograms, failed to confirm this period, or to suggest any other candidate. The true period might well be 580 days, revealed by the periodicity of the x-ray flare-ups, but the lowness of the amplitude/ orbital inclination may conspire to prevent detection. A further problem with the Be/x-ray systems is that the extent of contamination by emission components arising in the disk is not yet clear, and may mask the velocity variations even when they should be apparent.

7.2 Future Work

Irrespective of the quality of the spectrograms, the derivation of reliable mass-ratios depends on the size of the non-keplerian velocity distortions applied to the raw data. Although the corrections for gravity-darkening and tidal distortion are based on well-determined parameters which are independent of the distance to the star, this is not the case for the "reflection effect" caused by the proximity of the neutron star. As is discussed in Chapter 3, the influence of the neutron star is difficult to assess, since the beaming geometry and energy must somehow be inferred from the pulse and flux data. It is therefore vital to study the spectral and photometric variations of the B star to infer its temperature profile. Although there seems little hope of determining unique parameters from such studies, owing to the variety of configurations which can produce the same light variations, they can be used to ascertain the validity of various working models. Even in a relatively simple system such as QV Nor, in which there is probably no disk, the observed light curve is highly asymmetric about its

minima, something which can obviously not be explained within the context of purely ellipsoidal variations. There is therefore, much scope for further study in even the best understood of the high-mass x-ray binaries. To conclude, the following avenues of attack are suggested:

(1) Spectroscopy of all bright, short-period eclipsing systems, including Cen X-3 and LMC X-4. These systems should provide mass estimates of comparable accuracy to those seen in SMC X-1 and QV Nor, using the techniques of this study.

(2) Establish the status of A0538-66: is it a Be/x-ray system of short orbital/pulse period, or is it a RLOF system in the process of being circularised? One night's fortuitous observing may be sufficient to answer this question!

(3) Improved photometry should be performed on all the systems discussed in this study, ideally within one cycle, to avoid zero errors. This should test various hypotheses of Roche filling, disk configurations and temperature gradations.

(4) Simultaneous x-ray/optical/polarimetric/UV studies to elucidate accretion process and flux "reprocessing". This will offer a better insight into the heating effect, and thus enable the velocities to be interpreted with greater confidence.

(5) Establish that rotational velocities of primaries in RLOF/wind-driven systems are consistent with current model, using $V \sin i$ calibrations for luminous, rapidly rotating stars specific to the observed lines.

(6) Determine orbital periods of Be/x-ray systems such as X Persei independently of x-ray flare observations.

7.3 References

Joss, P.C., Rappaport, S.A., 1984. *Ann. Rev. Astr. Astrophys.*, **22**, 537.